

Development of a calculation tool to determine the shading tolerability of PV modules

Nida Rukhshi

Development of a calculation tool to determine the shading tolerability of PV modules

by

Nida Rukhshi

in partial fulfilment of the requirements for the degree of

Master of Science
in Sustainable Energy Technology

at the Delft University of Technology,
to be defended publicly on Thursday August 25, 2022 at 3:00 PM.

Student number:	5378451		
Thesis committee:	Dr. Hesam Ziar	TU Delft, ESE-PVMD	Supervisor
	Ir. Alba Alcañiz Moya	TU Delft, ESE-PVMD	Daily supervisor
	Prof. dr. Olindo Isabella	TU Delft, ESE-PVMD	Internal committee member
	Dr. Aleksandra Lekić	TU Delft, ESE-IEPG	External committee member

This thesis is confidential and cannot be made public until August 25, 2024.

Front page image: Taken from <https://www.solibro-solar.com/solar-power-101-how-the-best-solar-panels-cope-with-shade/> (Modified)

An electronic version of this thesis is available at <http://repository.tudelft.nl/>.

Acknowledgements

I would first and foremost like to sincerely thank my daily supervisor, Alba Alcañiz Moya, for her dedicated help and support throughout this thesis; for always being available for questions and for the discussions (short and long) whenever required. I would also like to thank my main supervisor, Dr. Hesan Ziar, for always being ready to discuss any doubts I had, and for providing his helpful insights on various topics, as well as his general support throughout. I would also like to extend my thanks to Yilong Zhou for his support with the laboratory measurements in this project, and to him and Dr. Malte Ruben Vogt for taking the time to answer various questions that I had periodically about specific topics throughout my thesis. Special thanks also to Eurac Research for kindly providing us with the measurement data that was used for validation of the IV simulations. Finally, I would like to thank the PVMD group for the opportunity to pursue my Masters thesis in this topic.

Nida Rukhshi
Delft, August 2022

Abstract

In recent years, photovoltaic technology has become one of the leading renewable alternatives for energy production. One main factor in the diminished performance of a photovoltaic module is partial shading, due to the resulting mismatch conditions in the module. However, it is difficult to understand how a specific PV module reacts to shading in comparison with others, as currently the ability of a module to withstand shading is usually expressed in vague qualitative terms on its datasheet. In this work, the development of a shading tolerability calculator in MATLAB was completed. This tool can relatively easily and quickly calculate the shading tolerability of a module as a numeric parameter (ST), which can then be used for characterization and comparison purposes.

First a MATLAB based model to simulate the IV characteristics of a PV module under different conditions was developed. Irradiance and temperature impacts on the relevant parameters were taken into account to simulate outputs at partial shading conditions. The model was developed at a cell level, which was used to calculate the IV characteristics at a module level by taking the series connection of cells into account. This included modeling the impacts of reverse bias and bypass diodes operation. Validation with experimental data was performed where errors in P_{MPP} were found to remain below 4.5%.

The next step was to define and develop the shading scenarios to be considered when calculating ST. The objective was to determine P_{MPP} of a given PV module under all possible shading scenarios, using the IV simulation model developed. The possible shading scenarios were based on sectioning a PV module into 12 (geometrically) equal parts, and considering two irradiance levels that could occur: $100 W/m^2$ for shaded sections, and $1000 W/m^2$ for unshaded ones. To improve the speed of the model, which was an important aim within this project, the existence of equivalent scenarios based on the symmetry of the module was taken advantage of. The P_{MPP} value then only needed to be simulated once for every unique scenario. In this way, the required number of simulations, and consequently the required simulation time, was greatly reduced.

Based on the above, the development of a calculator for the shading tolerability parameter of a PV module was accomplished. The ST values for more than 40 PV modules were calculated and the results were presented. The ST% values ranged between 22% and 29%. Based on the results, correlations between different module parameters were explored to see their impact, if any, on ST. One main result seen was the impact of the number/configuration of bypass diodes on ST, specifically the considerable positive effect of a higher number of bypass diodes for similar configurations of modules. Another was the positive correlation between temperature coefficient of open circuit voltage and ST calculated.

Finally, a case study for the calculation of shading tolerability for a half-cell butterfly module was implemented. This involved the modeling of parallel connections in PV modules, as well as updating the IV simulation model to include this new type of PV module configuration. The ST values for two half-cell butterfly modules were calculated and the results presented. The calculated ST values were around 42%, significantly higher than those calculated for the conventional modules, highlighting the improved shading tolerance of half-cell butterfly modules. The adaptability of this model to be able to calculate the shading tolerability of any type of configuration of PV module was also demonstrated through this case study, paving the way for future research.

Contents

Acknowledgements	iii
Summary	v
1 Introduction	1
1.1 Impact of shading on PV modules	1
1.2 Shading Tolerability parameter (ST)	3
1.3 Literature review	4
1.4 Thesis aim and research objectives	6
1.5 Thesis outline	7
2 IV Curve Generator	9
2.1 IV Curve	9
2.2 Parameter Extraction Models	10
2.3 Two Diode Model	12
2.4 Cell Level	14
2.4.1 STC	14
2.4.2 NonSTC	14
2.5 Module Level	16
2.5.1 Homogeneous conditions	16
2.5.2 Partial Shading	17
2.6 Bypass Diode Implementation	21
3 Validation	25
3.1 Cross Verification	25
3.1.1 Module level	26
3.2 LASS Validation	28
3.3 Canadian Solar Validation	30
4 Shading Tolerability Calculator	37
4.1 Shading Scenarios	37
4.2 Reduction of simulation time	38
4.3 In search of symmetry	41
4.3.1 Symmetry when splitting	41
4.3.2 Vertical Symmetry	44
4.3.3 Additional Symmetry	46
4.4 Shading Tolerability Calculation	49
4.4.1 Calculation of P_{MPP} for each shading scenario	49
4.4.2 Calculation of shading tolerability parameter	50
4.5 Discussion	52
4.5.1 Analysis of results	54
4.5.2 ST visualization	58
4.6 Interesting insights on model from results	60
4.6.1 Example of same module with 3 bypass diodes and 6 bypass diodes	60
4.6.2 Effects of lower breakdown voltages	62
4.6.3 Type of bypass diode	62
4.6.4 Effect of splitting configuration	63
4.7 Further Recommendations	65
5 Half-Cell Butterfly Module Case Study	67
5.1 Half-Cell Modules	67
5.2 Half-cell Butterfly IV Characteristics Modelling	68

5.3	Shading Tolerability	71
5.3.1	Equivalent Scenarios	72
5.4	Results and Discussion	77
6	Conclusion/Recommendations	79
6.1	Conclusions	79
6.2	Further Recommendations	80
	References	83
A	Canadian Solar Validation Results	89

List of Figures

1.1	IRENA data showing solar PV installed capacity worldwide by year, from 2010 to 2020. Figure taken from [1].	1
1.2	Current-Voltage (IV) and Power-Voltage (PV) curves showing impact of a shaded module with one bypass diode activated. Figure taken from [10].	2
1.3	Indoor experimental setup for shading tolerability measurements. Figure taken from [28].	5
2.1	Representative current-voltage (IV) curve (and corresponding power-voltage (PV) curve) of a solar cell (figure taken from [38]).	9
2.2	Representative current-voltage (IV) curves showing impacts of irradiance and temperature of a Topsola PV module [39].	10
2.3	One Diode Model Equivalent Circuit (figure taken from [40]).	11
2.4	Two Diode Model Equivalent Circuit (figure taken from [40]).	11
2.5	Plot showing IV characteristics at STC and Non STC conditions for a Shell S36 Multi-crystalline module.	17
2.6	Plot showing two solar cells facing different irradiances, $800W/m^2$ and $600W/m^2$	19
2.7	Plots showing methods 1 and 2 of calculating I_{sc}	19
2.8	Forward voltage-current characteristic of F1200 p-n diode. Figure taken from [86].	22
2.9	Plots showing IV and PV curves of 21 cells connected in series with different irradiance levels and no bypass diodes	23
2.10	Plots showing IV and PV curves of 21 cells connected in series with different irradiance levels and 3 bypass diodes	23
3.1	Validation of results at a module level at STC.	26
3.2	Errors at non STC conditions at a module level for the Shell S36 module.	27
3.3	Plot showing improvement of fitting of simulated to measured IV curves with changes in model (one cell shaded), module temperature $28^{\circ}C$	29
3.4	Plot showing improvement of fitting of simulated to measured IV curves with changes in model (two cells shaded), module temperature $31^{\circ}C$	29
3.5	Canadian Solar Shading Pattern	31
3.6	IV and PV plots showing calculated values in comparison to measured values for the Canadian Solar CS6 230P module under partial shading conditions. Shaded Irradiance: $0 W/m^2$, Unshaded Irradiance: $1000 W/m^2$; All cells in first column of cells shaded 50% horizontally Errors: $I_{MPP} : 0.68\%$, $V_{MPP} : 0.04\%$, $P_{MPP} : 0.64\%$	32
3.7	IV and PV plots showing calculated values in comparison to measured values for the Canadian Solar CS6 230P module under partial shading conditions. Shaded Irradiance: $0 W/m^2$, Unshaded Irradiance: $700 W/m^2$; All cells in first column of cells shaded 50% horizontally Errors: $I_{MPP} : 0.76\%$, $V_{MPP} : 0.02\%$, $P_{MPP} : 0.78\%$	33
3.8	IV and PV plots showing calculated values in comparison to measured values for the Canadian Solar CS6 230P module under partial shading conditions. Shaded Irradiance: $0 W/m^2$, Unshaded Irradiance: $200 W/m^2$; All cells in first column and all cells in third column of cells shaded 20% horizontally Errors: $I_{MPP} : 1.83\%$, $V_{MPP} : 4.31\%$, $P_{MPP} : 2.41\%$	34
3.9	Errors at maximum power point for all Canadian Solar measurements. Different irradiances are represented by orange for $200 W/m^2$, yellow for $700 W/m^2$ and green for $1000 W/m^2$	35
4.1	Various possible shading scenarios for a representative PV module split into 12 sections.	38
4.2	72 cell module, 12 rows, 6 columns, 3 bypass diodes, split into 12 sections in a 4x3 configuration.	39

4.3	Various possible shading scenarios for one section shaded in a 72 cell module split into 12 sections.	39
4.4	Various possible shading scenarios for two sections shaded in a 72 cell module split into 12 sections.	40
4.5	72 cell module split into 12 sections in 3x4 or 4x3 configuration- checking most symmetric splitting configuration.	42
4.6	Examples of splitting of various configurations of modules and resulting sections.	43
4.7	Examples of shading scenarios for 12 sections and 2 possible irradiance levels.	44
4.8	Shading Scenarios Examples.	44
4.9	96 cell module, 12 rows x 8 columns, 3 bypass diodes in a [2 4 2] configuration (covering 24 cells, 48 cells, 24 cells in series, respectively), and scenarios example table.	45
4.10	96 cell module, 12 rows x 8 columns, 3 bypass diodes in a [2 4 2] configuration (covering 24 cells, 48 cells, 24 cells in series, respectively), with reshaped scenarios and vertical symmetry impact illustrated.	45
4.11	Examples showing equal vs equivalent sections in 96 cell module (12 rows x 8 columns, 3 bypass diodes in a [2 4 2] configuration).	47
4.12	Example showing further symmetry of module taken into account to determine all duplicate scenarios.	48
4.13	Probability distributions of shading of PV module for various numbers of irradiance levels <i>i</i> . Figure taken from [28].	52
4.14	Shading Tolerability Percentage (ST%) as a function of N_s (number of cells in series in the PV module) for different PV module and bypass configurations (BD represents number of bypass diodes).	55
4.15	Visualization of ST for each module configuration (Module shaded area vs. operating power as a function of module nominal power).	59
4.16	60 cell module shown with 3 and 6 bypass diodes, with splitting configuration illustrated.	61
4.17	Forward voltage-current characteristic of JAMECO 80SQ Series Schottky diode [94]	63
4.18	72 cell module with 4x3 and 3x4 splitting configurations illustrated.	64
5.1	120 half-cell butterfly module, with series-parallel-series schematic shown. Figure taken from [95].	68
5.2	Plots showing two cells in parallel and methods of calculating V_{oc}	69
5.3	IV characteristic of a representative half-cell butterfly module (JA Solar JAM60S10 Half-Cell Module) with one substring partially shaded. Shaded cells (grey) receive irradiance of $100 W/m^2$, while unshaded cells (blue) receive irradiance of $1000 W/m^2$	70
5.4	IV characteristic of a representative half-cell butterfly module (JA Solar JAM60S10 Half-Cell Module) with two substrings (connected in parallel) partially shaded. Shaded cells (grey) receive irradiance of $100 W/m^2$, while unshaded cells (blue) receive irradiance of $1000 W/m^2$	71
5.5	72 cell conventional module layout vs 144 half-cell butterfly module layout.	72
5.6	72 cell conventional module substrings vs 144 half-cell butterfly module substrings.	73
5.7	All possible shading scenarios shown separately for top and bottom sections of the half cell butterfly module.	73
5.8	Example showing vertical symmetry of each of the top and bottom sections of the half-cell module for one scenario.	74
5.9	Putting the scenarios of the top and bottom parts of the module back together.	75
5.10	Example scenarios showing consideration of symmetry of parallel substring pairs in half-cell butterfly module.	76
5.11	Example scenarios showing consideration of symmetry of top and bottom parts in half-cell butterfly module.	76
5.12	Visualization of ST for two configurations of half-cell butterfly modules (Module shaded area vs. operating power as a function of module nominal power).	78
A.1	IV and PV plots showing calculated values in comparison to measured values for the Canadian Solar CS6 230P module under partial shading conditions, with errors at MPP. Shading case G200_Oratio_0strings.	89

A.20 IV and PV plots showing calculated values in comparison to measured values for the Canadian Solar CS6 230P module under partial shading conditions, with errors at MPP. Shading case G1000_08ratio_1strings.	99
A.21 IV and PV plots showing calculated values in comparison to measured values for the Canadian Solar CS6 230P module under partial shading conditions, with errors at MPP. Shading case G1000_08ratio_2strings.	99

List of Tables

3.1	Datasheet parameters for Shell S36 (multi-crystalline), Shell SP-70 (mono-crystalline), and Shell ST40 (thin-film) modules used for cross-verification purposes [62].	25
3.2	Datasheet parameters for BenQ SunForte PM096B00 module.	28
3.3	Datasheet parameters for Canadian Solar CS6 230P module [87].	30
4.1	Reduction in simulation times when taking duplicate scenarios due to symmetry into account for various module configurations.	49
4.2	Shading tolerability parameter results.	54
4.3	Pearson correlation coefficients when comparing K_V with ST% for each module configuration.	57
4.4	ST calculation for same PV module - modelling impact of T_{NOCT}	58
4.5	ST calculation for two 60 cell modules with 6 bypass diodes vs with 3 bypass diodes.	60
4.6	ST calculation for same PV module - modelling impact of type of bypass diode (p-n vs Schottky).	63
4.7	ST calculation for same 72 cell modules with different splitting configurations.	64
5.1	ST calculation for two half-cell butterfly PV modules.	77

Introduction

The rise of the uptake of renewable energy in order to combat climate change has resulted in an exponential growth of photovoltaic (PV) installations worldwide. Between 2015 and 2020 alone there was an increase of over 200% in PV installations worldwide, as can be seen in figure 1.1 [1]. This upsurge has also resulted in an increase in PV systems being installed in urban areas, which by nature are more prone to shading. In order to be able to effectively utilize PV systems and get the best performance out of them, it is important to be able to understand and classify the performance of PV modules under shading conditions.

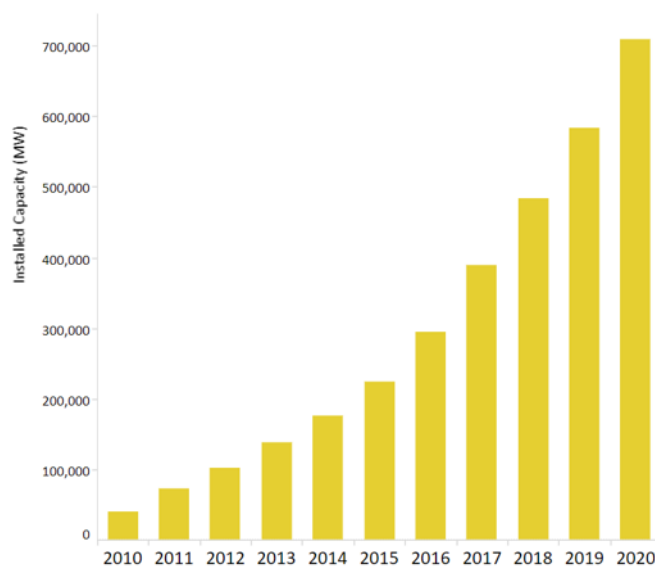


Figure 1.1: IRENA data showing solar PV installed capacity worldwide by year, from 2010 to 2020. Figure taken from [1].

1.1. Impact of shading on PV modules

There are a number of aspects that have the potential to affect the performance of a photovoltaic (PV) module. Irradiation, temperature, degradation and aging of cells are some of the factors that have an impact on the output power of a photovoltaic module [2, 3, 4, 5, 6]. Lower values of irradiance, for example, directly lead to reduced operating power of PV modules. One of the factors that can have a major negative impact on the performance of a PV module is partial shading or non homogeneous irradiation on the surface of the module.

Partial shading/non homogeneous irradiation can occur due to a number of reasons. Urban areas, by nature are more prone to partial shading – specifically static shading that occurs as a result of nearby

structures such as trees, buildings, chimneys, antenna towers, power lines, poles, etc. [7, 8, 9, 10]. Dynamic shading, unpredictable shading, and/or soiling is also always a potential issue, which could happen due to passing clouds, leaves, dust, dirt, snow, or bird droppings [2, 9, 11, 12]. Even in large PV plants, which usually do not deal with the same kind of static shading as detailed above for residential areas, there could be shadows cast by neighbouring modules, and dynamic shading could also be an issue [2, 8].

Partial shading is a major source of mismatch losses, which can drastically reduce the energy yield of a PV system [12, 9, 8, 3, 13, 14, 15, 16, 10]. Generally, all or part of the solar cells in a PV module are connected in series. When cells are connected in series, all of them carry the same current. Therefore, when some of the cells are shaded, this leads to a reduction of output current in those cells. This in turn limits the current in the other cells connected in series, reducing the amount of power those cells can produce. In this way, the total output of the solar module is reduced. [17, 10].

Moreover, when the current generated by the unshaded cells flows through a shaded cell, the cell would become reverse biased and begin operating at negative voltages. Thereby it would be dissipating power, and leading to a further reduction in output power of the PV module. What is of more concern is that this sort of power dissipation can lead to rising temperatures in the shaded cells resulting in what is known as hot spots, and can lead to local defects, and permanent damage and degradation of PV modules. [2, 7, 8, 9, 18, 14, 19, 20, 6].

One of the solutions proposed for the above problem is the inclusion of bypass diodes within the PV module [10, 20]. However, it has been shown that the presence of bypass diodes does not necessarily completely eliminate the occurrence of hot spots [21, 22]. Additionally when bypass diodes are activated during operation, this leads to multiple peaks in the resulting power curves. An example of this is illustrated in figure 1.2. This diminishes the accuracy of maximum power point trackers (MPPTs) to find the global MPP. This is because they often end up finding and operating at a local peak (local MPP), which can cause substantial energy losses. [23, 24, 25, 20, 6, 4, 26, 27, 17].

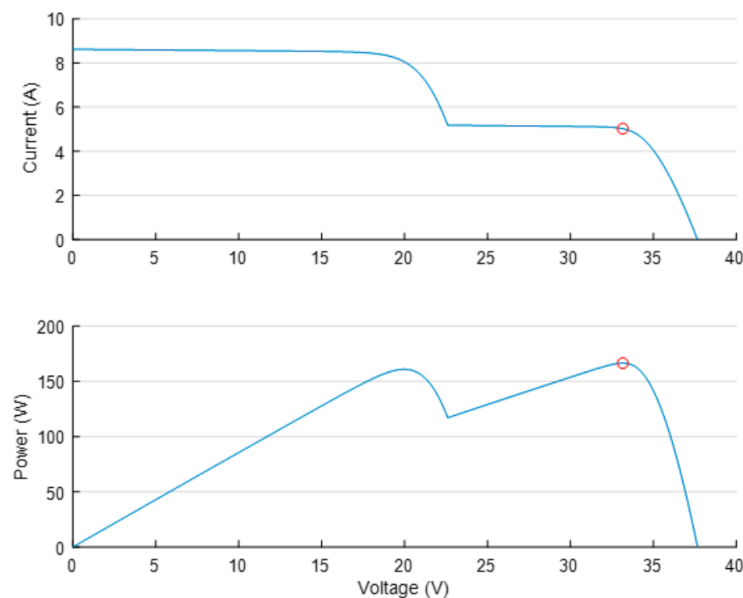


Figure 1.2: Current-Voltage (IV) and Power-Voltage (PV) curves showing impact of a shaded module with one bypass diode activated. Figure taken from [10].

It can be seen from figure 1.2 that the global MPP is the point highlighted in red, as that has the higher power value out of the two peaks. However, a maximum power point tracker may identify the other peak value (the local MPP) as the overall maximum power point by mistake, based on the strate-

gies used in the algorithm.

Partial shading can impact the performance ratio (PR) of a PV module (which is a measure of the actual energy output of a PV module when compared to its theoretical energy output) by up to 25%, and has been shown to result in a more than 10-20% decrease in power output in residential applications [28, 7]. Given these reasons, the proper selection of PV modules is of paramount importance in the design of PV systems, which can be made even more challenging when the location is prone to shading.

1.2. Shading Tolerability parameter (ST)

Currently on PV Module datasheets, the ability of the module to oppose shading effects is generally expressed qualitatively, with phrases such as 'better shading response' [29], 'outstanding low light behaviour' [30], 'shade tolerant' [31], etc. However, such general qualitative statements can make it difficult for a PV system designer to compare between the modules when trying to select the most suitable module for a specific location. Therefore a group of researchers suggested to have a quantified numerical parameter for shading tolerability which can be used to rank, compare and choose the optimum module for a certain location in terms of cloudiness or shading [28]. The defining of such a parameter was initiated by Ziar et al. in 2017 [28]. Experiments done have shown that accurate selection of a PV module based on shading tolerability can improve the resulting performance ratio by over 20%, underscoring the benefits of such a parameter [28]. In this section, the theory behind the calculation of the shading tolerability parameter (ST) will be briefly explained.

Ziar et al. introduced ST as a numerical parameter that can be measured for PV modules, and which reflects the ability of a PV module to withstand shading [28]. This was done through a probabilistic approach as follows.

When dealing with something random, like shading, probability laws can give the right tools to work with and analyse such data [32]. An important step in probability theory is to create and look at the sample space of such a random trial, which should include all possible events that could occur in this trial [32]. Here we can see the first significant hurdle. In the case of shading of a photovoltaic module, there are an infinite number of possibilities with respect to shading profiles. This in turn implies an infinitely large sample space. To work with the shading scenarios more effectively, Ziar et al. made two main assumptions in order to simplify the process [28]:

1. Irradiation across the surface of a PV cell (within a PV module) is homogeneous, and incident irradiance can be any value between 0 and 1000 W/m^2 , with every value having an equal probability of occurring.
2. The probability of different cells in a module being shaded is also equal and does not depend on the location of the cells in the module (or the location of the PV module in an array).

Using the above assumptions, the number of all possible shading profiles for a PV module can be calculated based on the number of cells in the modules and the number of irradiance levels being considered. Considering the number of cells to be c and the possible irradiance levels to be i , the total number of shading profiles that could occur would be i^c . When considering the possibility of any unique shading profile occurring, it should be kept in mind that there are infinite levels of irradiance between the limits of 0 and 1000 W/m^2 that have been set. Therefore, the probability of each unique shading profile occurring can be represented by $\lim_{i \rightarrow \infty} (1/i^c)$. While the number of possibilities of shading scenarios is still infinite, the above assumptions and calculations have allowed for the sample space to be established clearly [28].

Now to move on to the definition of the shading tolerability parameter (ST). ST is defined as a "mathematical expectation of power production" of a PV module under shading [28]. For a random variable x which has a $p(x)$ chance of occurring, its expected value $E(x)$ can be calculated as [33]:

$$E(x) = \sum_{k=1}^{\infty} x_k p(x_k) \quad (1.1)$$

Applying the same concept to shading tolerability, ST is therefore defined as [28]:

$$ST_{(i,c)} = \frac{1}{P_{mod_{mpp}}} \sum_{k=1}^{k=i^c} P_k \left(\frac{1}{i^c} \right) \quad (1.2)$$

where:

- $ST_{(i,c)}$: shading tolerability
- c : total number of cells the PV module consists of
- i : number of irradiance levels
- P_k : maximum power at each shading profile [W]
- $P_{mod_{mpp}}$: maximum power of the PV module (at STC) [W]

In equation 1.2, the utilization of division by $P_{mod_{mpp}}$ acts as a way to normalize the calculated value and essentially allows PV modules having different nominal powers to be compared effectively. In this way, shading tolerability (ST) has been defined as a numerical parameter, where PV modules which have higher values using equation 1.2 should have superior performance under shading conditions.

1.3. Literature review

In this section, shading tolerability and its calculation in literature will be discussed.

Ziar et al

Ziar et al. performed the calculation of shading tolerability through experimental means for a number of modules [28]. In the previous section, it was explained how the numerical calculation of ST is performed. When considering equation 1.2, it is clear that the value of ST cannot be determined experimentally when using this equation as is, since, as mentioned before, the number of potential irradiance levels between 0 and 1000 W/m^2 tends to infinity.

In order to be able to experimentally measure shading tolerability, the following proposal was set by Ziar et al: while equation 1.2 cannot be practically measured for an infinite number of irradiance levels ($i \rightarrow \infty$), it can however be done for a specific, small number of irradiance levels, such as 2 for example ($i = 2$). This method can be used to calculate ST if it can be shown that a module which gives a higher ST under the conditions of $i = 2$ also gives a higher ST under the conditions of $i \rightarrow \infty$. This was proved as follows.

Ziar et al. calculated the general equation for ST of a PV module through mathematical permutation [28]:

$$ST_{(i,c)} = \left(\frac{m}{c} \right) \left(\frac{1}{i^n} \right) \left[\sum_{k=1}^{k=j} \binom{n}{j} k + \sum_{a=1}^{a=j-1} n \binom{j-a}{j} \sum_{b=1}^{b=n-1} \binom{n}{b} a^{n-b} \right] \quad (1.3)$$

where $c = n \cdot m$, and n represents the number of PV cells connected in series, while m represents the number of PV cell strings the module consists of; and where $j = i - 1$.

For the case of $ST_{(i=2,c)}$, $i = 2$ can be substituted into equation 1.3, and the result is:

$$ST_{(i=2,c)} = \left(\frac{1}{2^n} \right) \quad (1.4)$$

Using both equation 1.3 and equation 1.4, one can derive the following:
Consider two PV modules: Module 1 and Module 2

- Given $ST_{(i=2,c)}$ is greater for Module 1 when compared to Module 2

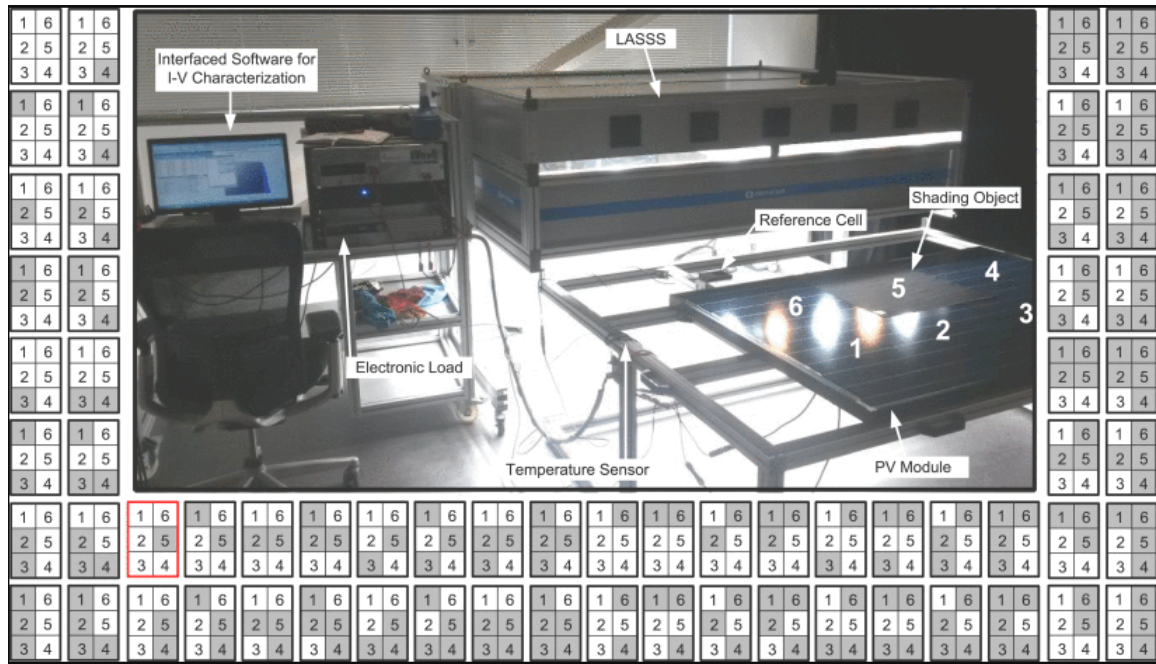


Figure 1.3: Indoor experimental setup for shading tolerability measurements. Figure taken from [28].

- This implies, based on the above equations, that $n_1 < n_2$
- If $n_1 < n_2$, this in turn gives a greater value for $ST_{(i \rightarrow \infty, c)}$ for Module 1 than for Module 2

Essentially

$$ST_{(i=2, c)}^{(Module_1)} > ST_{(i=2, c)}^{(Module_2)} \Rightarrow ST_{(i \rightarrow \infty, c)}^{(Module_1)} > ST_{(i \rightarrow \infty, c)}^{(Module_2)} \quad (1.5)$$

proving that it is valid to measure ST for $i = 2$ and use it instead of ST for $i \rightarrow \infty$ [28].

Ziar et al. utilized the above implication, and experimentally measured the value of $ST_{(i=2, c)}$ for a specific number of commercial PV modules through indoor laboratory testing. For the experiments, the PV module was chosen to be split into 6 geometrically equal sections. Since the smallest possible area of the PV module that can receive a different homogeneous irradiance level is one section, this gives c equal to the number of sections the PV module is split into; in this case $c = 6$. This gives the number of possible shading scenarios to be $2^6 = 64$.

The PV modules are chosen to be split into 6 sections specifically since, as the value of c increases, the number of possible shading scenarios (which is equal to 2^c as shown earlier), and therefore the number of experimental tests that need to be carried out (as well as the time required to carry them out), increases exponentially. A larger number of sections therefore would require a significantly large amount of time with respect to experimental measurements, and therefore would reduce the possibility for industrial application of ST [28].

Apart from the relatively lower time for measurements, another advantage given for choosing $c = 6$ is that PV modules can then be easily divided into 3 times 2 sections (as 6 is an even number) [28].

The experiments were carried out for 11 modules, with all possible 64 shading profiles being applied to each module. The sections were either shaded or unshaded, with the unshaded sections having an irradiance of 1000 W/m^2 , and the shaded sections being exposed to an incident irradiance of 250 W/m^2 (the reasoning being that due to diffuse irradiation, shaded conditions in real life applications still have a certain amount of incident irradiance). The applied irradiance and measurements were done using an EternalSun large area steady state solar AAA-class simulator (AM 1.5), with the I-V characteristics being measured for each scenario. Ambient temperature was kept constant at 25°C .

The setup can be seen in figure 1.3. The total amount of time taken for all measurements was around 63.11 hours coming to an average of 5.73 hours of measurement time for each module (which includes the time required for data saving and exporting), which is a substantial amount of time [28].

Mishra et al

Mishra et al. expanded upon the research done by Ziar et al. in [28], and a main aim was to formulate a correlation between ST and ambient temperature, to check whether ST is an innate property of a PV module [34]. Module temperature was modeled using the NOCT model. The effect of temperature in ST was modeled analytically using a combination of the NOCT model as well as γ , the temperature coefficient for power. ST was experimentally measured for four different PV modules at three different ambient temperatures (25°C, 30°C, and 35°C). The experimental setup was the same as that used by Ziar et al. and shown in figure 1.3, with 6 sections being considered again ($c = 6$, giving 64 shading scenarios for each module at each ambient temperature value). The same conditions were applied with respect to irradiance values of shaded and unshaded sections, and the output power at each shading profile for each value of ambient temperature was noted. The results for the tested modules showed an average measured change in ST value with respect to ambient temperature being 0.17%/°C, showing that the shading tolerability parameter of a PV module can be considered practically independent from the ambient temperature, and therefore ST can be considered an intrinsic property of a PV module. [34]

The experimental time for each module (for each ambient temperature) in this case was around 4.18 hours, showing that still a significant amount of time was required for experimental analysis of ST in this case [35].

Klassen et al

Klassen et al. have also worked in the concept of the shading tolerability parameter [36]. They examined and compared the performance of four different PV module layouts (conventional, butterfly, shingle string, shingle matrix) under partial shading conditions, through simulations using LTSpice. In this work, Monte Carlo shading scenarios are utilized, considering both rectangular and random shading. A similar method to calculating ST is used to calculate the "average normalized power for partial shading \bar{P}_{ps} ", which is the parameter used in this work to compare the shading tolerability of different types of modules [36].

In the simulations, a set of 30 cells connected in different ways with respect to the four different configurations is characterized. The current-voltage (IV) characteristics of each module are given by LTSpice. A two diode model is used to get the corresponding parameters for shingle solar cells (by fitting with measured data [37]), which are then scaled to half-cut and full-sized solar cells to be used as inputs for the simulations [36].

The shading scenarios are generated randomly, and the smallest unit of shading is considered one pixel. The scenarios are created for a shingle solar cell, or for the size of a shingle solar cell (the shading scenarios are created for the shingle layouts and then transferred to the other types of layouts), which is split into 25x25 pixels. As mentioned earlier, the scenarios consider both rectangular and random shading, with the shaded area of the module, A_{sh} , being the main independent parameter being changed. One advantage of this model is the detail within the shading scenarios, with the smallest unit being a pixel ($(\frac{1}{625})^{th}$ of the area of a shingle solar cell), and with multiple irradiance levels between 0 and 1000 W/m^2 being considered. However, this work also deals with a large number of simulations which could be quite time consuming, and only presents results for one representative module per configuration type considered.

1.4. Thesis aim and research objectives

As shown, there has been research done in the past on evaluating shading tolerability of certain PV modules. This has been either done through experimental means (for a specific number of PV Modules) or through simulation of representative models for specific PV configurations. However, both of these processes were quite time consuming and were only able to calculate ST for only a certain number of modules. Additionally, the experimental process required the physical modules themselves.

Therefore, the objective of this thesis is to develop a MATLAB based tool to calculate shading tolerability as a parameter for PV modules. This work aims to build upon the work already done by Ziar et al [28]. The goal is to have a tool that can relatively quickly calculate shading tolerability of a PV module given specific inputs that are easily available in a datasheet (such as number of cells; characteristic values of current, voltage, and power; etc.). In this way, a database can be created of ST values for a large number of photovoltaic modules.

In order to achieve this, the following points are the main objectives of this project:

1. Develop a MATLAB based code to simulate the current voltage (IV) characteristics of PV modules under different conditions
2. Simulate and study different solar modules' performance under various shading conditions
3. Design a MATLAB based calculator for shading tolerability parameter (ST)
4. Calculate ST for a number of PV modules and analyse results to check for possible correlations

1.5. Thesis outline

The overview of the layout of this thesis can be found below.

Chapter 2 - IV Curve Generator: In Chapter 2, the theory behind the development of the MATLAB based code to generate current, voltage, and power data for PV modules, under different irradiation and temperature conditions will be discussed.

Chapter 3 - Validation of Model: Chapter 3 will detail the validation process of the model developed in Chapter 2, providing results and analysis.

Chapter 4 - Shading Tolerability Calculator: In Chapter 4, the development of the shading tolerability (ST) calculator based on the model created will be explained. A discussion on defining and working with the shading scenarios, and how they are incorporated into the calculator is also included in this chapter. An analysis of the calculated ST results will be presented.

Chapter 5 - Half-Cell Butterfly Module Case Study: In Chapter 5, a case study will be carried out to determine the shading tolerability of two half-cell butterfly modules, based on the work done in this thesis.

Chapter 6 - Conclusions/Future Work: Finally, in Chapter 6, a summary of the results of the research objectives, and the conclusions derived, as well as recommendations for future work, will be presented.

2

IV Curve Generator

The final objective of this thesis is to create a 'calculator' that can determine the parameter ST (shading tolerability) for a PV module. In order to do this, it is important to be able to evaluate the performance of the PV module at various shading conditions. This requires an understanding of the current and voltage (and consequently power) characteristics of the PV module under different conditions. Therefore, in this chapter the development of a MATLAB model to generate the current-voltage (IV) characteristic of a PV module will be discussed and presented.

In section 2.1, a brief introduction to IV curves and the important points on them is given. Section 2.2 discusses the parameter extraction models used to determine IV characteristics that exist in literature. Section 2.3 presents the two diode model used in this work. The implementation of the model at a cell level and consequently at a module level is discussed in sections 2.4 and 2.5 respectively. Finally the modelling of the operation of bypass diodes within this model is presented in section 2.6.

2.1. IV Curve

First, the IV characteristic of a PV cell along with its important points will be described and explained. The IV curve represents the current and voltage characteristics of a PV module. A representative IV curve can be seen in figure 2.1 as an example.

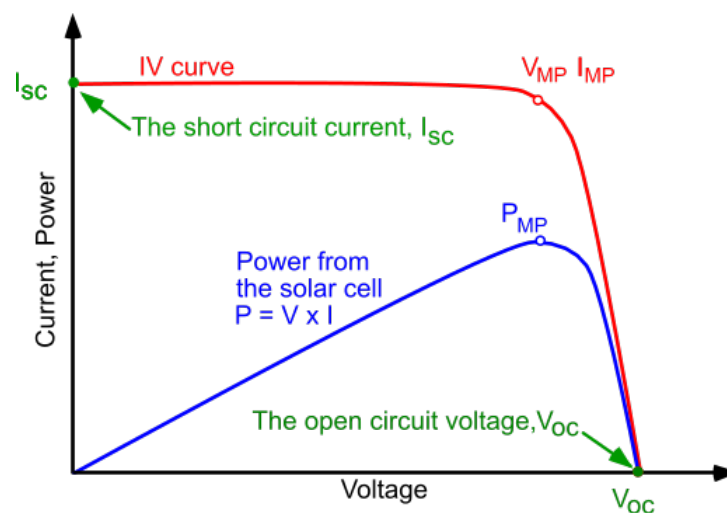


Figure 2.1: Representative current-voltage (IV) curve (and corresponding power-voltage (PV) curve) of a solar cell (figure taken from [38]).

The short circuit point is the point at which the IV curve intersects the y-axis. This corresponds to the values of $V = 0V$ and $I = I_{sc}$, which is called the short-circuit current. The short-circuit current, I_{sc} ,

is the current that can be measured in the external circuit of a solar cell when its electrodes are short circuited. I_{sc} is dependent on the irradiance that is incident on the cell (and therefore consequently also the area of the cell), as well as other intrinsic properties of the solar cell.

The open circuit point is the point at which the IV curve intersects the x-axis. It corresponds to the values of $I = 0A$ and $V = V_{oc}$, also known as the open circuit voltage. It is the maximum possible voltage of a solar cell (and can also be defined as the voltage when the current flowing through the external circuit is zero).

The maximum power point, as the name suggests, is the point at which the maximum power of the PV module is reached. The power at this point, (represented by P_{MP} in figure 2.1) is also known as the operating power of a PV module (or nominal power). This is essentially the power a PV module provides under the given conditions. This point varies with external conditions such as irradiance and temperature (as do current and voltage). V_{MP} and I_{MP} shown in figure 2.1 are the voltage and current values at the maximum power point, respectively.

Two more important factors are the series and parallel (shunt) resistances, R_s and R_p respectively, which are related to various losses in a solar cell. With respect to the IV curve specifically, R_s is related to the slope of the IV curve near the open-circuit point, while R_{sh} is related to the slope of the IV curve near the short-circuit point.

As mentioned, irradiance and temperature have an impact on the IV characteristics of a PV cell (and therefore PV module), and consequently on its performance. Generally as irradiance on a PV cell decreases (while temperature of the cell remains constant), the I_{sc} decreases proportionally, while the V_{oc} also slightly decreases. As temperature increases (while irradiance is kept the same), mainly the V_{oc} mainly decreases, while the I_{sc} increases slightly. An example of this can be seen in figure 2.2, taken from a Titan PV module datasheet [39].

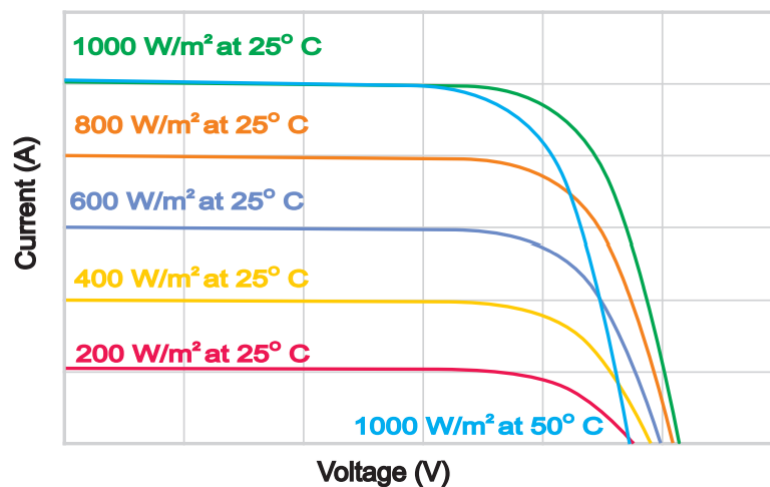


Figure 2.2: Representative current-voltage (IV) curves showing impacts of irradiance and temperature of a Topsola PV module [39].

2.2. Parameter Extraction Models

When trying to determine the IV characteristics of a PV module, there are two main models that are used in literature: the one diode model and the two diode model. The equivalent circuits corresponding to each model can be seen in figures 2.3 and 2.4 respectively, and the corresponding characteristic IV equations in equations 2.1 and 2.2 respectively. It can be seen that, as the name implies, the two diode model utilizes a second diode in its equivalent circuit, which leads to two additional parameters corresponding to that diode in the model when compared to the one diode model.

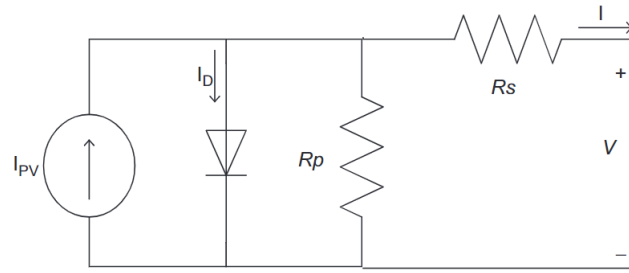


Figure 2.3: One Diode Model Equivalent Circuit (figure taken from [40]).

One Diode Model Characteristic IV Equation [40]:

$$I = I_{PV} - I_o \left[\exp\left(\frac{V + IR_s}{aV_T}\right) - 1 \right] - \left(\frac{V + IR_s}{R_p}\right) \quad (2.1)$$

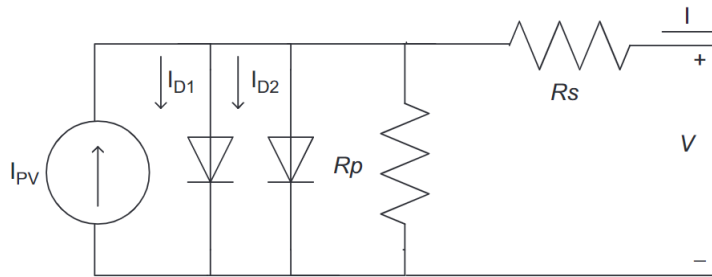


Figure 2.4: Two Diode Model Equivalent Circuit (figure taken from [40]).

Two Diode Model Characteristic IV Equation [40]:

$$I = I_{PV} - I_{o1} \left[\exp\left(\frac{V + IR_s}{a_1 V_{T1}}\right) - 1 \right] - I_{o2} \left[\exp\left(\frac{V + IR_s}{a_2 V_{T2}}\right) - 1 \right] - \left(\frac{V + IR_s}{R_p}\right) \quad (2.2)$$

where:

I is the output current

V is the output voltage

I_{PV} is the photogenerated current (current generated in the solar cells due to the incident light on the surface of the cells)

I_{o1}/I_{o1} and I_{o2} represent the reverse saturation currents of diode 1 and diode 2 in the models respectively

a/a_1 and a_2 refer to the diode ideality constants of diode 1 and diode 2 in the models respectively

V_{T1} and V_{T2} represent the thermal voltages of the respective diodes

- where the thermal voltage $V_T = \frac{N_s k_B T}{q}$
- with N_s being the number of cells connected in series, k_B being the Boltzmann constant ($1.38 \cdot 10^{-23} J/K$), q being the electron charge ($1.60 \cdot 10^{-19} C$), and T representing the temperature of the module

R_s is the series resistance

R_p is the parallel (or shunt) resistance

The one diode model is used more commonly in literature, as, due to the reduced number of parameters, it is slightly less complex to solve [41, 27]. However, it has been shown that the two diode model is more accurate, especially at lower irradiances [42, 43, 44, 45, 46]. Since the main aspect

of this work is to characterize the performance of PV modules under different shading conditions, the accuracy at lower irradiances is quite important. Therefore, in this work a two diode model was used to determine the IV characteristics of a PV module.

Literature methods

There are many methods used for parameter extraction for the one diode and two diode models in literature.

One of the more non conventional methods to solve for the parameters that has been used in recent times is the utilization of metaheuristic algorithms, which are optimization algorithms based on artificial intelligence. Some examples are a bird mating optimizer based approach [41], harmony search based algorithm [47], flower pollination algorithm [48], particle swarm optimization [49, 50], [51]), and genetic algorithm [52, 53]). However such algorithms can be quite complex to implement.

Out of the more traditional methods, one of the commonly used methods is using known points on the IV characteristic curve (such as short circuit point, open circuit point, and maximum power point for example) to develop a system of equations with unknowns to be solved simultaneously [54, 42]. In order to reduce the number of unknowns that need to be solved for, simplified approaches have been implemented where series and/or shunt resistances have been neglected in the solving of the model [55, 56, 57]. This is done to reduce time and complexity, however this can come at the cost of accuracy. Some of the common methods of solving the system of unknown equations is through methods and functions involving Lambert W function, Newton Raphson, iteration and/or explicit methods [58, 16, 59, 60, 61, 43]. These are some of the more common and straightforward approaches, however, depending on the complexity of the set of unknowns and respective equations, some of these methods can take a long time for simulation/convergence. One of the main aims of this work is to have a model with comparatively low simulation times, in order to be able to relatively quickly calculate the shading tolerability of a number of PV modules, which was taken into account when deciding the method of solving for the IV characteristic as explained in the next section.

2.3. Two Diode Model

The model this work has taken as main reference is the model developed by Ishaque et al. which utilizes a two diode model approach for parameter extraction [62].

The two diode model has seven unknown parameters which need to be determined/extracted: I_{PV} , I_{o1} , I_{o2} , R_s , R_p , a_1 , and a_2 . The model by Ishaque et al. makes certain simplifications in order to reduce the complexity and simulation time that would be required to solve for seven unknown parameters. These simplifications are detailed below.

Firstly, I_{PV} is calculated through an explicit equation given in literature [62, 63]:

$$I_{PV} = (I_{PV,STC} + K_I \Delta T) \frac{G}{G_{STC}} \quad (2.3)$$

$$I_{PV,STC} = I_{sc,STC}$$

where

$I_{PV,STC}$ is the photogenerated (light generated) current at STC (and is considered equal to short circuit current at STC, $I_{sc,STC}$)

K_I is the temperature coefficient of the short circuit current

ΔT is the difference in the temperature of the module/cell with respect to the temperature at STC, which is $25^\circ C$, or $298.15 K$ ($\Delta T = T - T_{STC}$)

G is the incident irradiance on the module/cell

G_{STC} is the value of irradiance at STC, which is $1000 W/m^2$

The saturation currents I_{o1} and I_{o2} are also calculated through explicit means. An explicit equation for the saturation current I_o in the one diode model has been developed in literature [64]:

$$I_o = \frac{(I_{sc,STC} + K_I \Delta T)}{\exp[(V_{oc,STC} + K_V \Delta T)/aV_T] - 1} \quad (2.4)$$

where

$V_{oc,STC}$ is the open circuit voltage at STC, $I_{sc,STC}$)

K_V is the temperature coefficient of the open circuit voltage

Ishaque et al. adapt this explicit equation to make one simplified explicit equation for both the reverse saturation currents [62]:

$$I_{o1} = I_{o2} = I_o = \frac{(I_{sc,STC} + K_I \Delta T)}{\exp[(V_{oc,STC} + K_V \Delta T)/(\frac{a_1+a_2}{p} V_T)] - 1} \quad (2.5)$$

where $p = a_1 + a_2$.

It is important to note that this is an assumed simplification for the purposes of more efficient calculation. Having an explicit equation for the reverse saturation current(s) not only simplifies the calculation in this case, but also consequently significantly reduces the computation time required when compared to other methods used to solve for the reverse saturation currents, such as iteration for example [62].

Next, the diode ideality factors a_1 and a_2 are considered, which represent the diffusion and recombination current components respectively. Based on Shockley's diffusion theory, a_1 can be taken to be equal to one [62, 65, 66]. The value of a_2 is now to be determined. In Ishaque et al.'s work, through carrying out numerous simulations, it was found that the best fit between the modeled IV curve and the actual IV curve was observed when a_2 was greater than or equal to 1.2. Therefore the value of a_2 can be arbitrarily chosen to be a value greater than or equal to 1.2 (and/or consequently p can be chosen to be a value greater than or equal to 2.2, since $a_1 = 1$) [62].

Taking the above definitions and assumptions into account, the characteristic IV equation can be written in the form [62]:

$$I = I_{PV} - I_o \left[\exp\left(\frac{V + IR_s}{V_T}\right) + \exp\left(\frac{V + IR_s}{(p-1)V_T}\right) - 2 \right] - \left(\frac{V + IR_s}{R_p}\right) \quad (2.6)$$

Now, out of the seven unknown parameters to be determined mentioned earlier, only R_s and R_p are remaining. The modified characteristic IV equation at maximum power point (MPP) conditions can be written as:

$$I_{mpp} = I_{PV} - I_o \left[\exp\left(\frac{V_{mpp} + I_{mpp}R_s}{V_T}\right) + \exp\left(\frac{V_{mpp} + I_{mpp}R_s}{(p-1)V_T}\right) - 2 \right] - \left(\frac{V_{mpp} + I_{mpp}R_s}{R_p}\right) \quad (2.7)$$

It follows then, that R_p can be written in terms of R_s as follows:

$$R_p = \frac{V_{mpp} + I_{mpp}R_s}{I_{PV} - I_o \left[\exp\left(\frac{V_{mpp} + I_{mpp}R_s}{V_T}\right) + \exp\left(\frac{V_{mpp} + I_{mpp}R_s}{(p-1)V_T}\right) - 2 \right] - \frac{P_{mpp,E}}{V_{mpp}}} \quad (2.8)$$

In the above equation, the only two unknowns are R_p and R_s ; given the value of one, the other can be calculated. Therefore, R_p and R_s are proposed to be calculated through a simple iteration method,

using a power matching method. Essentially, at each iteration, the values of R_p and R_s at that iteration step are used along with the remaining parameters to calculate the value of the maximum power point, $P_{mpp,C}$. This value is then compared with the actual (experimental) value of the maximum power point $P_{mpp,E}$ obtained from the manufacturer's datasheet of the PV module. The iteration process continues until the margin of error between the actual and calculated values lie within a certain range [62]. This initial value of R_s for the iteration is chosen to be 0, while for R_p , it is given by the following equation [62]:

$$R_{po} = \left(\frac{V_{mpp}}{I_{sc} - I_{mpp}} \right) - \left(\frac{V_{oc} - V_{mpp}}{I_{mpp}} \right) \quad (2.9)$$

Therefore, now all the unknown parameters in the model have been determined. Since they are all determined either explicitly or otherwise through a simple iterative method, the speed of this simulation model is quite fast. This is a significant advantage for the purposes of this work, since one of the factors to optimize was the amount of time taken.

2.4. Cell Level

In this work, the two diode model was implemented in MATLAB. There were a few modifications made to the above model as part of the work done in this thesis. The first modification that will be discussed in this section is the adjustment to the equations to calculate the IV characteristics at a cell level instead of a module level. The main way this is done is to just neglect the N_s term in the thermal voltage V_T which is included in the characteristic IV equation. Essentially the N_s term, which corresponds to the number of cells connected in series in the module, is set to the value of one, to obtain the IV characteristics at a cell level. The second modification is the implementation of the dependence of the parameters on irradiance and temperature, specifically for R_s and R_p . This is done by implementing irradiance and temperature dependencies, based on models in literature, to the values obtained at STC.

2.4.1. STC

The first implementation of this model was at a cell level at standard test conditions (1000 W/m^2 , AM 1.5, 25°C).

The datasheet parameters required as inputs to the model at this point are the variable p as defined earlier, as well as the values of V_{oc} , I_{sc} , I_{mpp} , V_{mpp} , P_{mpp} at standard test conditions. All parameters mentioned, apart from p , can be found on the manufacturer's datasheet of the relevant module. Since we are calculating at a cell level, the datasheet parameters are scaled down to the parameters for a single cell to be used as inputs to the MATLAB function. The parameter p is chosen to be 2.5 (based on the option to arbitrarily choose it to be greater than or equal to 2.2 as defined earlier).

According to the process, I_{PV} and I_o were calculated at STC using the equations already defined. Then the iteration process for R_p and R_s was carried out until the calculated P_{mpp} lay within 0.1% of the given P_{mpp} from the datasheet. The IV characteristic equation was solved in MATLAB using the `fzero` function, which is a nonlinear root solving function [67]. The voltage points were defined in MATLAB within a certain range using the V_{oc} value from the datasheet as a reference. Then, along with the determined parameters, they were used with the `fzero` function in Matlab to solve for a set of datapoints for current, corresponding to each voltage point defined. In this way, a set of data points describing the IV characteristics at a cell level at STC was obtained.

2.4.2. NonSTC

The next step was to implement the ability for the calculation of IV characteristics at a cell level under non STC conditions. This is also where the next modification was made to the reference model.

In order to be able to determine the IV characteristics at non STC conditions, the dependencies of the parameters on irradiance and temperature have to be implemented. As can be seen from the

equations for I_{PV} and I_o , irradiance and temperature dependencies are already taken into account for these two parameters. However, for the R_s and R_p , it is not clear whether these dependencies are accounted for in the model provided by Ishaque et al. [62]. There are two possible options: either it is assumed that R_s and R_p are constant at their STC values even under different irradiance and temperature conditions, or, during the iteration process to calculate for R_s and R_p , the actual measured values of I, V, and P at the maximum power point at the relevant non STC irradiance and/or temperature conditions are required.

Both of these options are non-ideal. Using the actual measured values at the maximum power point under any possible irradiance and temperature condition is inefficient, as it would not only require time, but also the modules themselves (as well as a measurement setup). Since the main purpose of the model of this work is to be able to calculate the maximum power point value (P_{mpp}) to a certain degree of accuracy, it would also defeat the purpose of this code. Alternatively, keeping R_s and R_p constant is also not ideal. It has been shown in literature that R_s and R_p do have some temperature and irradiance dependencies. Therefore, the action carried out in this work is to apply temperature and irradiance dependencies to the two resistances based on models in literature. The equations can be found below [18]:

$$\frac{R_s}{R_{s,ref}} = \frac{T}{T_{ref}} \left(1 - 0.217 \ln \frac{G}{G_{ref}} \right) \quad (2.10)$$

$$\frac{R_p}{R_{p,ref}} = \frac{G_{ref}}{G} \quad (2.11)$$

where the 'ref' subscript in this case refer to their values at STC.

Therefore, the process is to first calculate the parameters at standard test conditions, using the method described in the previous section. The next step is then to apply the relative irradiance and temperature dependencies, based on their non STC values given, using equations 2.3, 2.5, 2.10, and 2.11.

Then the parameters calculated at the non STC conditions are used again in the IV characteristic equation, using the *fzero* function in Matlab to solve for the IV data points. In this way, the IV characteristic at a cell level at irradiance and temperature values different from STC can now be determined.

NOCT Model

An important point to note here is that the input of temperature to the code is the ambient temperature, as this is generally the information that is known. However, the equations utilize the cell/module temperature as mentioned earlier. In order to go from the ambient to the cell temperature, the NOCT model is used in this work.

NOCT stands for 'Nominal Operating Cell Temperature'. The NOCT model is a method used to calculate the cell temperature from the ambient temperature. This is required as the temperature of a PV module in operation is generally not equal to the ambient temperature, especially the longer it is in operation. This is due to the fact that the module generally heats up during operation, both due to the incident irradiance, as well as the heat produced during electrical activities. The NOCT value of a PV module is defined to be the actual temperature of the module under the conditions of 800 W/m^2 irradiance, 20°C ambient temperature, and a wind speed of 1 m/s , and the characteristic equation is as follows [68, 69]:

$$T_M = T_a + \frac{T_{NOCT} - 20^\circ}{800} G_M \quad (2.12)$$

where T_a is the ambient temperature, T_{NOCT} is the NOCT value of the PV module, and G_M is the incident irradiance on the module. The NOCT model is derived from measurements demonstrating that the incident irradiance on a module (G_M) and the difference in the ambient temperature and the resulting module temperature ($T_M - T_a$) have a relatively linear relationship [68].

The NOCT model is a fairly commonly used model to calculate the cell temperature. However, it does have certain drawbacks, due to its simplified nature. One is that it does not take into account the impact of wind speed. It also does not consider the influence of the mounting configuration of the PV module. Both these factors in reality would have an impact on the temperature of the module. Another shortcoming is that as this is a steady state model, it does not take into account the variation of the conditions and the temperature with time. Therefore for real life conditions, this simplified, steady-state model may not be the best method of accurately predicting the module temperature, and there are better, more comprehensive models out there [68].

However, for the purposes of this work, the drawbacks do not really have a big impact, as the wind speed and mounting configuration details are not relevant here. Since the objective of this project is to be able to calculate the 'shading tolerability' as a general characteristic parameter of a PV module for classification and comparison purposes, it does not require specific details about the location and mounting of the PV module. In order to compare models objectively, it would anyway be assumed these are the same across modules. Additionally, one of the requirements of this work is to have a model which only requires simple, easily obtainable inputs, such as parameters given on the datasheet of a PV module. Here, the NOCT model has a significant advantage, which is that the T_{NOCT} of a PV module can be easily found on its respective datasheet.

2.5. Module Level

Now that the model has been created at a cell level, the next step is to be able to generate the IV characteristics of at a module level. It will be considered that the cells in the module are all connected in series, which is one of the most common configurations in solar modules.

In a series connection of cells, the voltages of the cells add up, while the current running through all the cells is the same, and is determined by the cell in the string having the lowest current [68]. As an example, take the case of two solar cells connected in series, with one solar cell having V_{oc} value of 0.7 V and I_{sc} value of 8 A, and the other solar cell having a V_{oc} of 0.8 V and I_{sc} also of 8 A. The resulting V_{oc} and I_{sc} of the series connected pair of cells would be 1.5 V and 8 A respectively. Therefore, to find the resulting voltage of cells connected in series, the voltage values at each current point can simply be added up.

2.5.1. Homogeneous conditions

In the case of all the cells of the module being under the same conditions (irradiance, temperature, etc.), the conversion from cell to module is fairly straightforward. Under the same conditions, two identical cells will produce the same voltage and current characteristics. Therefore, in a series connection, it is possible to just then multiply the voltage characteristics by the number of cells in the module, while keeping the current characteristics the same, in order to obtain the voltage current characteristics of the PV module.

The other option, which gives the same result, is to add up the corresponding values of voltage for each cell connected in series, at each current point. In this case, since all the cells are at the same conditions, the current and voltage points for each cell are identical too (as explained in the previous paragraph). Therefore, in the model, this is a simple case of adding all voltage arrays of each cell to each other (adding each row of each voltage array to the corresponding row in each of the other arrays). The final result would be an array containing the voltage data points for the PV module at each current point (as calculated earlier).

So to determine the IV characteristics of a module at STC, or at homogeneous non STC conditions, either one of the above two methods can be used. The result of this would be a matrix of values of voltage of the module and corresponding current.

Homogeneous Non STC conditions indicate that, while the irradiance and/or temperature of the

module are different from standard test conditions, the respective irradiance and temperature are the same across the module. This once again means that all the cells in the module are under the same conditions, with respect to irradiance and temperature, although these are non STC values. Therefore, the method to obtain the voltage and data points of the PV module from the cell level data is the same.

An example of the output of this section can be seen in figure 2.5.

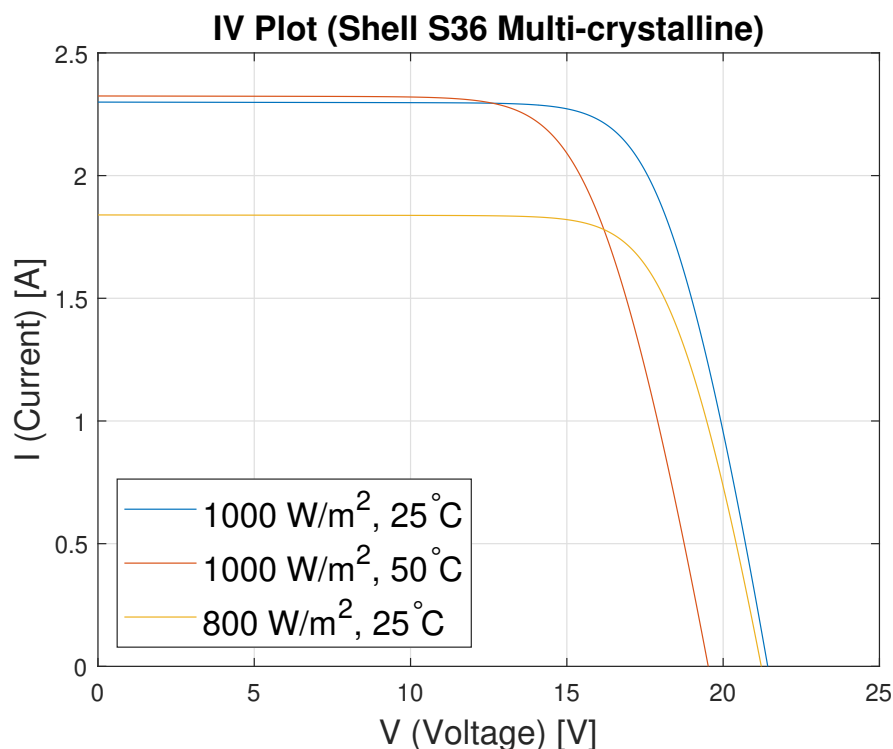


Figure 2.5: Plot showing IV characteristics at STC and Non STC conditions for a Shell S36 Multi-crystalline module.

Figure 2.5 shows the IV characteristics at a module level at STC conditions (blue curve), as well as the resulting IV characteristics at homogeneous non STC conditions across the module. The expected effects of temperature and irradiance can be seen with these curves. For example, the yellow and the blue curves represent the same temperature, but different irradiances. It can be seen that, the yellow curve which represents the lower irradiance has a much lower I_{sc} and a slightly lower V_{oc} than the blue, which is expected. Similarly, the blue and red curves compared, which both represent the same irradiance level but different temperatures. Here it can be seen that the red curve representing the higher temperature has a slightly higher I_{sc} and a lower V_{oc} than the blue, which is the expected behaviour.

2.5.2. Partial Shading

Partial shading is an example of non-homogeneous conditions that a PV module faces. Partial shading occurs when irradiance conditions on the module are different at different locations of the module.

Here, the calculation in the model becomes slightly more complex. The first step in the process stays the same, where the parameters for the two diode model, and subsequently the IV characteristics at a cell level, are calculated at STC conditions. The next step, as before, is to first apply the temperature and irradiance dependencies to the parameters of the two diode model (based on the temperature and irradiance of the cell), and then use the results to determine the IV characteristics at a cell level at the given non STC conditions. Earlier since all the cells in the module were at the same conditions, it was enough to perform this process for one cell, since the resulting data would be the same for all the cells. However, since this is no longer the case, it would be necessary to go through

the full process of calculating the non STC IV characteristics for each cell in the module.

Since running the *fzero* function so many times (as it needs to be run for each cell now) could significantly add to the simulation time of the model, an improvement to the code with regards to speed was implemented at this point. In order to reduce the amount of time the calculation takes, this model first checks for identical conditions on different cells. For any groups of cells facing the same non STC conditions, this model solves for the non STC IV characteristics only once for each unique condition. Then it equates the data from that cell to the other cells under the same conditions. This considerably reduces the simulation time required at this step, improving the overall speed of this model.

At this point, the next complication of the non homogeneous conditions comes into effect. As mentioned earlier, in a series connection of cells, the current through the cells is the same, while the voltages at each current point are added up. For homogeneous condition on a PV module, to go from cell level to module level was pretty straightforward. However, for non homogeneous conditions the IV characteristic data sets are no longer identical for all cells. This has two implications with respect to going from cell level to module level characteristics.

Firstly, since the data points are not identical anymore (specifically the current data points) – it is no longer possible to just add the already existing voltage arrays to each other (at each row) to get the module voltage data set. Therefore, some form of interpolation is required here. As explained earlier, the method to obtain the IV characteristics at a cell level involves starting with defining the voltage points to be used, and then using *fzero* in MATLAB along with the characteristic IV equation as well as the determined parameters to calculate the corresponding I points. Since the voltage data points are defined, the resulting voltage arrays are identical for all cells. However, since the corresponding current data points are calculated, and now here since the cells are at different conditions, the corresponding current at each defined voltage data point will be different for cells at different conditions.

In order to be able to effectively calculate the IV characteristic of a PV module from the cell level, it would be more efficient to have the current data points identical for each cell connected in series, and obtain the corresponding voltage at each point. Then the resulting voltage arrays can simply be added together as before. In this model this is done by defining the current points for each cell and then, using the already calculated IV data for all the cells from the previous step, utilizing interpolation to obtain the corresponding voltage at each current point.

The step of interpolation has impacts on simulation time. Therefore, once again, in order to improve the speed of the code, this calculation is done only once for cells at each unique set of conditions, and the results are simply duplicated for cells under identical conditions. This has a significant reduction on simulation time. Finally once all the current and voltage data sets are obtained for each cell, the voltage arrays can simply be added up at each current point as before.

The second implication of going from cell to module level under non homogeneous conditions relates to the fact as mentioned that the current characteristic is not the same across all the cells. For cells in series, the current running through all the cells should be the same. As mentioned earlier, in the case of cells have different current characteristics, the overarching current is determined by the cell having the lowest current. However the current is not simply that of the cell with the lowest incident irradiance.

To explain how to determine the resulting current, an example will be given. Consider the IV characteristics of two cells with each under a different incident irradiance as shown in figure 2.6.

If two cells having different currents are connected in series, such as the ones shown in figure 2.6, one way to determine the resulting short circuit current point is by plotting the IV curves of both cells, then flipping one across the y axis and considering the intersection point of the two curves in the fourth quadrant. The value of the current at the intersection will be the resulting short circuit current of the set of the two cells in series. This method is illustrated in figure 2.7a.

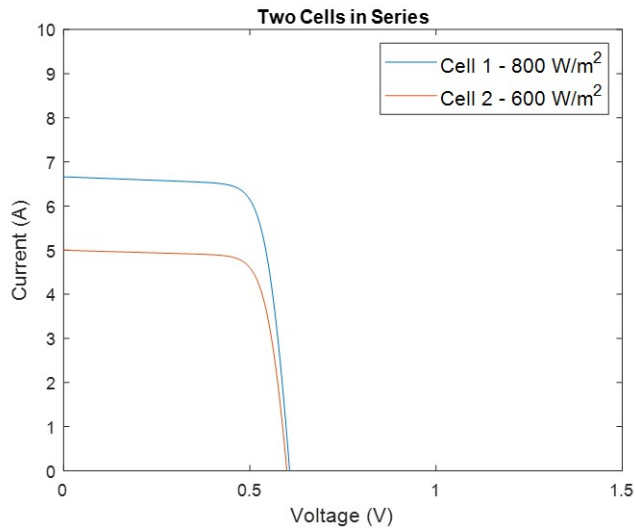
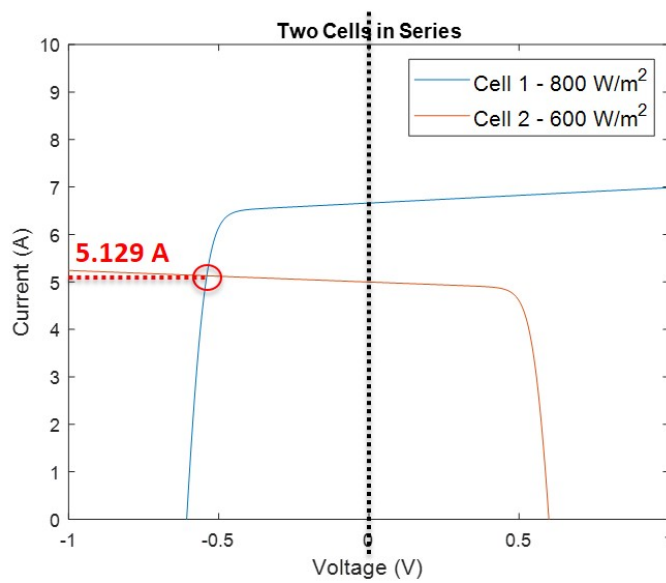
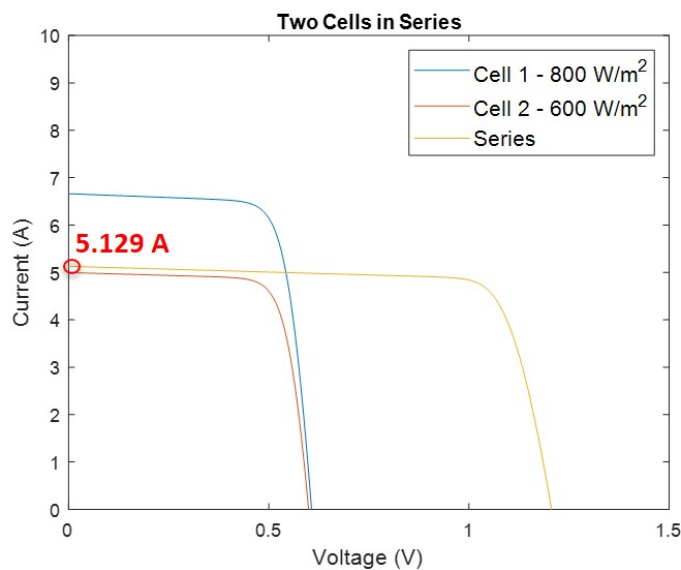


Figure 2.6: Plot showing two solar cells facing different irradiances, $800W/m^2$ and $600W/m^2$.



(a) Method 1: Plot showing intersection of two solar cells facing different irradiances, $800W/m^2$ and $600W/m^2$, with one plot flipped across the y-axis.



(b) Method 2: Plot showing resulting IV curve of two solar cells in series facing different irradiances, $800W/m^2$ and $600W/m^2$, obtained by the addition of the voltage points (including negative voltages).

Figure 2.7: Plots showing methods 1 and 2 of calculating I_{sc}

The same value can be obtained if all the voltage values at each current point are added up, including the negative voltage points. This can be seen in figure 2.7b. As can be noted, the resulting short circuit current is the same in both cases (in this case 5.129 A). In this way, the resulting IV characteristic of cells in series can be calculated in a simple manner using the methods already implemented in the model.

Less Than Cell Level Shading

An additional application was implemented at this stage, which was the modeling of less than cell shading, for example when different areas of the same PV cell are facing different irradiance levels. This was done in a simple way as shown in equation 2.13.

$$G_{cell} = G_1 \frac{A_1}{A_{total}} + G_2 \frac{A_2}{A_{total}} + \dots \quad (2.13)$$

where G_1 , G_2 , etc., represent the values of the different irradiance levels on the cell, and A_1 , A_2 are the respective areas of the cell each irradiance level is affecting. A_{total} is the total area of the cell. Therefore an average irradiance across the cell is calculated from the different irradiance conditions a single cell may be facing. In this way, the capability to work with less than cell level shading is also implemented in this model.

Reverse Bias

The calculation of the negative voltages was initially done in a simple manner where it was assumed that the IV characteristics of the cells continues into the fourth quadrant following the same slope. However, this was updated based on the results of the initial validation with LASS measurements (which will be discussed later). It was decided to model the reverse bias region of the IV characteristic. This was done a simple way in order to not add to the complexity and/or simulation time of the model.

The reverse bias characteristic refers to the part of the IV characteristic in the fourth quadrant, where voltage is negative. Shaded cells can become reverse biased as a consequence of the requirement of all cells connected in series to be working at the same current [70]. As explained in the previous section, while the current of the string is determined by the cell producing the lowest current, the resulting short circuit current of the string is generally slightly higher than that of that specific cell. At currents higher than its short circuit current, the shaded cell(s) is/(are) operating in the reverse bias region.

Cells operating in the reverse bias region result in power dissipation [70, 71]. At low negative voltages, the slope of the reverse bias IV characteristics tends to follow a fairly linear function [70]. In this region, heating occurs but generally happens more homogeneously [70]. However, as the voltage becomes more and more negative, the slope starts increasing more and more – once a certain point is reached, the solar cell goes into reverse breakdown, a region which is defined by considerably high reverse currents [72]. This leads to heating of the cell and the formation of hot spots in the PV module, which can cause degradation and, in serious cases, severe permanent damage to the module [72, 73, 74]. One way to deal with these issues is through the utilization of bypass diodes which will be explained in the next section.

Reverse Bias Model

The reverse bias region has been modeled many times in literature. One of the oldest and most referenced models is the model developed by Bishop [75]. The premise of this model is the addition of an extension term in the IV characteristic equation to model the reverse bias/breakdown region in the fourth quadrant. Quaschnig et al. provided an adaptation of the two diode model with an extension term modeling the breakdown region implemented [76]:

$$I = I_{PV} - I_{o1} \left[\exp\left(\frac{V + IR_s}{a_1 V_{T1}}\right) - 1 \right] - I_{o2} \left[\exp\left(\frac{V + IR_s}{a_2 V_{T2}}\right) - 1 \right] - \left(\frac{V + IR_s}{R_p}\right) - a(V + IR_s) \left(1 - \frac{V + IR_s}{V_{Br}}\right)^{-n} \quad (2.14)$$

where the last term is the extension term, and V_{Br} refers to the breakdown voltage value, and a and n are constants which differ slightly for different modules.

This equation was used as reference to model the reverse bias region (negative voltage region) in this work. Since this work only required a simple implementation, which has inputs that can be easily found (ideally on the datasheet of a PV module for instance), the constants a and n were kept constant for all modules. There are a number of values in literature for these two parameters, but they are all quite similar. For the purposes of this work, the values used were $a = 2.0 \cdot 10^{-3}$ and $n = 3$, from the work of Kawamura et al. [23]. These values were specifically chosen after trying values from a few other works as these worked best with a large range of breakdown voltages, whereas the other values attempted would often run into convergence issues when solving the IV characteristics.

Regarding the breakdown voltage, initially an average breakdown voltage of -18 V was used for all modules. This was based on the fact that the breakdown voltage of a crystalline silicon PV cell has been shown to generally lie in the range of -13 V to -20 V, although could also go from -10 V up to -30 V [77, 78, 70, 79]. This was amended later on in the code based on initial validations done with certain LASS measurements, which will be discussed later. IBC cells tend to have earlier breakdown at smaller voltages, with the absolute value of breakdown voltage values generally falling below 6 V [79]. Since the initial measurements with LASS showed that the breakdown voltage had a high impact on the accuracy of the IV curve of the module, in cases where only one or two cells were shaded, it was decided in this model to have breakdown voltage as an input if the value was known. If the value of breakdown voltage is not known exactly, then it is estimated based on the type of cell/connection. For example, if the cell/connection type is unknown, then the average voltage of -18 V is used for the breakdown voltage. If the cells are FBC (front back connected cells), the average voltage of -18 V is also used, as generally the values for FBC cells lie between -10 V and -20 V [80]. For IBC cells, since the values generally lie between 0 than -6 V as mentioned earlier, an average value of -4.5 V is chosen. CIGS and CdTe technologies also have pretty low breakdown voltages, with ranges of around -2 V to -6/7 V seen in literature, therefore an average value of -4.5 V is chosen for them as well [81, 82, 83].

2.6. Bypass Diode Implementation

As mentioned in section 2.5.2, there are a number of potential issues that can occur due to partial shading and reverse bias of cells in a PV module. One way to deal with the issues mentioned (hot spot formation, cell breakdown, etc.) is through the use of bypass diodes [9, 84, 71]. Bypass diodes are usually connected across a section containing a number of series connected cells, and help in the form of constraining the maximum reverse voltage that can occur when cells are reverse biased [59, 85]. A bypass diode is activated when the overall voltage of a string of cells connected to it drops below the forward voltage of the diode. Then the reverse voltage is limited to the forward voltage across the bypass diode. The forward voltage of the bypass diode depends on the type of bypass diodes used and is usually around 0.6-0.8 V for a p-n diode, while it is lower for a Schottky diode, usually in the range of 0.2-0.4 V. Therefore, the reverse voltage of the string is limited to quite a small value, reducing the risk of high power dissipation in the reverse bias region, as well as the more severe issues associated with that.

Bypass diodes also help in dealing with another major issue of partial shading, especially in series connected modules. As mentioned earlier, in a set of series connected cells, the current running through the cells is limited by the cell with the lowest current. This means that in the case of partial shading (or other issues such as faults occurring with cells, etc.), even if only a few cells are shaded, the power output of the entire module is limited by those cells. However, with the utilization of bypass diodes, only the output of the string connected together by the bypass diode is affected, and the rest of the module is not. In this way (depending on the number of bypass diodes, their configuration, and the configuration of the shaded cells) having a few cells shaded will not limit the total output power of the module as significantly as before. The power loss will be much lower, and will depend on the forward voltage of the diode in operation, and the current running through it. The difference can be seen in figures 2.9 and 2.10, discussed at the end of this chapter.

One drawback of bypass diodes, however, is when activated (in cases of partial shading, etc.) – they result in multiple peaks in the resulting PV curve of the module. This can lead to issues when it

comes to maximum power point tracking (MPPT), as was explained in section 1.1. The operation of a PV module is at its maximum power point at any given condition. This is obtained through the use of MPPT algorithms, which, as the name suggests, search for and track the peak of the PV curve, which is the maximum power point, during the time of operation, and make sure the PV module is operating around that point. In the case of many peaks in the resulting PV curve of the module, this can lead to issues with the MPPT algorithms tracking local peaks instead of the global peak of the PV curve. This can lead to losses with respect to the operating power of the PV module [27]. There have been a number of solutions offered with respect to the MPPT algorithms regarding this issue, such as using artificial intelligence, multi-variable perturb and observe algorithms, etc. [20].

The inclusion of bypass diodes in a PV module and their operation and impact were also modelled in this work. The inputs required for the implementation of the operation of bypass diodes in this model are the number of bypass diodes and their configuration in the module. Based on this, the number of cells and the configuration of bypass strings in the module is determined. This allows to understand which cells are connected to each other in one bypass string, which has implications for the impacts of partial shading.

The bypass diode activation is modeled for a p-n diode by taking into account the minimum forward voltage of the diode as well as its IV characteristic. A typical IV characteristic for a p-n diode can be seen in figure 2.8, which was used to model the characteristics of a p-n type bypass diode in the model. The curve was modeled using a straight line correlation based on the trend from $I = 0.1$ A to $I = 10$ A (as this is the general operating range), and specifically the 25°C curve as shown was considered for this modeling.

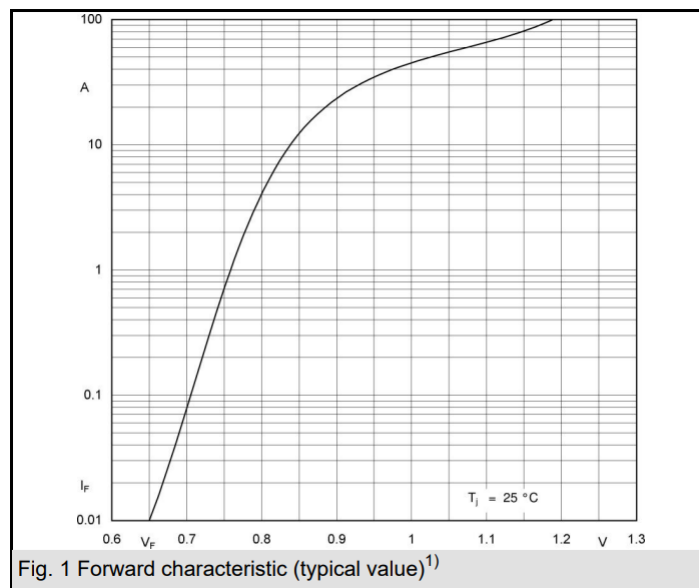


Figure 2.8: Forward voltage-current characteristic of F1200 p-n diode. Figure taken from [86].

The process for taking bypass diodes into account in the final IV characteristic of the module is as follows. Based on the process mentioned earlier, the current and voltage data points of each cell are calculated based on the given irradiance and temperature conditions. Then, once again based on the method explained earlier, the current voltage characteristics of each bypass diode string of series connected cells is calculated. The amendment to this part is that the activation of the bypass diode is now taken into account. Based on the minimum forward voltage and the IV characteristic of the bypass diode (to calculate the forward voltage V_F of the diode at the respective current), the bypass diode gets activated when the voltage of the string drops lower than $-V_F$ (the negative of the forward voltage of the bypass diode), and limits the reverse voltage of the string to $-V_F$. Then the current voltage characteristics of each bypass diode string are added together taking into account that they are connected

in series.

An example of the implementation and impact of bypass diodes can be seen in figures 2.9 and 2.10. The figures represent the IV and PV curves of a set of 21 cells connected in series, with cells 1 to 16 facing an irradiance level of 900 W/m^2 , and cells 17 to 21 facing an irradiance level of 200 W/m^2 . Figure 2.9 demonstrates the results when the cells are connected in series without any bypass diodes, whereas in figure 2.10, the case for the inclusion of 3 bypass diodes (each covering 7 cells) is shown.

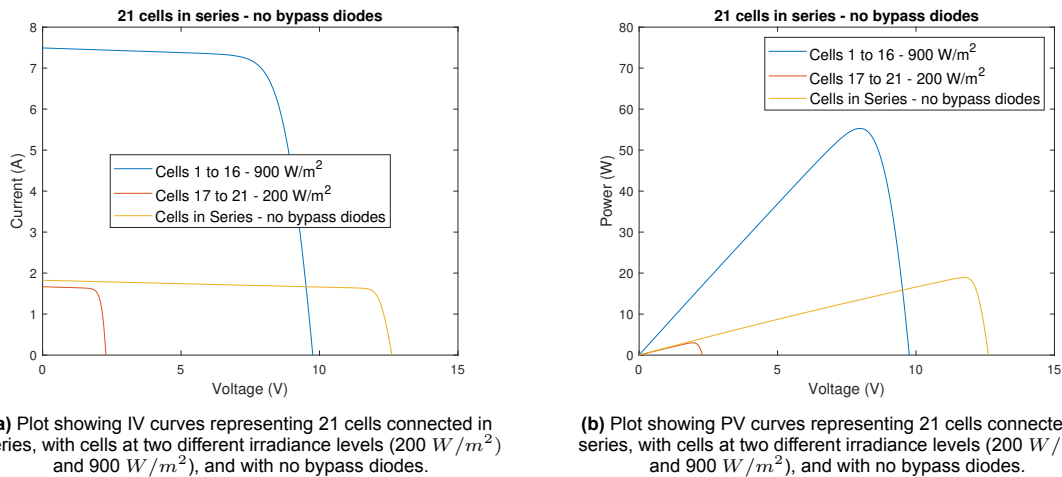


Figure 2.9: Plots showing IV and PV curves of 21 cells connected in series with different irradiance levels and no bypass diodes

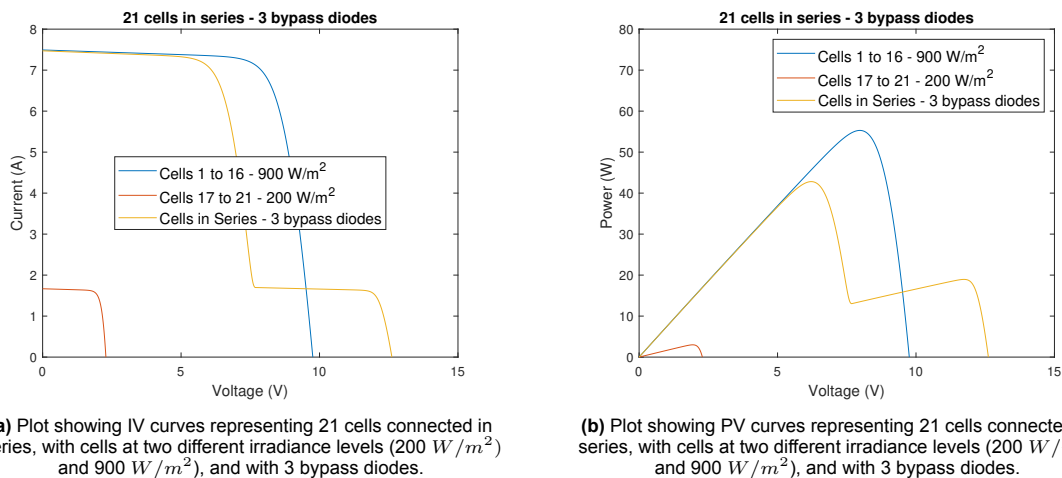


Figure 2.10: Plots showing IV and PV curves of 21 cells connected in series with different irradiance levels and 3 bypass diodes

The significant negative impact of partial shading on cells connected in series is demonstrated in figure 2.9. As can be seen, just having 5 cells shaded with an irradiance of 200 W/m^2 has a serious impact on the output power of the string of cells, reducing the MPP to 18.95 W . With the MPP if all cells were at 900 W/m^2 being approximately 72 W , this means the resulting output power is only 26.3% of the nominal. The impact of connecting bypass diodes to a set of cells in series is shown in figure 2.10. It can be seen that there is a substantial improvement to the overall MPP, with P_{MPP} here being 42.8 W , more than double the power seen without bypass diodes.

In conclusion, in this chapter, the implementation of a MATLAB based model to simulate the IV characteristics of a PV module under various irradiation and temperature conditions has been demon-

strated. The inclusion of the reverse bias region as well as the capability to integrate the effect of bypass diodes was also shown. The next step is the validation of this model, which is discussed in the next chapter.

3

Validation

In this chapter, the validation process for the IV curve simulator developed in Chapter 2 will be demonstrated. First, a cross verification with the modules mentioned in Ishaque et al.'s work is done, which is shown in Section 3.1. Then, major insights gained from laboratory measurements with a large area solar simulator, which have impacts on the model, will be discussed in Section 3.2. Finally, the main validation of this model with lab measurement data provided for a Canadian Solar CS6 230P module will be presented in Section 3.3.

One point to note here is that, as will be explained in Chapter 4, in the shading tolerability calculator, the value that is used in the calculation is the power at the maximum power point, P_{MPP} . Therefore, the accuracy at the maximum power point at different conditions is of the most importance, and so, during validation, the errors at the resulting maximum power point will be evaluated.

3.1. Cross Verification

The first step in the process was to cross validate the results of the model, by checking the errors when using the same modules used in the work by K. Ishaque et al. [62]. Three modules used in the paper, whose datasheet parameters are given in Table 3.1 below, were used for the purposes of this validation [62].

Table 3.1: Datasheet parameters for Shell S36 (multi-crystalline), Shell SP-70 (mono-crystalline), and Shell ST40 (thin-film) modules used for cross-verification purposes [62].

	Shell S36	Shell SP-70	Shell ST40
$P_{mpp}(W)$	36	70	40
$V_{mpp}(V)$	16.5	16.5	16.6
$I_{mpp}(A)$	2.18	4.25	2.41
$V_{oc}(V)$	21.4	21.4	23.3
$I_{sc}(A)$	2.3	4.7	2.68
$K_V(mV/^\circ C)$	-76	-76	-100
$K_I(mA/^\circ C)$	1	2	0.35
N_s	36	36	42

As explained in section 2.4, this work first models the IV characteristics at a cell level. Based on the parameters given for the module, the cell level parameters were calculated. For a module with cells connected in series, this was done as shown below:

$$\begin{aligned}P_{mpp_{cell}} &= P_{mpp}/N_s \\V_{mpp_{cell}} &= V_{mpp}/N_s \\I_{mpp_{cell}} &= I_{mpp}\end{aligned}$$

$$V_{oc_{cell}} = V_{oc}/N_s$$

$$I_{sc_{cell}} = I_{sc}$$

$$K_{V_{cell}} = K_V/N_s$$

$$K_{I_{cell}} = K_I$$

Using the above parameters, the cell level IV characteristics were simulated for these modules. Then, using the method explained in section 2.5, the module level IV characteristics were able to be determined from the cell level calculated values. Both cell level and module level results were cross validated. However, since the results were very similar, the results of the module level cross verification will be focused on. The validation of the module level results also implicitly validate the cell level results as well as the modelling to go from cell level to module level.

3.1.1. Module level

As discussed, the first step of this model was to model the IV curve at cell level under STC conditions. Therefore, this was the first set of results that was cross verified using the datasheet parameters as given in table 3.1. The next step was to validate the model under both STC and homogeneous non STC conditions at a module level. Once again, the modules and their parameters as given in table 3.1 were utilized for this step.

STC

The model was first validated at a module level under standard test conditions. The results can be seen in figure 3.1.

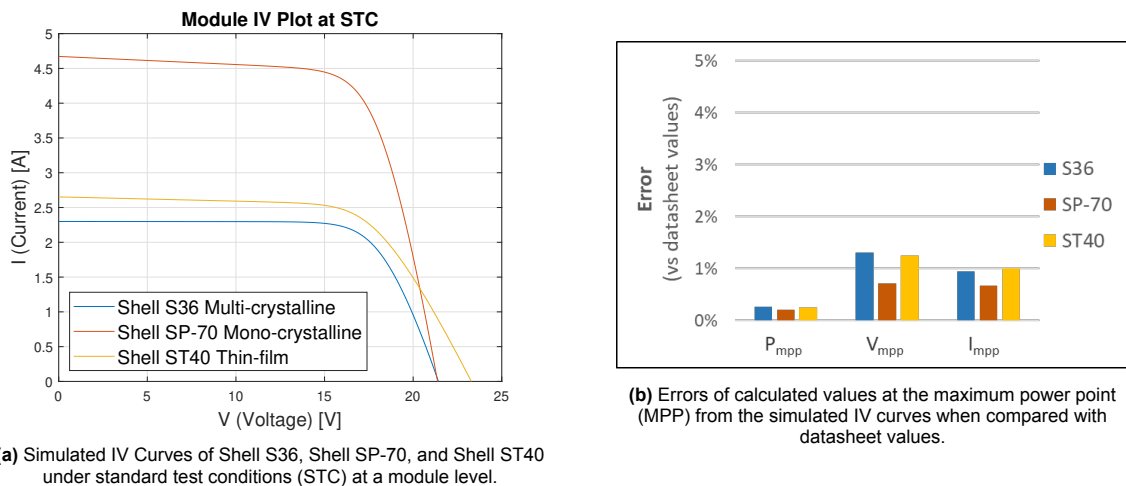


Figure 3.1: Validation of results at a module level at STC.

Figure 3.1a shows the IV characteristics simulated at STC conditions for the three modules given in table 3.1. The errors at the maximum power point for each module are given in figure 3.1b, with the colors corresponding to the colors of the curves.

It can be seen that the P_{mpp} errors seem to be the lowest here. As explained in section 2.4.1, the parameters for calculating the IV characteristics under STC conditions were determined through P_{mpp} matching (with the P_{mpp} value at STC given on the datasheet of the module). This can explain why the STC errors with respect to P_{mpp} are so low, all falling below 0.5%. It also explains why they are the lowest errors out of the three variables.

All values here are considerably low, all falling below 1.5%, with most below 1%. These results give a good validation for the model at a module level under standard test conditions (STC).

Non STC (Homogeneous)

The next step was the validation at non STC conditions. In Ishaque et al., numerical measured values were given for the modules exposed to various temperatures, therefore these were the parameters used to validate the model in this instance. The errors at maximum power point for one of the modules (Shell S36) can be seen in figure 3.2.

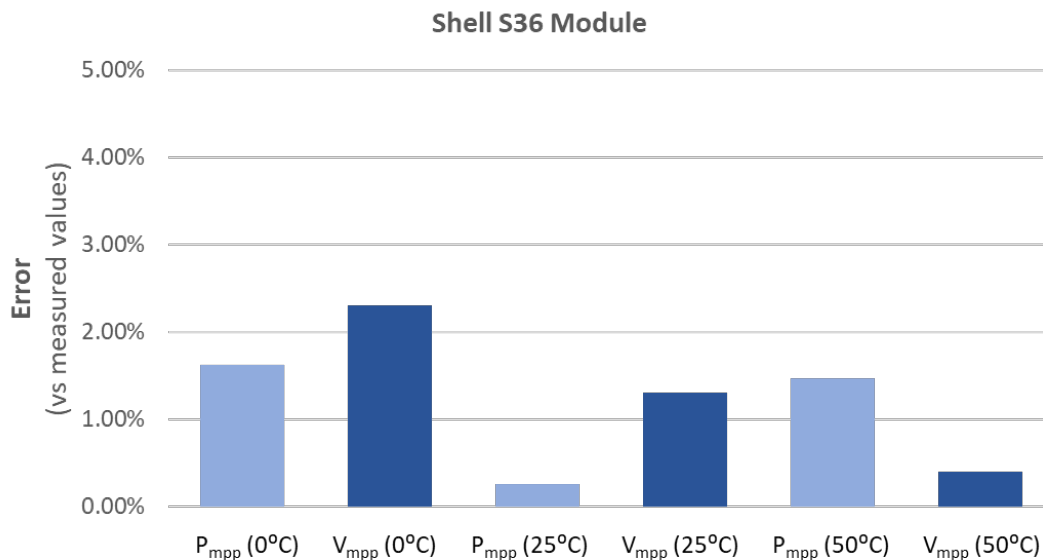


Figure 3.2: Errors at non STC conditions at a module level for the Shell S36 module.

Two main things can be noticed from figure 3.2: P_{mpp} value is no longer the lowest at all levels, and there seem to be generally higher levels of error seen for temperatures different from 25°C. This can likely be explained by the fact that the P_{MPP} matching to calculate the parameters is done for STC values. When calculating for non STC conditions, irradiance and temperature dependencies are applied within the equations for the two diode model parameters, to go from their calculated STC values to their corresponding non STC values, as explained in section 2.4.2. This was done based on models found in literature. This additional step in moving from STC to non STC adds another level for error potential, which is most likely what is contributing to the generally higher levels of errors overall seen for temperatures different from STC temperature (25°C).

These errors, as well as STC errors were also compared with the errors that Ishaque et al. obtained. It was found that mostly the errors calculated in this work were slightly different from the values given by Ishaque et al. [40]. However, it did not seem like they were overall better or worse, or that any correlation could be observed. There are a few reasons why the values seen in this work could be different from those calculated by Ishaque et al. As has been mentioned in section 2.4, this model first calculates the IV characteristics at a cell level, and then modeled the series connection of a PV module with cells connected in series to use the results to obtain the module level IV characteristics. In Ishaque et al., the characteristics are directly calculated at a module level [40]. This difference in process could be one of the aspects contributing to the difference in values seen. Another point is that when solving for the IV characteristic, Ishaque et al. used the Newton Raphson method, whereas this work uses the `fzero` function in MATLAB. This is an additional difference in methods. One more thing to note is that, in Ishaque et al.'s work, the exact value of acceptable error used in the P_{mpp} matching step is not mentioned. Therefore the level of error used in the P_{mpp} matching step could be different. This would definitely lead to differences in the value of errors seen between this work and that of Ishaque et al. A final aspect is that, as explained in section 2.4.2, there is most likely a difference in methods used to solve for R_s and R_p at non STC conditions. Since these parameters have a direct impact on the IV characteristics, this could also be one of the reasons for the differences in values observed.

However, here it can be seen that errors of the values at maximum power point of the simulated IV curves when compared to the measured values are still relatively low, all falling below 2.5%, with most actually falling close to or below 1.5%. This gives sufficient credibility to the model at this point and also validates the process by which the model calculated the IV characteristics at a module level from the respective characteristics at a cell level (homogeneous conditions). This thereby concludes the cross verification part of the validation.

3.2. LASS Validation

The next step was validating with in-lab measurements at TU Delft using an EternalSun large area solar simulator (LASS) for specific modules. A number of measurements were carried out for three modules, considering various partial shading scenarios. However, afterwards, it was found that there were certain issues with the large area solar simulator, thereby making some aspects of the measurements incorrect, especially around the top half of the IV curve, near the short circuit current point. Therefore, these were not the measurements used for the final validation of this model. However, during the course of validation with the LASS measurements, there were certain important points noted that made an impact on the implementation of the IV simulation model of this work, which greatly improved the fit around the open circuit voltage point. Therefore, it was decided to briefly discuss here only two representative cases of those measurements.

The module for which the results will be discussed is a BenQ Sunforte module with 96 cells in a 12 rows x 8 columns configuration. It has 3 bypass diodes, where the first one covers the first two columns of cells (24 cells), the second the next four columns (48 cells), and the third the last two columns (24 cells). It should also be noted that this module utilizes Interdigitated Back Contact (IBC) cells. The details of the datasheet parameters of the module are given in table 3.2.

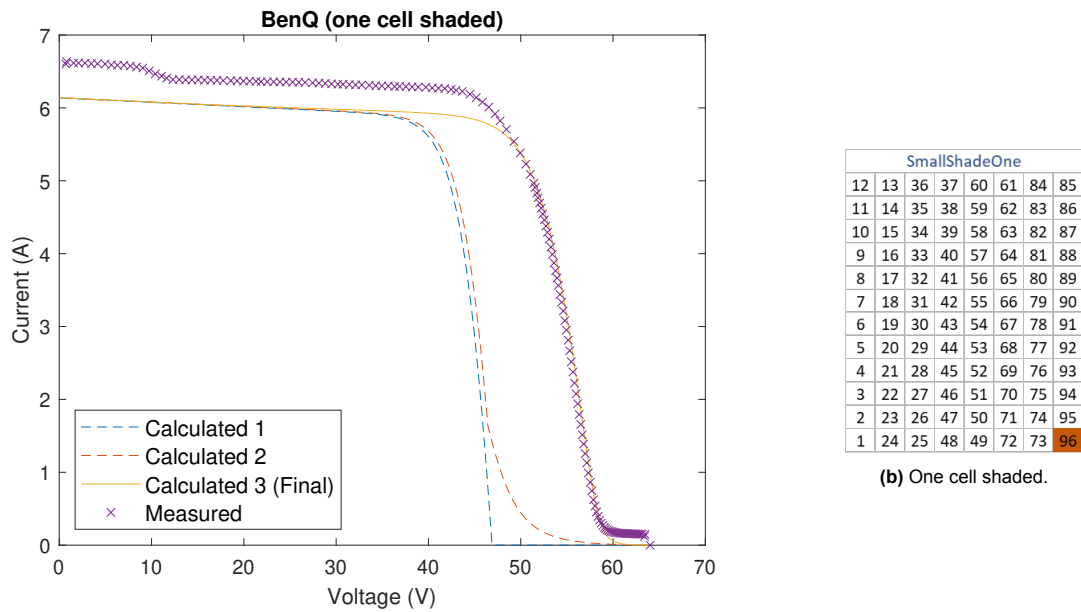
Table 3.2: Datasheet parameters for BenQ SunForte PM096B00 module.

	BenQ SunForte PM096B00
$P_{mpp}(W)$	335
$V_{mpp}(V)$	54.7
$I_{mpp}(A)$	6.13
$V_{oc}(V)$	64.9
$I_{sc}(A)$	6.62
$K_V(mV/^\circ C)$	-0.16874
$K_I(mA/^\circ C)$	0.008
N_s	96

Two representative results for the laboratory measurements can be seen in figures 3.3 and 3.4. Figure 3.3a shows the IV characteristics in the case where one cell is fully shaded, represented by the dark brown square in the configuration shown in figure 3.3b. Figure 3.4a gives the IV characteristics for two fully shaded cells, as illustrated in figure 3.4b (here each cell is in a different bypass diode string). The IV plots show the progression of the development of the code (from the blue dashed line to the red dashed line to the final yellow solid line) and the results observed. These figures are just shown to illustrate the improvement in fit around the open circuit area, and due to the issues with the LASS measurements as explained, the top part of the curves (the area near the short circuit current point), are disregarded.

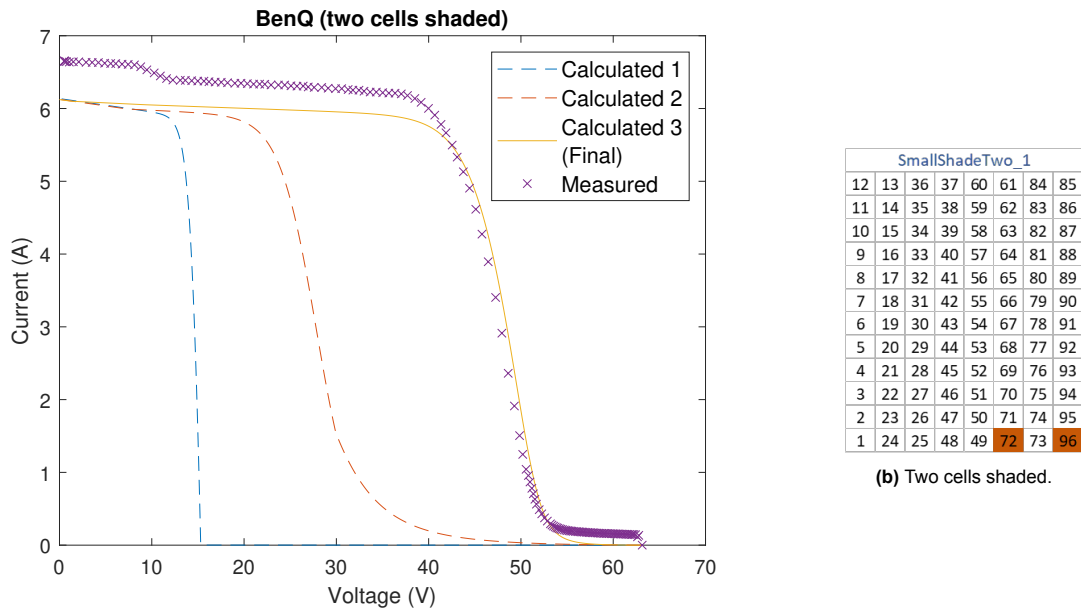
It was noticed that for the cases where only one or two cells of the module were shaded, there seemed to be a large difference between the simulated curve from the MATLAB model and the measured one (the initial blue dashed curves in figures 3.3 and 3.4). There were two aspects that were decided to be checked based on this: the bypass diode activation and the reverse bias region. For the first curve seen in this plot, the reverse bias region had not yet been modeled in the code. Therefore, the first amendment made to the model based on the LASS results was to include the reverse bias region based on the methods explained in chapter 2. The bypass diode activation was also amended to have the model check the string voltage at every voltage point and have the bypass diode activated

once the string voltage dropped below the forward voltage of the bypass diode. This insertion changed the shape of the curve to the dashed red one. One can see now a tail close to the open circuit voltage point, caused by the shaded cell operating in the reverse region.



(a) Progression of simulated IV Curves with respect to measured values, with amendments to code.

Figure 3.3: Plot showing improvement of fitting of simulated to measured IV curves with changes in model (one cell shaded), module temperature 28°C.



(a) Progression of simulated IV Curves with respect to measured values, with amendments to code.

Figure 3.4: Plot showing improvement of fitting of simulated to measured IV curves with changes in model (two cells shaded), module temperature 31°C.

As can be seen, these initial amendments made a positive difference to the simulated IV curve. One can see a shift of the simulated curve to the right, getting closer to the measured one in both values and shape. The final curves are represented by the yellow continuous lines in both plots, which can be

seen to have a much better fit with the measured curves when compared to the previous red and blue dashed curves. It was found that the effect of the breakdown voltage value had a significant impact in cases with IBC cells for instance (which is what was used in the BenQ module as mentioned), where the breakdown voltages are much lower, specifically in cases where only one or two cells were shaded. This is due to the fact that the bypass diode then does not necessarily get immediately activated when only one cell is shaded for example, since the resulting reverse bias string voltage with these cells shaded does not fall below the limit of the bypass forward voltage. In the initial simulations, the value for breakdown voltage used was -18 V , as an average breakdown voltage as explained in section 2.5.2. However, since the BenQ module used IBC cells, this breakdown voltage was now changed to -6 V , which is closer to the average breakdown voltages of IBC cells [79]. The result is shown with the third and final calculated curve. As can be seen, the fitting between the simulated and measured curves has improved significantly in the right part of the curve, around the open circuit voltage point. In this way, with this validation against the LASS measurements, the reverse bias region and the bypass diode activation modeling was updated and finalized in this model, taking into account the importance of the accuracy of the value of the breakdown voltage when dealing with shading of a small number of cells.

Despite all the amendments, the difference between the two curves was still significant, mainly with respect to the top part of the IV curves (and consequently the resulting maximum power point). However, it was not possible to continue the validation of these curves due to the already mentioned problems of the LASS. Therefore, other measurements were required for further validation, which will be discussed in the next section.

3.3. Canadian Solar Validation

With the completion of the updating of the model based on the LASS measurements validation, the final validation was carried out against lab measurements of a Canadian Solar CS6P 230P module under various partial shading conditions [87]. This measurement data was directly provided by EURAC (and was also used in the following works: [88, 89]). This module has 60 cells connected in series with 6 columns and 10 rows. There are 3 bypass diodes, each one covering 20 cells in series. the relevant datasheet parameters are given in table 3.3.

Table 3.3: Datasheet parameters for Canadian Solar CS6 230P module [87].

	Canadian Solar CS6 230P
$P_{mpp}(W)$	230
$V_{mpp}(V)$	29.6
$I_{mpp}(A)$	7.78
$V_{oc}(V)$	36.8
$I_{sc}(A)$	8.34
$K_V(mV/^\circ C)$	-0.12512
$K_I(mA/^\circ C)$	0.005421
N_s	60

The shading conditions considered during the measurements (and the respective naming) are as follows:

- Shading is done by covering a certain percentage of all cells in the first and/or third column, from left to right, as illustrated in figure 3.5. There are 4 shading conditions.
 - Unshaded: None of the cells are shaded
 - 02ratio: 20% shaded: all cells in the respective column(s) are partially shaded, with 20% of their area in a horizontal direction being shaded
 - 05ratio: 50% shaded
 - 08ratio: 80% shaded
- As mentioned either all the cells in the first column or all the cells in both the first column and the third column are partially shaded.

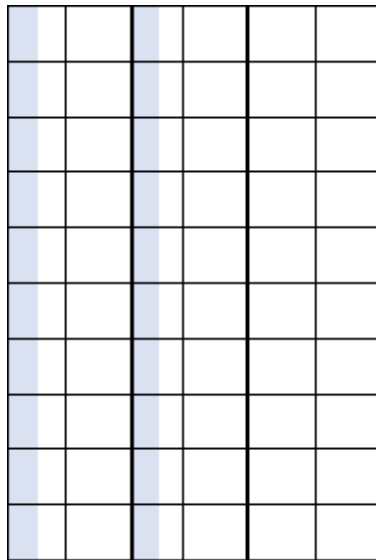


Figure 3.5: Canadian Solar Shading Pattern

- 0strings: Unshaded
- 1strings: 1 string shaded (all cells in the first column are partially shaded)
- 2strings: 2 strings shaded (all cells in the first and third columns are partially shaded)

The case illustrated in figure 3.5 corresponds to the parameters 05ratio and 2strings, as explained by the definitions given.

The unshaded cells receive an irradiance of either 1000 W/m^2 , 700 W/m^2 , or 200 W/m^2 . A selection of the results are shown here in figures 3.6, 3.7, 3.8, with the shading details and errors at maximum power point given in the figure captions.

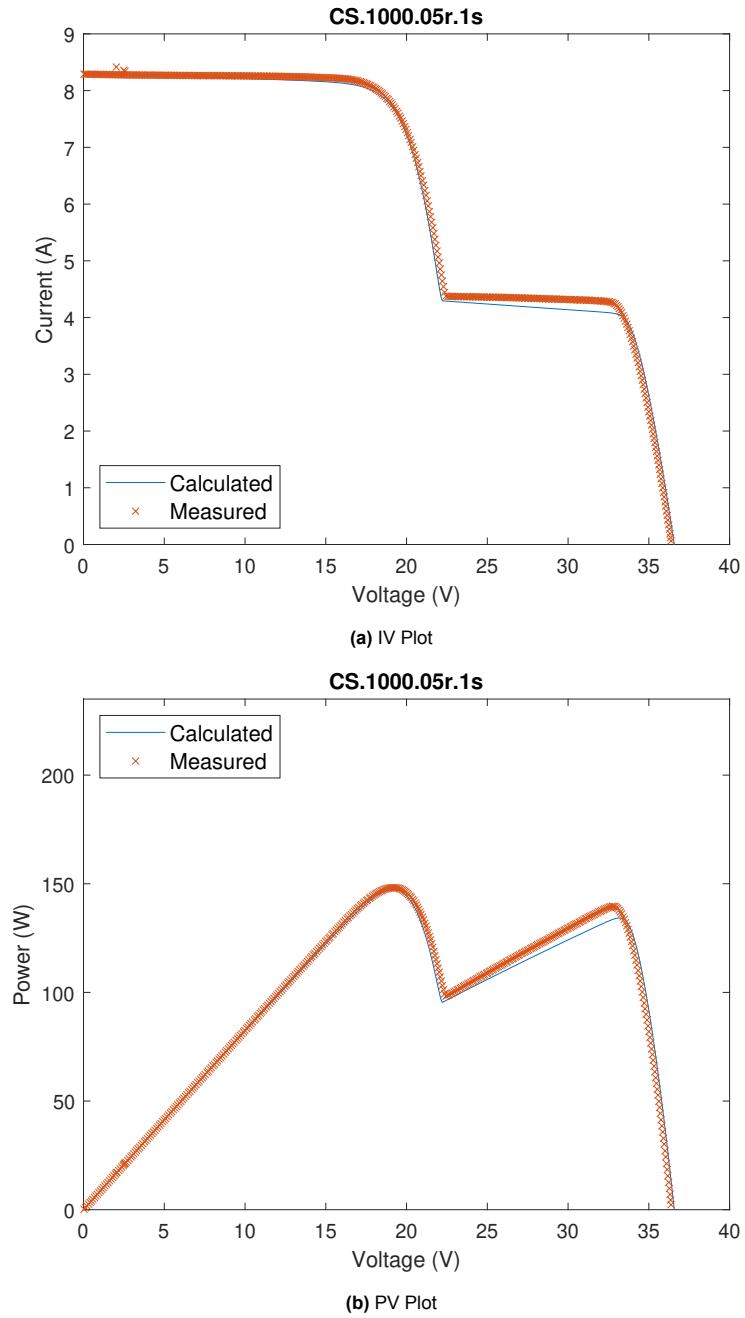


Figure 3.6: IV and PV plots showing calculated values in comparison to measured values for the Canadian Solar CS6 230P module under partial shading conditions.

Shaded Irradiance: 0 W/m^2 , Unshaded Irradiance: 1000 W/m^2 ; All cells in first column of cells shaded 50% horizontally
 Errors: $I_{MPP} : 0.68\%$, $V_{MPP} : 0.04\%$, $P_{MPP} : 0.64\%$

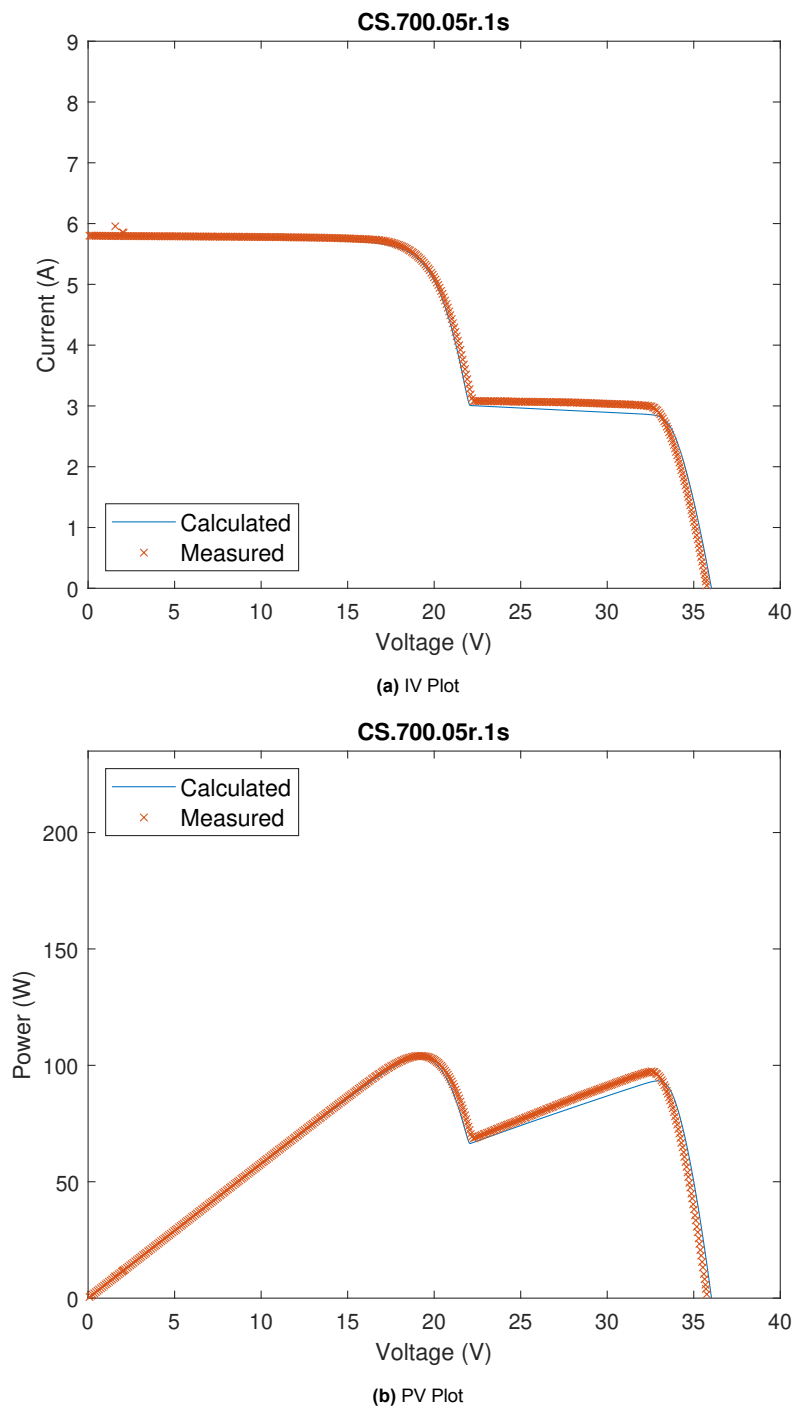


Figure 3.7: IV and PV plots showing calculated values in comparison to measured values for the Canadian Solar CS6 230P module under partial shading conditions.

Shaded Irradiance: 0 W/m^2 , Unshaded Irradiance: 700 W/m^2 ; All cells in first column of cells shaded 50% horizontally
 Errors: $I_{MPP} : 0.76\%$, $V_{MPP} : 0.02\%$, $P_{MPP} : 0.78\%$

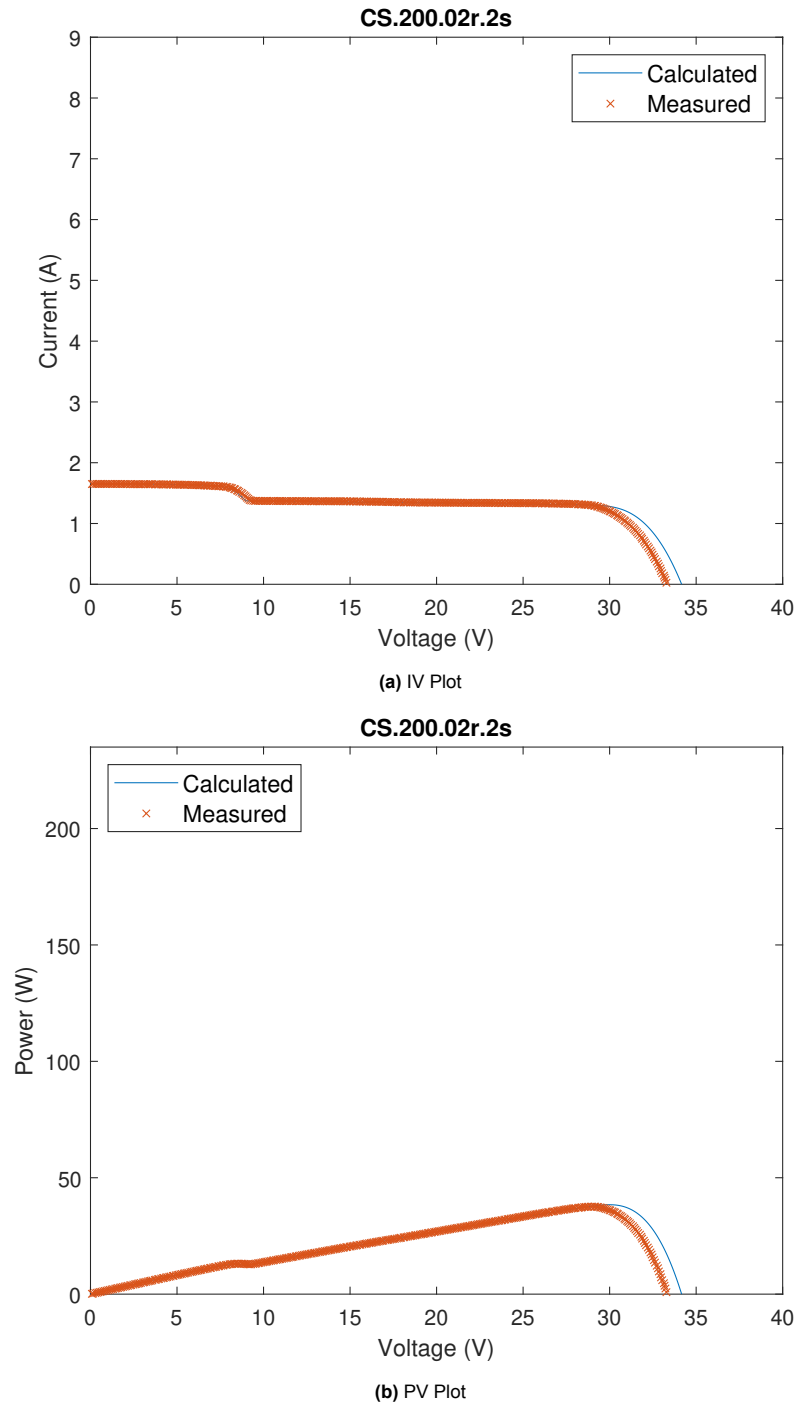


Figure 3.8: IV and PV plots showing calculated values in comparison to measured values for the Canadian Solar CS6 230P module under partial shading conditions.

Shaded Irradiance: 0 W/m^2 , Unshaded Irradiance: 200 W/m^2 ; All cells in first column and all cells in third column of cells shaded 20% horizontally

Errors: I_{MPP} : 1.83%, V_{MPP} : 4.31%, P_{MPP} : 2.41%

There were 21 measurements done in total. The remaining results can be seen in Appendix A. The results of the errors at maximum power point for each of the 21 scenarios can be seen in figure 3.9.

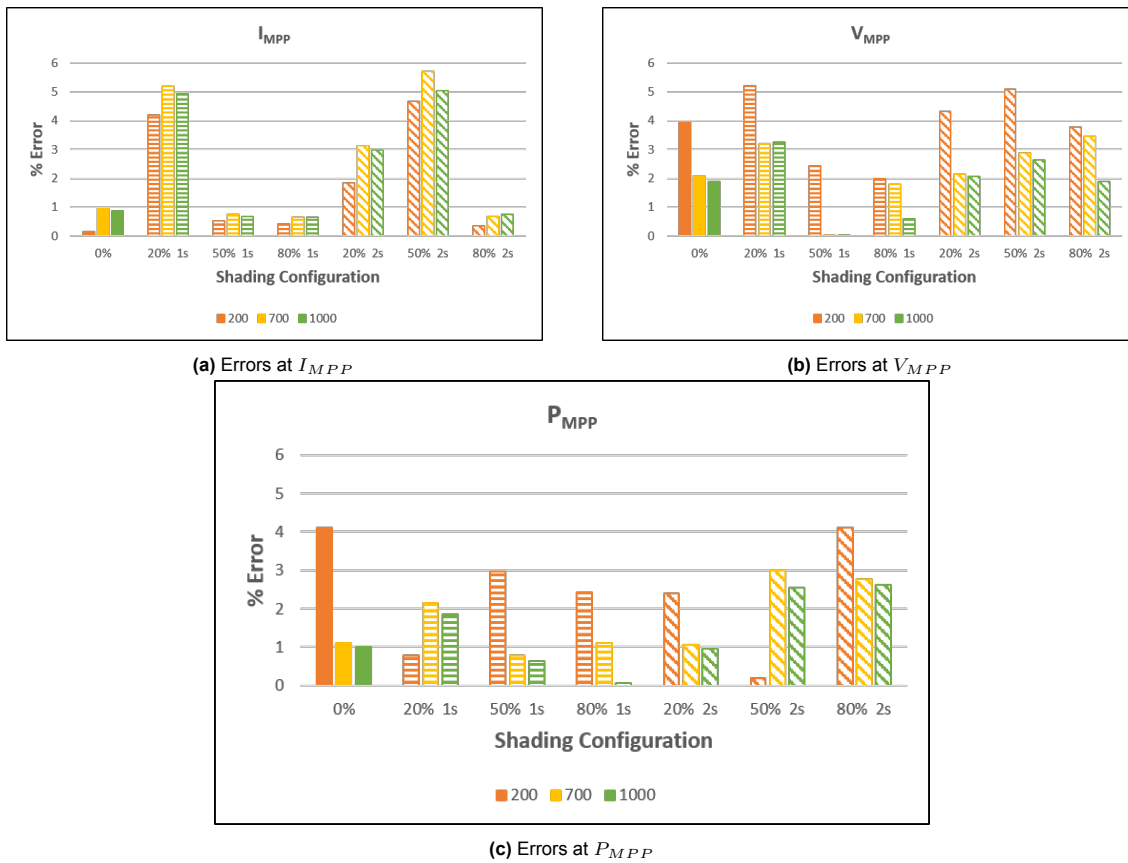
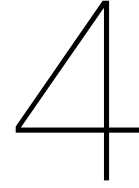


Figure 3.9: Errors at maximum power point for all Canadian Solar measurements. Different irradiances are represented by orange for 200 W/m^2 , yellow for 700 W/m^2 and green for 1000 W/m^2 .

Figure 3.9 shows the errors at the maximum power points for each measurement done. Errors at the different irradiance levels are represented by different colours (orange: 200 W/m^2 , yellow: 700 W/m^2 , green: 1000 W/m^2). One of the observations that can be made is that it seems across that for each shading configuration, the errors for the irradiance level of 1000 W/m^2 seems to be the lowest (compared with the other irradiance levels). As also mentioned in section 3.1, this could be due to the fact that the module calculates the initial parameters at STC (which corresponds to an irradiance level of 1000 W/m^2) through P_{MPP} matching. Therefore it makes sense that the accuracy around the MPP point is generally the highest when conditions are similar to STC. For V_{MPP} and P_{MPP} it can also be observed that it seems that the errors are generally highest for the case where the irradiance is 200 W/m^2 (although this trend is not observed for I_{MPP}). This could indicate that the accuracy decreases the further away you get from STC conditions, which would make sense. The results of the trends in the errors for each variable could also be impacted by the methods used to calculate temperature and irradiance dependencies. With respect to the area of shading, there do not really seem to be any clear correlations, implying that the shading configuration does not really seem to have an impact on the model, which is a positive finding.

From the IV and PV curves shown (as well as the errors at maximum power point), it can be seen that the calculated IV and PV data from this model (and the consequent simulated IV and PV curves) have quite a good fit with the measured values. The maximum power point errors at P_{MPP} all lie below 4.5%, with most actually below 3%. The errors at V_{MPP} and I_{MPP} remain below 5.5% and 6% respectively (again with most below 4% and 5% respectively). The other point to note here is that these measurements also validate the less than cell level shading modeling done in this work, as the cells were all partially shaded as explained earlier. In this way, the validation of the IV/PV simulation model of this work has been completed. The next step is to use this model in the development of a shading tolerability calculator, which is discussed in the next chapter.



Shading Tolerability Calculator

In this chapter, the development of the shading tolerability calculator in Matlab will be discussed. In section 4.1, an brief explanation on shading scenarios will be given. Section 4.2 will detail the necessity of the reduction of simulation time and how this could be achieved. In section 4.3, the identification of symmetry with respect to the modules and shading scenarios will be discussed, as well as how this contributes to reducing the unique scenarios that need to be simulated. Section 4.4, the method for calculating the shading tolerability parameter (ST) will be explained, taking into account the steps taken in the previous sections, and the results of ST values for over 40 modules are presented as well. Section 4.5 performs an analysis of the ST results obtained, and section 4.6 provides some insights into the methods used in calculating the shading tolerability in this work. Finally, section 4.7 lays out some recommendations for further development of this model.

4.1. Shading Scenarios

As discussed in section 1.2, the equation for the calculation of shading tolerability is [28]:

$$ST_{(i,c)} = \frac{1}{P_{mod_{mpp}}} \sum_{k=1}^{k=i^c} P_k\left(\frac{1}{i^c}\right) \quad (4.1)$$

where:

- $ST_{(i,c)}$: shading tolerability
- c : total number of cells the PV module consists of
- i : number of irradiance levels
- P_k : maximum power at each shading profile [W]
- $P_{mod_{mpp}}$: maximum power of the PV module (at STC) [W]

As explained, all possible shading scenarios are not possible to take into account physically in this equation (in the case of for example $i \rightarrow \infty$), as this would not be physically possible to measure. In the work of Ziar et al., it was proved that [28]:

$$ST_{(i=2,c)}^{(Module_1)} > ST_{(i=2,c)}^{(Module_2)} \Rightarrow ST_{(i \rightarrow \infty,c)}^{(Module_1)} > ST_{(i \rightarrow \infty,c)}^{(Module_2)} \quad (4.2)$$

Therefore, it was decided to use $i = 2$ in the ST calculations.

The first step in the development of the shading tolerability calculator is the definition of the shading scenarios that will be considered. The total number of scenarios can be calculated by i^c , where c represents the number of cells of the module. In actuality, 'c' can be thought of the number of sections the module is split into where each section is the smallest possible area that can be shaded at any given time. Taking the assumption that 'c' is the number of cells - for a 60 cell module the total number of shading scenarios would be $1.15 \cdot 10^{18}$, which is tremendously large, and not really possible to calculate

either, therefore it is necessary to simplify this.

In the previous work on shading tolerability done by Ziar et al and Mishra et al, which involved experimental measurement of ST, the PV module was split into 6 sections [28], [34]. This resulted in $2^6 = 64$ total possible shading scenarios, a much more reasonable number to experimentally test.

In this work, in order to define the shading scenarios, the PV module will be split into 12 (geometrically) equal sections, and the results are simulated computationally (and not as measurements in the lab). As can be seen, this work has a significant increase in the number of shading scenarios that is explored. One of the limitations of the previous work was that, since the IV characteristics of each shading scenario were measured physically in the laboratory, there was a constraint with respect to time and energy with how many measurements could be carried out. However, since the work done in this thesis plans to calculate the shading tolerability through simulation of IV characteristics of PV modules under the various shading conditions, and not in-lab measurements, this allows for testing over a larger range of scenarios (and modules). The simulations themselves also take some time, therefore it was decided to not go higher than 12 sections at this point.

Based on the decision to consider two irradiance levels ($i = 2$), it was considered that a section can be either shaded or unshaded. If unshaded, an incident irradiance of 1000 W/m^2 will be taken into account, whereas if shaded, the irradiance will be 100 W/m^2 . This value was chosen as the diffuse irradiance component is generally considered to be around 10% of the global horizontal irradiance (GHI), therefore 10% of 1000 W/m^2 was used.

Based on these parameters, all possible shading scenarios are considered in the calculation. The total number of all possible combinations of 2 irradiance levels (100 W/m^2 and 1000 W/m^2) over 12 sections is equal to $2^{12} = 4096$ possible shading scenarios in total. To give more of an idea on what the shading scenarios represent, a brief example is given below.

Consider a PV module split into 12 sections as shown in figure 4.1a. As mentioned earlier, a section can be either shaded or unshaded. Figures 4.1b-4.1e show certain shading scenarios for two irradiance levels (with the grey squares representing the shaded sections). These figures illustrate a few different ways in which 12 sections of a PV module could be shaded, with number and position of the shaded sections changing.

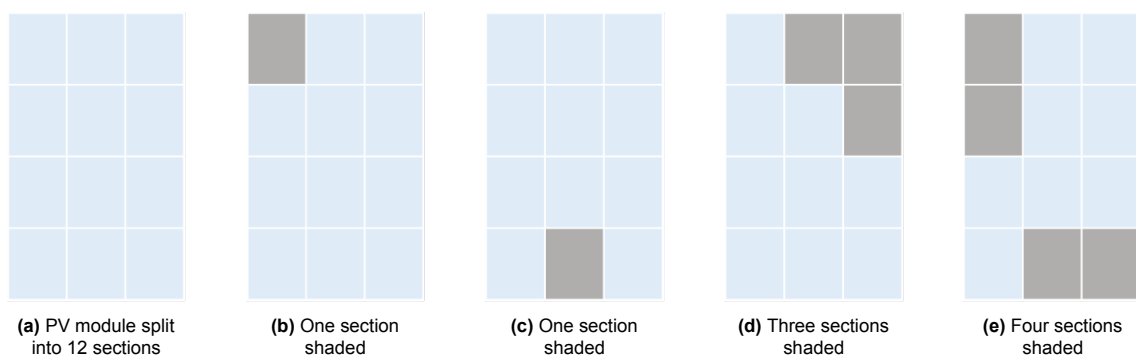


Figure 4.1: Various possible shading scenarios for a representative PV module split into 12 sections.

4.2. Reduction of simulation time

It should be taken into account here that the simulation for each shading scenario takes around 1.75 mins. That means that to run simulations for 4096 shading scenarios would take on average 120 hours for each module. This is a significant amount of time, and would severely limit the number of modules that shading tolerability could be calculated for within a specific time. Therefore it is an important requirement to find a way to effectively reduce the total simulation time.

One interesting aspect that could help with this is the existence of equivalent scenarios. Two shading scenarios are considered equivalent if the resulting IV characteristics (and therefore subsequent operating power P_{MPP}) of the module are the same for both. Based on the configuration of the module (and the resulting sections), there may be a number of equivalent scenarios that could exist.

To explain what is meant by equivalent scenarios, take an example of a module with 72 cells in series in a 12x6 configuration, having 3 bypass diodes, each covering 24 cells in series (this can also be thought of each covering 2 columns of cells, in a [2 2 2] layout). Take this module to be split into 12 sections in a 4x3 configuration. An illustration can be seen in figure 4.2. In this figure, the orange vertical lines split the module into the three strings which are each connected to a bypass diode. As can be seen from the figure, each of the 12 sections contains 6 cells.

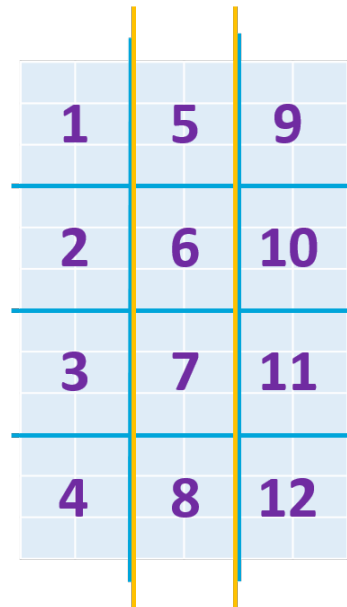


Figure 4.2: 72 cell module, 12 rows, 6 columns, 3 bypass diodes, split into 12 sections in a 4x3 configuration.

Now, take the example of one section shaded. One section can be shaded in 12 different ways (either section 1 is shaded, or section 2, or section 3, and so on). In figure 4.3, 4 of the different ways one section can be shaded are illustrated.

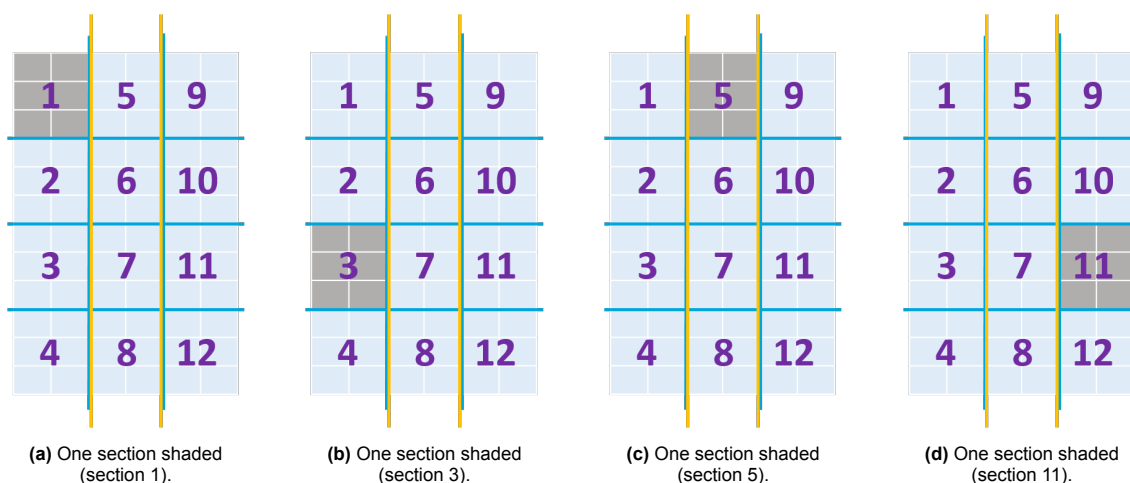


Figure 4.3: Various possible shading scenarios for one section shaded in a 72 cell module split into 12 sections.

What should be noted from this illustration, is that all the 4 (and subsequently all 12) scenarios can

be considered equivalent. This is because no matter which of the 12 sections is shaded, the case is always 6 cells shaded within a bypass diode string (a string of 24 cells in series, connected to a bypass diode). So whether section 1 is shaded, or section 3, 5, or 11, the impact on the resulting output power should be the same. Therefore, for 1 section shaded, in this specific case, there are 12 possible shading scenarios, but since they are all equivalent, there is only one resulting unique scenario.

Another example with two sections shaded can be seen in figure 4.4. For two sections shaded, there are 66 possible scenarios (this is calculated using combination theory: $\frac{12!}{(12-2)!2!} = 66$). In figure 4.4, 6 possibilities are shown.

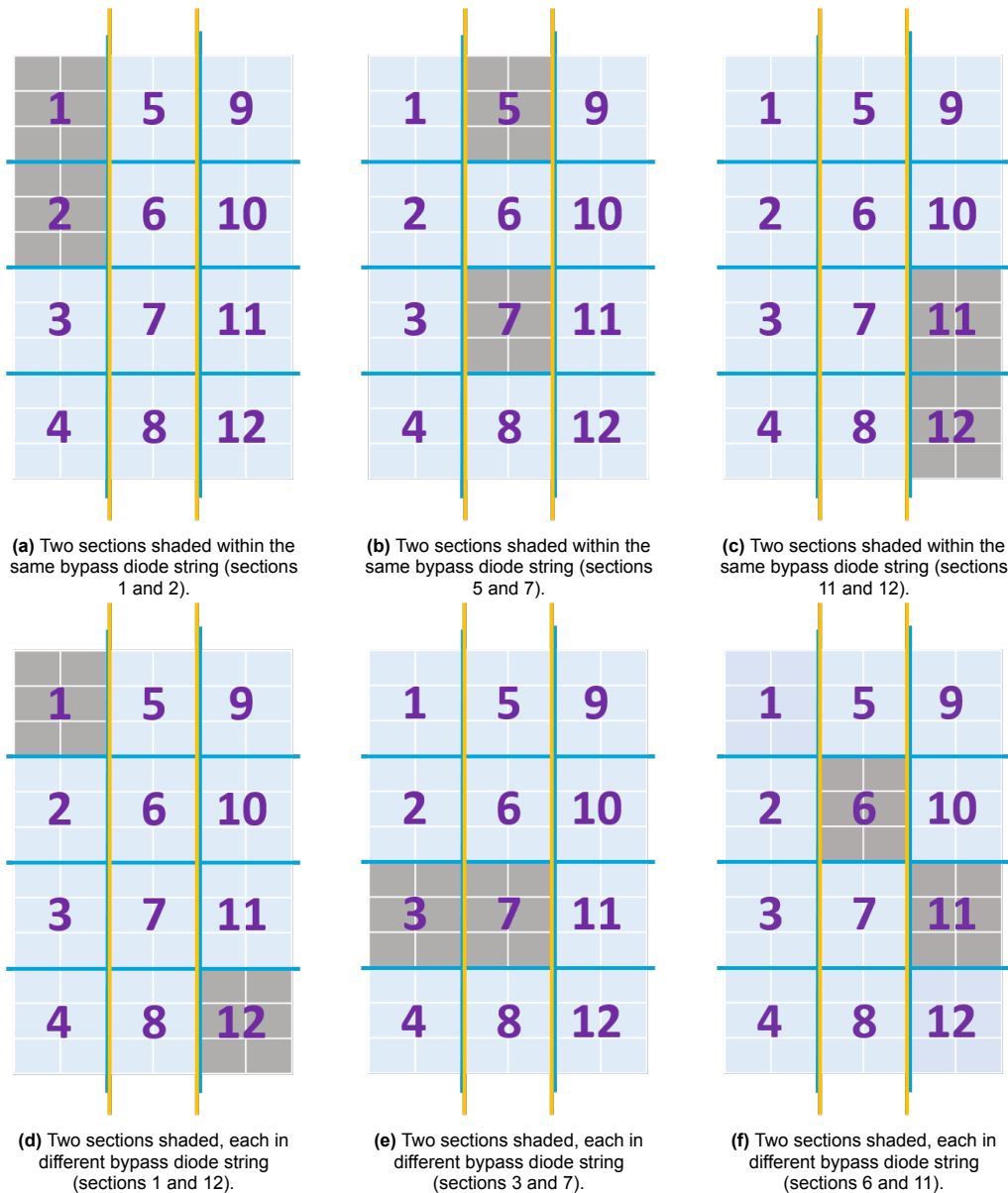


Figure 4.4: Various possible shading scenarios for two sections shaded in a 72 cell module split into 12 sections.

As is illustrated, there are only 2 possible ways in which 2 sections (out of the 12 sections) can be shaded in this specific scenario. Either both shaded sections are within one bypass diode string, as depicted in figures 4.4a-4.4c, or each of the two shaded sections is in a different bypass diode string (figures 4.4d-4.4f). Therefore out of the 66 possible scenarios for 2 sections shaded, there are only two unique scenarios, with the rest being equivalent (to be precise, there are 18 equivalent scenarios

for 2 sections being shaded within the same bypass diode string, and 48 equivalent scenarios for each being in a different string).

With these two examples, the existence of equivalent scenarios has been demonstrated for one section or two sections shaded. Similarly for any n number of sections shaded (with n being any integer value from 0 to 12, inclusive), there exist a number of equivalent scenarios for each. It is important to note here that the type and number of equivalent scenarios depends on the module and its configuration, the configuration of the bypass diodes, and the configuration of how the module is split into 12 sections.

As mentioned earlier, equivalent scenarios by definition mean that the IV characteristics and subsequent operating power (P_{MPP}) are the same for each respective scenario. In this way, equivalent scenarios can be taken advantage of to reduce the required simulation time for the shading tolerability calculator. Instead of having to simulate the IV characteristics/ P_{MPP} value for each of the 4096 scenarios as mentioned earlier, it would be enough to just calculate/run the simulation once per unique scenario, and duplicate it for the number of equivalent scenarios that exist. Based on the examples given above, the impact on simulation time can already be seen. For one section shaded with the configuration in the given example, instead of running the simulation 12 times, it would only need to be run once, reducing the simulation time for this scenario from around 20 mins to 1.75 mins. Similarly for 2 sections shaded, simulation time would be reduced from around 1.75 hours (for 66 scenarios), to approximately only 3.5 mins (for 2 unique scenarios). This would be different for modules with different configurations but, as can be seen, it results in a significant reduction on required simulation time, which is a great advantage.

4.3. In search of symmetry

As explained, the presence of equivalent scenarios really makes a considerable impact in reducing the time required for simulation. Since one of the goals is to have a calculator that can relatively quickly compute shading tolerability for a number of modules, reducing the time for simulation is of utmost importance.

4.3.1. Symmetry when splitting

The number of equivalent scenarios, as explained, depends on the configuration of the module and its components, as well as the configuration on how it is split into 12 sections. The more symmetrical the module and the sections are, the more equivalent scenarios there should be. Given this, it was decided to add to the model the ability to find out the most symmetrical way to split a given PV module. In this way, the number of equivalent scenarios is maximised, and the required simulation time minimised. In this section, the modeling of how to determine how to split a module as symmetrically as possible will be explained.

First it is considered that splitting a module into 12 sections can be done in either a 3x4 or 4x3 configuration, therefore these are the two configurations to choose between. The inputs to this part of the model are the number of cells in the PV module (N_s), the number of rows and number of columns in the module, the number of bypass diodes, and the configuration of the bypass diodes. Then, based on each splitting configuration, 3x4 or 4x3, the following options are checked in order and the configuration is chosen if the conditions are satisfied (with the most symmetrical option being first, and each subsequent option getting less symmetrical).

1. **The module is completely equally split.** This means that each section contains full cells (no cells are cut in half), and that each of the 12 sections is contained within a single bypass string (all cells within each section belong to the same bypass diode string).
2. **The module is split with a granularity of 0.5, keeping within bypass diodes.** This means that each section can contain cells that are either full cells or cut in half, and that each of the 12 sections is contained within a single bypass string.
3. **The module is split with a granularity of 0.5, across a bypass diode string.** This means

that each section can contain cells that are either full cells or cut in half, and sections can be distributed equally across two bypass strings.

In order to illustrate how this works, a few examples will be given. Consider the 72 cell module shown earlier, with 72 cells in series, in a 12 rows x 6 columns configuration, with 3 bypass diodes each covering 24 cells in series. Both configurations of splitting 3x4 and 4x3 are checked against this module, taking into account the conditions laid out above.

First option 1 is checked with both configurations.

- With a configuration of 3x4, as can be seen by figure 4.5a, option 1 is not satisfied, since the second and fifth columns of cells are split in half. Therefore, each section contains cells that are split in half.
- However, with a configuration of 4x3, as can be seen by figure 4.5b, all conditions of option 1 are satisfied. No cells are split in half, and each section lies within a single bypass diode string.

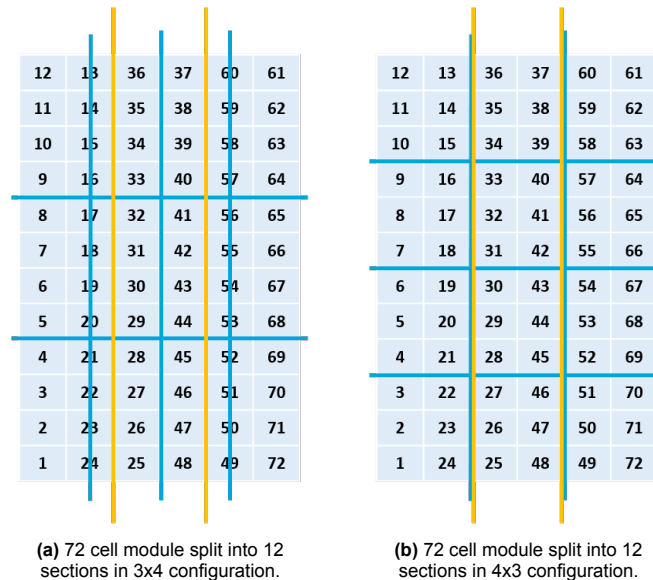


Figure 4.5: 72 cell module split into 12 sections in 3x4 or 4x3 configuration- checking most symmetric splitting configuration.

Since option 1 is the most symmetric option, the model stops checking here, and selects the 4x3 configuration to split the module into 12 sections.

It should be noted that, when splitting the module into 12 sections, the model numbers each section (as can be seen in figure 4.2), and notes the numbers of the cells that are within that section. For example, from figure 4.2 and figure 4.5b, it can be seen that section 1 contains the cells 10 to 15. Based on the splitting of the module, the model also notes which cells are cut in half (if any). For example, if the module was split as shown in figure 4.5a, columns 2 and 5 are split in half vertically, so cells 13 to 24 and cells 49 to 60 are split in half during the sectioning. This means that section 1 in this case has the cells 9 to 16, but cells 13 to 16 are cut in half, with only half of each of them within this section. This information becomes important when assigning irradiance levels to each cell based on the shading scenario, which will be discussed later in this chapter.

In a similar way this is done for other configurations. Figure 4.6 shows a few different examples illustrating the results of checking for symmetry when splitting for different configurations of PV modules.

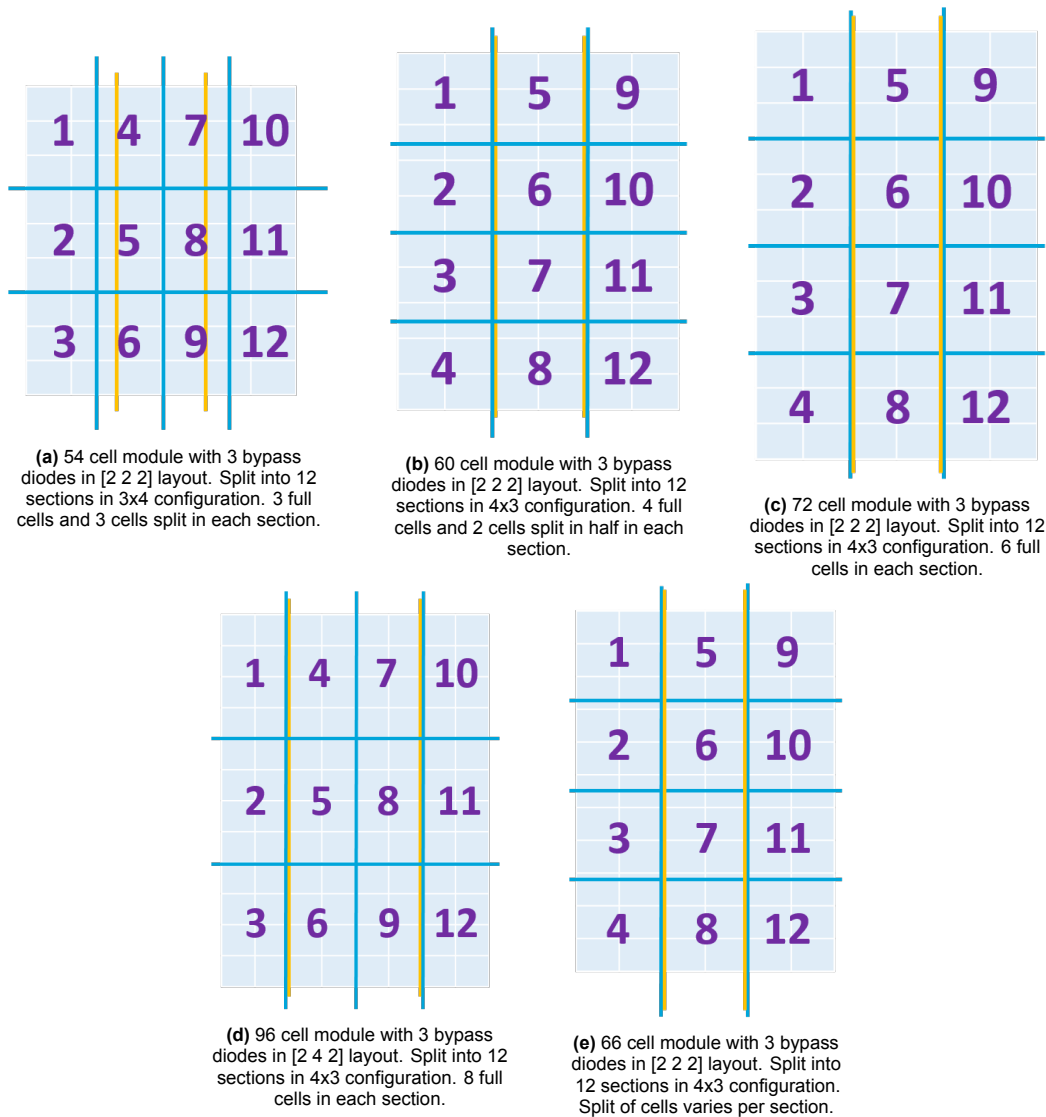


Figure 4.6: Examples of splitting of various configurations of modules and resulting sections.

Here the different possible splitting configurations when taking symmetry into account (as explained at the beginning of this section) are illustrated. For example, figure 4.6b shows the case of a 60 cell module which is split with a granularity of 0.5, keeping within bypass diodes. Here, each section contains 4 full cells and 2 cells split in half (thereby the granularity of 0.5). Figure 4.6a shows the case where a 54 cell module is split with a granularity of 0.5, across a bypass diode string. It can be seen that sections 4 to 9 contain cells that belong to two different bypass strings. Cells are also split in half in this case. Figures 4.6c and 4.6d show cases where the module is completely equally split (no cells are split and all sections are within a single bypass diode string). One point to note is the last example given here in figure 4.6e, which is a 66 cell module with 3 bypass diodes in a [2 2 2] layout. Currently the model is not optimized for cases like this, where the module cannot be split in any of the three ways defined earlier for the best symmetry. The splitting of this module in a 4x3 configuration as shown would result in the split of cells varying between sections. For example section 1 has 4 full cells and 0.75 of 2 cells each. Whereas section 3 has 4 full cells, 0.25 of 2 cells each, and 0.5 of a different 2 cells each. In this case, the symmetry of the sections decreases, illustrating the importance of splitting at a 1 or 0.5 level whenever possible (as opposed to 0.25, 0.3, 0.75, etc.).

Now that the modules have been split as symmetrically as possible, the next step is to consider the specific symmetries of the module to check for equivalent scenarios.

4.3.2. Vertical Symmetry

Each of the scenarios are represented in MATLAB through a binary format. In a specific shading scenario, if a section is unshaded, it is represented by a 0, and if it is shaded then by a 1. All 4096 possible shading scenarios are modeled in MATLAB by taking into account all the possible ways 1 section can be shaded, 2 sections can be shaded, and so on until 12 sections. An example showing certain shading scenarios can be seen in figure 4.7.

	1	2	3	4	5	6	7	8	9	10	11	12
<u>1</u>	0	0	0	0	0	0	0	0	0	0	0	0
<u>2</u>	1	0	0	0	0	0	0	0	0	0	0	0
<u>3</u>	0	1	0	0	0	0	0	0	0	0	0	0
...
<u>1500</u>	0	0	0	1	0	1	1	0	1	1	0	0
<u>1501</u>	0	0	0	1	0	1	1	0	1	0	1	0
...
<u>4096</u>	1	1	1	1	1	1	1	1	1	1	1	1

Figure 4.7: Examples of shading scenarios for 12 sections and 2 possible irradiance levels.

Therefore, for example, in scenario 3, only section 2 is shaded, and all the other sections are unshaded; in scenario 1500, sections 4, 6, 7, 9, and 10 are unshaded, while the rest are unshaded, and so on. These examples can be seen in figure 4.8.

1	5	9
2	6	10
3	7	11
4	8	12

(a) Shading Scenario 2

1	5	9
2	6	10
3	7	11
4	8	12

(b) Shading Scenario 1500

Figure 4.8: Shading Scenarios Examples.

Take as example a 96 cell module, in a configuration of 12 rows by 8 columns. This specific example of module has 3 bypass diodes in a [2 4 2] configuration. This essentially means that the first bypass diode covers 2 columns of cells (so 24 cells in series), the second diode covers 4 columns (48 cells), and the last diode covers 2 columns (24 cells). Figure 4.9 shows the module and the table of scenarios showing examples from before as a reference. The numbers in the top row of the scenarios table correspond to the number of each section as shown in the figure of the module on the left.

A main point to be noted here is the vertical symmetry of the sections. What this means essentially, is that in any vertical column of sections, all sections within that column are equivalent. For example, in the first column, each section (1, 2 and 3) has 6 full cells within the first bypass string. In the second column, each section (4, 5 and 6) has 6 full cells within the second bypass string (and so on). There-

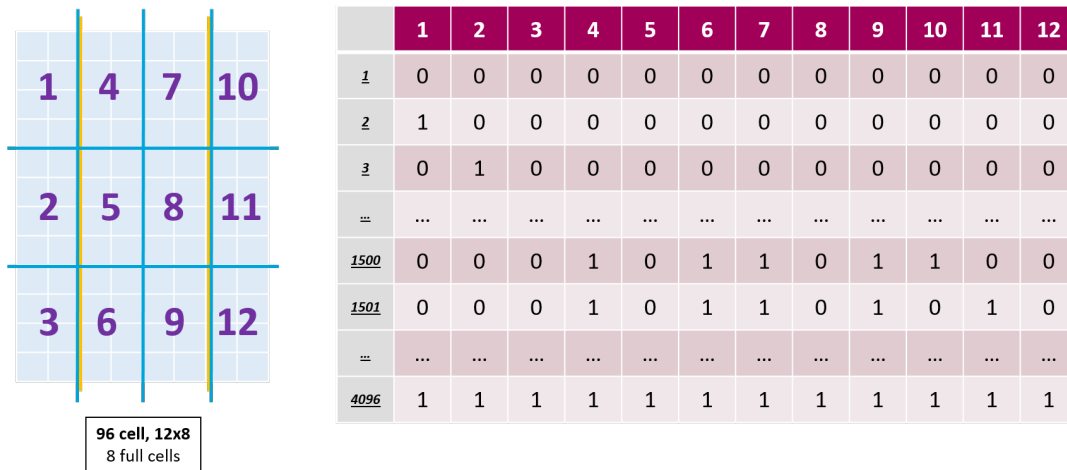


Figure 4.9: 96 cell module, 12 rows x 8 columns, 3 bypass diodes in a [2 4 2] configuration (covering 24 cells, 48 cells, 24 cells in series, respectively), and scenarios example table.

fore there are a number of equivalent scenarios here taking into account the vertical symmetry of the split module. The way this is modeled is as follows. First the scenarios are reshaped into the same configuration as the sectioned module. In figure 4.10, three specific scenarios are taken as examples: Scenarios 2, 3, and 1500. C1, C2, C3, and C4 represent the columns of sections in the module. Based on the numbers of each section, every scenario (each of which is a 1x12 array) is reshaped into the same configuration as the split module (in this case a 3x4 matrix), as shown in the figure.

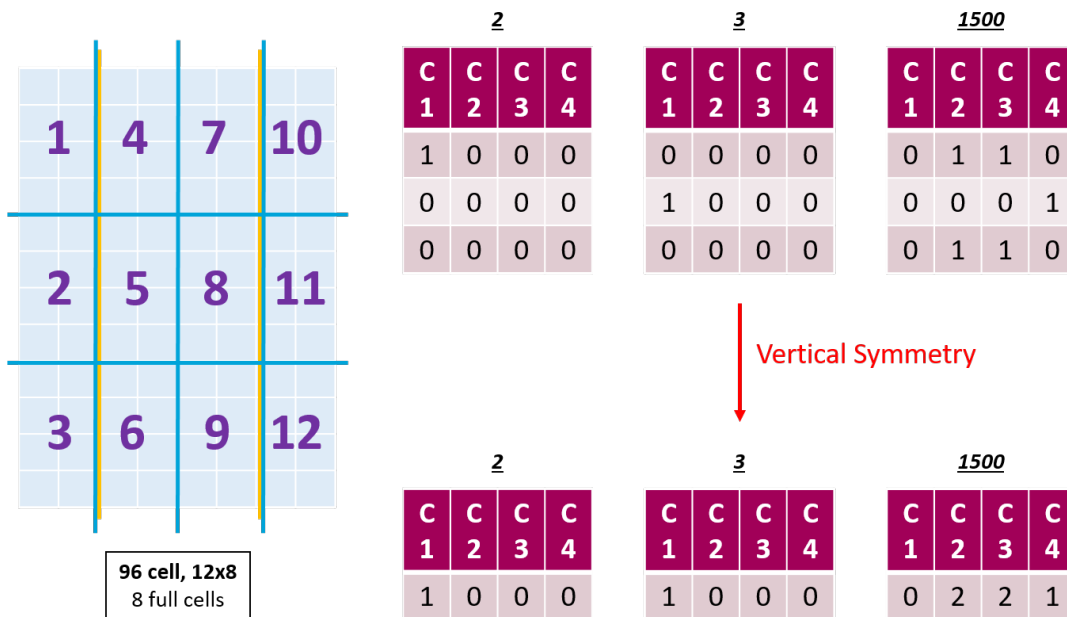


Figure 4.10: 96 cell module, 12 rows x 8 columns, 3 bypass diodes in a [2 4 2] configuration (covering 24 cells, 48 cells, 24 cells in series, respectively), with reshaped scenarios and vertical symmetry impact illustrated.

In the next step, the effect of using a binary format to represent shaded and unshaded sections is demonstrated. Since every column has vertical symmetry, as explained, what this means is that which specific section is shaded in the column does not matter, only the number of sections shaded does. So for example, in the first column, whether section 1 and 2 or section 1 and 3 or section 2 and 3 are shaded, all would have the same effect. It only matters that 2 sections in the first column are shaded. Taking this result of vertical symmetry into account, the sum of each column is taken, to get the number

of sections shaded in each column. The results for the given scenarios can be seen in figure 4.10.

Based on this, the results of modelling the vertical symmetry are shown. Scenario 2 has only section 1 shaded, while scenario 3 has only section 2 shaded, and therefore they initially are different scenarios. However, taking vertical symmetry into account, it can be seen that scenarios 2 and 3 are equivalent scenarios. This is done for all scenarios, with the model counting and removing duplicates, to arrive at the unique scenarios (with respect to vertical symmetry) and the number of times each occurs. In this case, for this specific type of 96 cell module, taking vertical symmetry into account reduces the number of scenarios to be calculated from 4096 scenarios to 256 unique scenarios. This is a significant reduction which considerably reduces the required simulation time.

Vertical symmetry is observed in all the types of modules considered in this work specifically (and is observed in general if sections either do not split cells, or split them exactly in half), and therefore is applied as a first step in checking for equivalent scenarios in the model.

4.3.3. Additional Symmetry

After the application of vertical symmetry, the next step is to check for additional symmetry based on the configuration of the specific module being considered and its sections. There are two types of equivalencies that can exist between sections: sections can be either equal or equivalent. The way this is classified is as follows:

- **Equal sections:** This means that the sections have the same number of cells (same number of full cells and same number of half cells), and essentially fall within the same bypass string (or have the same ratio between the same two bypass strings).
- **Equivalent sections:** This means that the sections have the same number of cells (full and half), but can fall in different bypass strings, as long as the respective bypass strings have the same size/configuration.

Once again, to illustrate the above, an example can be seen with the same 96 cell module discussed before. As mentioned earlier, this module has three bypass diodes covering 24, 48, and 24 cells respectively. As can be seen in figure 4.10, based on the configuration of this module:

- The first column (C1) lies within the first bypass diode string
- Both the second and third column (C2 and C3) lie within the second bypass diode string
- The fourth column (C4) lies within the third bypass diode strings

Therefore, based on the defined classification, column 1 (C1) sections and column 4 (C4) sections are equivalent. This is because bypass diode strings 1 and 3 are of equal sizes (both have 24 cells each). However, the second bypass diode string is of a different length, having 48 cells, therefore the sections in this string are not equivalent to those in bypass diode strings 1 and 3. This can be explained briefly by the fact that if one section in C1 or C4 is shaded, this is 6 cells shaded within a bypass diode string of 24 cells in series, whereas if one section in C2 (or C3) is shaded, it will be 6 cells shaded within a bypass diode string of 48 cells in series. Therefore the impacts of these two scenarios on the module output will be different.

Sections in columns 2 and 3 (C2 and C3), on the other hand, are considered equal. This is because they both fall within the same bypass diode string (2). Equal sections imply they can be added together. For example, if two sections in C2 are shaded versus if one section in C2 and one section in C3 are shaded, both scenarios mean 12 cells are shaded within the same bypass string of 48 cells. Therefore, shaded sections in C2 and C3 can be added together to check for duplicate scenarios.

An example illustrating equal sections vs equivalent sections for this module is given in figure 4.11.

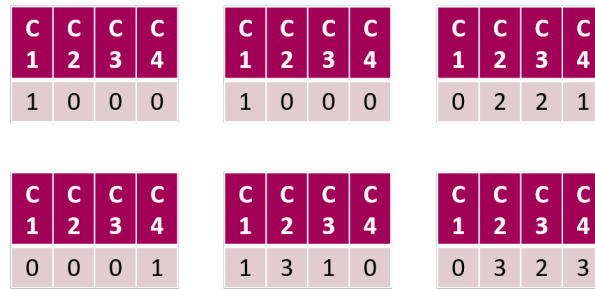


Figure 4.11: Examples showing equal vs equivalent sections in 96 cell module (12 rows x 8 columns, 3 bypass diodes in a [2 4 2] configuration).

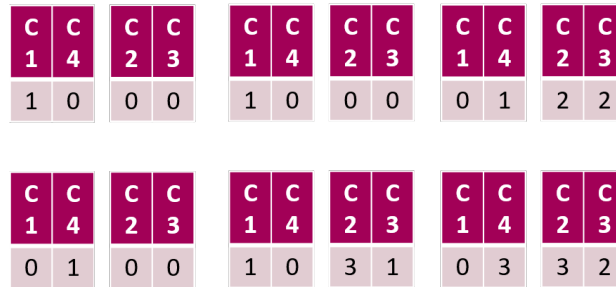
Equivalent scenarios cannot be added together to check overall equivalency. This can be explained by the fact that two sections shaded in C1 (12 cells shaded within one bypass string of 24 cells) does not have the same impact as one section shaded in C1 and one section shaded in C4 (6 cells each shaded in different bypass strings of 24 cells each). Since the order between equivalent columns/-sections does not matter, the way equivalent sections are dealt with in MATLAB is through the use of sorting. The sorting functions in MATLAB allow to effectively check for duplicate scenarios.

Once again, this can be better illustrated through the use of an example. Consider the six scenarios shown in figure 4.12a.

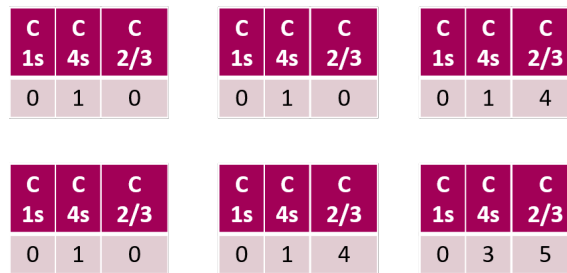
As shown in figure 4.12b, the columns are separated into two groups: C1 and C4 (which are equivalent to each other), and C2 and C3 (which are equal to each other). Then, as can be seen in figure 4.12c, the equivalent columns, C1 and C4, are sorted, whereas the equal columns, C2 and C4, are added together. Then, the columns are put back together. Now, the model can check for duplicate scenarios.



(a) Six example shading scenarios (after consideration of vertical symmetry) for 96 cell, 12 rows x 8 columns module with 3 bypass diode in [2 4 2] configuration.



(b) Splitting of columns in scenarios based on whether they are equivalent or equal.



(c) Final scenarios after equivalent and equal sections symmetry taken into account, showing duplicate scenarios.

Figure 4.12: Example showing further symmetry of module taken into account to determine all duplicate scenarios.

As can be seen from figure 4.12c, the top left, top middle, and bottom left scenarios are duplicate ones. The top right and bottom middle scenarios are also duplicate. The top right scenario had zero sections shaded in C1, 2 sections shaded in C2, 2 sections shaded in C3, and 1 section shaded in C4. Whereas, the bottom middle scenario had one section shaded in C1, 3 sections shaded in C2, 1 section shaded in C3, and zero sections shaded in C4. Once the sorting and adding of equivalent and equal columns, respectively, is done though, these two are visibly duplicate scenarios.

Once again, the model then checks for duplicates, after equivalent and equal sections are taken into account, and removes and counts them. At this point, it is important to note that the counts of duplicate scenarios from the previous vertical symmetry step also need to be taken into account here, to conserve the total number of scenarios. The total number of counts (and thus scenarios) should always sum up to the total possible scenarios, which is 4096 for the case of 12 sections and 2 irradiance levels.

For this specific example, this second symmetry/checking for duplicates step reduces the number of unique scenarios further down from 250 to a final 70 unique scenarios. This is a considerable reduction from the initial 4096 scenarios. Required simulation time decreases from the initial estimate of 120 hours for each module to around 2 hours instead, an extremely significant reduction. Thus, the goal of reducing simulation time has been achieved. This will allow for more modules to be tested under more shading scenarios.

Overall time reduction

The process of checking for equivalencies and duplicate scenarios is carried out for all module tested. A summary showing the results for the most common series configurations can be seen in table 4.1.

Table 4.1: Reduction in simulation times when taking duplicate scenarios due to symmetry into account for various module configurations.

N_s	Row	Col	Bypass Diodes	Bypass Diode Config	Split Config	Total Scenarios	Scenarios after Vertical Symmetry	Final Unique Scenarios	Initial Time (hours)	Final Time (hours)
72	12	6	3	[2 2 2]	4x3	4096	125	35	100 - 135	~1
60	10	6	3	[2 2 2]	4x3	4096	125	35	100 - 135	~1
96	12	8	3	[2 4 2]	3x4	4096	250	70	100 - 135	2.25
96	12	8	4	[2 2 2 2]	3x4	4096	256	35	100 - 135	~1
54	9	6	3	[2 2 2]	3x4	4096	250	100	100 - 135	2.75
48	8	6	3	[2 2 2]	4x3	4096	125	35	100 - 135	~1

As can be seen, the impact of checking and removing duplicate scenarios is significant in reducing the overall simulation times. At the end of this part of the model the details of each unique shading scenario and the number of times it occurs is available. Using these results, the next and final step can be commenced, which is the calculation of the shading tolerability parameter.

4.4. Shading Tolerability Calculation

For the shading tolerability calculation, as mentioned earlier, the final IV characteristics, and specifically, the P_{MPP} point are required for every possible scenario. In this section, how this value is calculated, and consequently, how the shading tolerability parameter is calculated, will be discussed.

4.4.1. Calculation of P_{MPP} for each shading scenario

As mentioned in the previous section, the final result gives every final unique scenario with the number of times each occurs. In this section, the development of the irradiance and cell temperature matrices with respect to each scenario will be discussed.

The IV characteristics are calculated on the basis of the irradiance matrix as an input (as well as the consequent cell temperature matrices, which will be discussed next). Therefore, while the shading scenarios have been determined, these now need to be converted to irradiance matrices.

An irradiance matrix is a $1 \times N_s$ array (where N_s represents the number of cells in the module), where each cell represents an irradiance value for the respective cell of the module. Based on the considerations for the shading scenarios, it is assumed that the shaded sections are facing an irradiance level of $100 W/m^2$ while the unshaded sections are facing $1000 W/m^2$, as has been defined at the beginning of this chapter.

The model determines which sections are shaded based on the specific shading scenario. The final scenarios give the number of sections shaded in each column (or in each bypass string). Based on this the specific sections shaded in each column/bypass string are assigned arbitrarily. Since the sections within a column/bypass string are either equal or equivalent, it does not matter which specific sections are shaded, as long as the total sections shaded are correct.

As explained in section 4.3.1, one of the functions of the model is that the cells and their ratios within each numbered section are determined when sectioning the module. So the number ID of each cell in the section, as well as whether it is a full cell or whether it is split in half is noted. This is important in this step, as based on the number IDs of the sections shaded, the specific number IDs of the cells which are shaded can be determined. This allows the model to assign the value of $100 W/m^2$ to those cells

in the irradiance matrix (based on their number IDs). An important point to note here is also whether the cell in the section is split in half or not. If a cell is split in half between two sections, then the final irradiance on that cell is dependent on the irradiance level on each half of the cell, which could be different if one of the sections is shaded while the other is unshaded. The final irradiance on the cell is then determined by the irradiance levels on each half of the cell, using the method of less than cell level shading as explained in section 2.5.2.

In this way, the final irradiance matrix giving the irradiance level for each cell in the module is calculated for each unique shading scenario.

Similarly, the cell temperature matrices for each shading scenario are determined. Using the irradiance level on each cell for the respective shading scenario, the temperature of each cell is calculated through utilization of the NOCT method, as explained in section 2.4.2.

Using the irradiance and temperature matrices obtained for each shading scenario, the IV characteristics and P_{MPP} of each scenario can now be calculated using the IV characteristics simulation model developed (explained in chapter 2). The final results are the final unique scenarios, the P_{MPP} of that scenario, and the number of times that scenario occurs.

4.4.2. Calculation of shading tolerability parameter

Shading Tolerability Parameter

The calculation of the shading tolerability parameter was briefly introduced in section 1.2.

The performance of a PV module is characterized by the amount of power it can produce. This is commonly referred to as the operating power, and is given by the maximum power point P_{MPP} (which changes based on the operating conditions). The P_{MPP} under STC conditions is referred to as the nominal power of the module. To take a simple example, consider two modules having the same nominal power operating under the same conditions. The module which has a higher operating power (P_{MPP}) under those conditions then can be thought to be the better performing one. This is essentially the philosophy behind the mathematical expression for the calculation the shading tolerability of a PV module (in addition to the probability aspect, also briefly explained in section 1.2).

As already shown in section 1.2, the equation for ST (shading tolerability) is given by equation 4.3 below [28].

$$ST_{(i,c)} = \frac{1}{P_{mod_{mpp}}} \sum_{k=1}^{k=i^c} P_k\left(\frac{1}{i^c}\right) \quad (4.3)$$

where:

- $ST_{(i,c)}$: shading tolerability
- c : total number of cells (or sections) the PV module consists of (whatever is considered the smallest possible area that can be shaded)
- i : number of irradiance levels
- P_k : maximum power at each shading profile [W]
- $P_{mod_{mpp}}$: maximum power of the PV module (at STC) [W]

It is considered that a module with a higher value of ST has a better performance when shaded [28]. The equation for ST considers the P_{MPP} of every possible shading scenario for i irradiance levels and c cells/sections of the module, and essentially takes the average of the P_{MPP} with respect to the total possible number of scenarios (i^c). Dividing by the nominal power of the module $P_{mod_{mpp}}$ allows to standardize the obtained value, and thereby be able to compare different PV modules which have different nominal powers [28].

Ideally this calculation should be done with $i \rightarrow \infty$, but that is not practically measurable [28]. As per the explanation in section 1.3, however, it was proven by Ziar et al. that a module that has higher ST with two irradiance levels ($i = 2$) will also have a higher ST as $i \rightarrow \infty$, as shown in equation 4.4.

$$ST_{(i=2,c)}^{(Module_1)} > ST_{(i=2,c)}^{(Module_2)} \Rightarrow ST_{(i \rightarrow \infty, c)}^{(Module_1)} > ST_{(i \rightarrow \infty, c)}^{(Module_2)} \quad (4.4)$$

Therefore, as explained earlier, it is enough to measure ST for $i = 2$ and use it instead of ST for $i \rightarrow \infty$ [28].

ST calculation

With the above proved, the shading tolerability calculation can now finally be carried out. For this work, since the module was split into 12 sections for the shading scenarios, $c = 12$. With two irradiance levels (shaded = 100 W/m^2 and unshaded = 1000 W/m^2), $i = 2$.

To perform the calculation, the results of the modeling of the shading scenarios will be used. As stated earlier, the results of modeling are the the final unique scenarios, the P_{MPP} of that scenario, and the number of times that scenario occurs. Taking this into account, consider the slightly reworked ST equation given in equation 4.5:

$$ST_{(i,c)} = \frac{1}{P_{mod_{mpp}}} \frac{1}{s_{u_{total}}} \sum_{u=1}^{u=u_{total}} P_{mpp_u} \cdot s_u \quad (4.5)$$

where

- u represents each unique scenario
- P_{mpp_u} is the maximum power value at the respective unique scenario u
- s_u represents the number of times the respective unique scenario u occurs
- $s_{u_{total}}$ is the total number of scenarios, which is simply equal to i^c (which is $2^{12} = 4096$ in this case)

Using equation 4.5, as well as the results of the shading scenarios modelling, and the IV characteristics simulations, the ST of a number of modules was calculated in order to make a database of values.

Percentage ST

The value of ST is used as a classification parameter, but there is another parameter that is also defined, which is percentage ST, ST%. ST% is defined by dividing the ST value by its maximum possible theoretical ST value [28]. In order to find this percentage value, it is first necessary to determine the maximum possible ST value, ST_{max} .

As was explained in section 1.2, ST is based on probability distribution. Under any uniform probability distribution, the average irradiance a PV cell faces is 500 W/m^2 (for irradiance levels between 0 and 1000 W/m^2 as defined). Therefore, based on this, the maximum $ST_{(i \rightarrow \infty, c)}$ would be equal to $\frac{1}{2}$. This can be demonstrated considering through an example. Consider figure 4.13 which shows the probability distributions of the irradiance levels when considering $i = 2$ to $i \rightarrow \infty$ [28].

Based on figure 4.13, take the case when $i = 3$ for a single PV cell. Maximum ST would be equal to [28]:

$$ST_{(i=3,c=1)} = \frac{1}{P_{cell}} \frac{1}{3^1} (0 + 0.5 + c \cdot 1) P_{cell} = 0.5 \quad (4.6)$$

It can be shown that this is the same even if the number of cells is two [28].

$$ST_{(i=3,c=2)} = \frac{1}{2 \cdot P_{cell}} \frac{1}{3^2} (0 + 0.5 + 0.5 + 1 + 1 + 1 + 1.5 + 1.5 + 2) P_{cell} = 0.5 \quad (4.7)$$

Therefore, the max ST for a probability distribution where the average irradiance is 500 W/m^2 can be defined as $ST_{max} = 0.5$. It should be noted that since the irradiance level on the shaded cells is considered to be 100 W/m^2 and not zero in this work, ST_{max} will actually be different in this case, as the shading object is passing 10% of the irradiance. Therefore the ST_{max} will increase by 10% and for this work can be defined as:

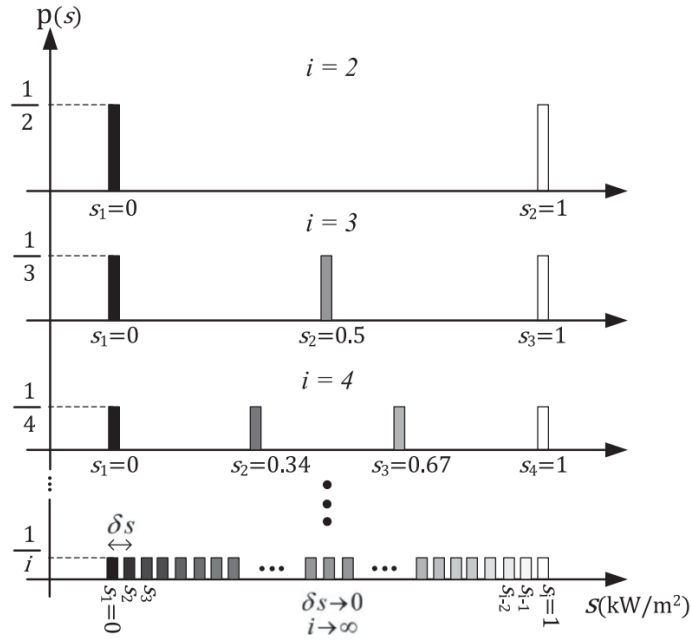


Figure 4.13: Probability distributions of shading of PV module for various numbers of irradiance levels i . Figure taken from [28].

$$ST_{max} = 0.5 + \frac{10}{100} \cdot 0.5 = 0.55 \quad (4.8)$$

Therefore, ST% has been defined by finding the percentage value of ST in this work when compared to the ST_{max} of 0.55.

Lambda coefficient

Ziar et al. also defined a coefficient $\lambda_{(i,c)}$ in order to take into account all the aspects of a PV module that could contribute to better shading tolerability [28]. Equation 1.3 only really takes into account the cells and their configuration (specifically series/parallel) in a PV module. However, there are a number of aspects that could contribute to the shading tolerability of a module. One example is number and type of bypass diodes. Therefore, the variable $\lambda_{(i,c)}$ was designed by Ziar et al. to include in equation 1.3 in order to model such aspects within the ST equation. It is taken into account that this coefficient could be dependent on number of cells, c , and irradiation levels i . In this way, the ST general equation is amended to the following equation 4.9 [28]:

$$ST_{(i \rightarrow \infty, c)} = \lambda_{(i \rightarrow \infty, c)} \frac{1}{n + 1} \quad (4.9)$$

Since $\lambda_{(i \rightarrow \infty, c)}$ could depend on a number of things that differ from module to module, a general mathematical equation for it is difficult to define. However, it was possible to determine the limits of the coefficient. If the additional properties of the PV module to make it more shade tolerant do not have any impact on the ST, this defines the lower limit of $\lambda_{(i \rightarrow \infty, c)}$, which is 1. To find the maximum limit of $\lambda_{(i \rightarrow \infty, c)}$ (in which case it is considered that the unshaded cells in a module are not impacted by the shaded cells), consider as described in section 4.4.2 that ST_{max} under a uniform probability distribution of irradiance levels between 0 and 1000 W/m^2 is 0.5. Therefore, this value can be substituted in equation 4.9, to obtain the limits of $\lambda_{(i \rightarrow \infty, c)}$ [28]:

$$1 \leq \lambda_{(i \rightarrow \infty, c)} \leq \frac{n + 1}{2} \quad (4.10)$$

4.5. Discussion

The modules for which the simulations were run and calculations were done and their parameters, along with their respective ST and ST% values can be seen in Table 4.2.

Modules of various configurations were used for the simulations, with a number of modules being selected for each main configuration, which are the following (these specific configurations were selected as they are the most common configurations for series connected PV modules):

- 48 cell PV module in a 8 rows x 6 columns configuration, with 3 bypass diodes (BD) in a [2 2 2] layout
- 54 cell PV module in a 9 rows x 6 columns configuration, with 3 BD in a [2 2 2] layout
- 60 cell PV module in a 10 rows x 6 columns configuration, with 3 BD in a [2 2 2] layout
- 72 cell PV module in a 12 rows x 6 columns configuration, with 3 BD in a [2 2 2] layout
- 96 cell PV module in a 12 rows x 8 columns configuration, with 3 BD in a [2 4 2] layout
- 96 cell PV module in a 12 rows x 8 columns configuration, with 4 BD in a [2 2 2 2] layout

Module	Cell Tech	N_s	Config	P_{mpp} (W)	BD	BD Con- fig	V_{br}	T_{NOCT}	ST	ST%
Enfoton 48E6	Poly c-Si	48	8x6	180	3	[2 2 2]	-18	47	0.1242	22.58%
PAHAL49Series	Poly c-Si	48	8x6	210	3	[2 2 2]	-18	48	0.1248	22.69%
Aleo S24	Poly c-Si	48	8x6	175	3	[2 2 2]	-18	47	0.125	22.73%
TPL P-48 Series	Poly c-Si	48	8x6	215	3	[2 2 2]	-18	45	0.125	22.73%
Pixon PIX PD2 48	Poly c-Si	48	8x6	200	3	[2 2 2]	-18	45	0.1262	22.95%
Schott Poly 185 DG	Poly c-Si	48	8x6	185	3	[2 2 2]	-18	48	0.1264	22.98%
Anji AJP-M648	Poly c-Si	48	8x6	190	3	[2 2 2]	-18	46	0.1267	23.04%
Pixon PIX MP3 48	Mono c-Si (PERC)	48	8x6	265	3	[2 2 2]	-18	45	0.1268	23.05%
Aleo X55L240	Mono c-Si (PERC)	48	8x6	250	3	[2 2 2]	-18	44.5	0.1283	23.33%
BenQ Green-Triplex PM048M00	Mono c-Si	48	8x6	225	3	[2 2 2]	-18	46	0.1298	23.60%
JSkyE ST54-P230	Poly c-Si	54	9x6	230	3	[2 2 2]	-18	45	0.1218	22.15%
Peimar SG230P	Poly c-Si	54	9x6	230	3	[2 2 2]	-18	45	0.1219	22.16%
TPL P-54 Series	Poly c-Si	54	9x6	235	3	[2 2 2]	-18	45	0.122	22.18%
Tenesol TE 2000	Poly c-Si	54	9x6	200	3	[2 2 2]	-18	45	0.1229	22.35%
TitanM6-54	Poly c-Si	54	9x6	190	3	[2 2 2]	-18	45	0.1231	22.38%
Solarday PX54 250W	Poly c-Si	54	9x6	250	3	[2 2 2]	-18	43	0.1242	22.58%
Anji AJP-M654	Poly c-Si	54	9x6	215	3	[2 2 2]	-18	46	0.1245	22.64%
Tenesol TE 2200	Poly c-Si	60	10x6	220	3	[2 2 2]	-18	45	0.1282	23.31%
Kyocera KU-60	Poly c-Si	60	10x6	270	3	[2 2 2]	-18	45	0.1289	23.44%
Talesun TP660P	Poly c-Si	60	10x6	230	3	[2 2 2]	-18	45	0.1293	23.51%
UPT Solar UPT-C245P60	Poly c-Si	60	10x6	245	3	[2 2 2]	-18	46	0.1296	23.56%
Solarday PX60 290W	Poly c-Si	60	10x6	290	3	[2 2 2]	-18	43	0.1297	23.58%
SunTech STP265S	Mono c-Si	60	10x6	265	3	[2 2 2]	-18	45	0.1299	23.62%
Qcells Q.PEAK-G5.1	Mono c-Si	60	10x6	310	3	[2 2 2]	-18	43	0.1328	24.15%
TPL S-72 Series	Mono c-Si	72	12x6	190	3	[2 2 2]	-18	45	0.1288	23.42%

PVSupers Series 72M	Mono c-Si (PERC)	72	12x6	390	3	[2 2 2]	-18	48	0.1307	23.76%
IberianSolar IBS72P	Poly c-Si	72	12x6	320	3	[2 2 2]	-18	45	0.131	23.82%
Axitec AC-310P/156-72S	Poly c-Si	72	12x6	310	3	[2 2 2]	-18	45	0.1313	23.87%
JASolar JAM72S01	Mono c-Si (PERC)	72	12x6	390	3	[2 2 2]	-18	45	0.132	24.00%
Panasonic VBHN245SJ25	HIT heterojunction cells	72	12x6	240	3	[2 2 2]	-18	44	0.1344	24.44%
Canadian Solar CS6U-335P	Poly c-Si	72	12x6	335	3	[2 2 2]	-18	43	0.1327	24.13%
DMEGC DM395G1-72SW	Mono c-Si (PERC)	72	12x6	395	3	[2 2 2]	-18	42	0.1349	24.53%
SunEarth TDB 250Wp	Mono c-Si	96	12x8	250	4	[2 2 2 2]	-18	46	0.148	26.91%
Topsola TSM96-125M	Mono c-Si	96	12x8	260	4	[2 2 2 2]	-18	45	0.1481	26.93%
Calrays CPM230-A-96	Mono c-Si	96	12x8	240	4	[2 2 2 2]	-18	45	0.1471	26.75%
Canadian Solar CS5P	Poly c-Si	96	12x8	220	4	[2 2 2 2]	-18	45	0.1479	26.89%
Galaxy Energy GS270M-96	Mono c-Si	96	12x8	270	4	[2 2 2 2]	-18	48	0.1484	26.98%
Silevo Triex U305	Triex	96	12x8	305	4	[2 2 2 2]	-18	46	0.1551	28.20%
Panasonic module HIT (VBHN330SJ47)	HIT heterojunction cells	96	12x8	330	4	[2 2 2 2]	-18	44	0.1581	28.75%
Panasonic HIT KURO (VBHN320KJ01)	HIT heterojunction cells	96	12x8	320	4	[2 2 2 2]	-18	44	0.1587	28.85%
BenQ SunForte PM096B00	Mono c-Si (IBC)	96	12x8	320	3	[2 4 2]	-4.5	45	0.1318	23.96%
SunPower SPR-X20-327-BLK	Mono c-Si (IBC)	96	12x8	327	3	[2 4 2]	-4.5	43	0.1336	24.29%

Table 4.2: Shading tolerability parameter results.

In this way, the shading tolerability parameter was calculated for a total of 42 modules as part of this work.

4.5.1. Analysis of results

Figure 4.14 shows the shading tolerability percentage (ST%) of the modules as a function of the total number of cells in the module, as well as the number/configuration of bypass diodes. In this section, possible aspects that could be influencing ST will be explored.

Number of bypass diodes

When comparing similar types of modules, one can compare the 96 cell PV module with 3 bypass diodes (in a [2 4 2] configuration) shown in green vs with 4 bypass diodes (in a [2 2 2 2] configuration) shown in light blue. There is a large difference in the STs of these two types of configurations, with the modules with more bypass diodes having considerably higher STs. This is of course expected to an extent, as for the same configuration of module, an increase in the number of bypass diodes should theoretically increase the shading tolerability of a module, as that is their function. This could also mean that num-

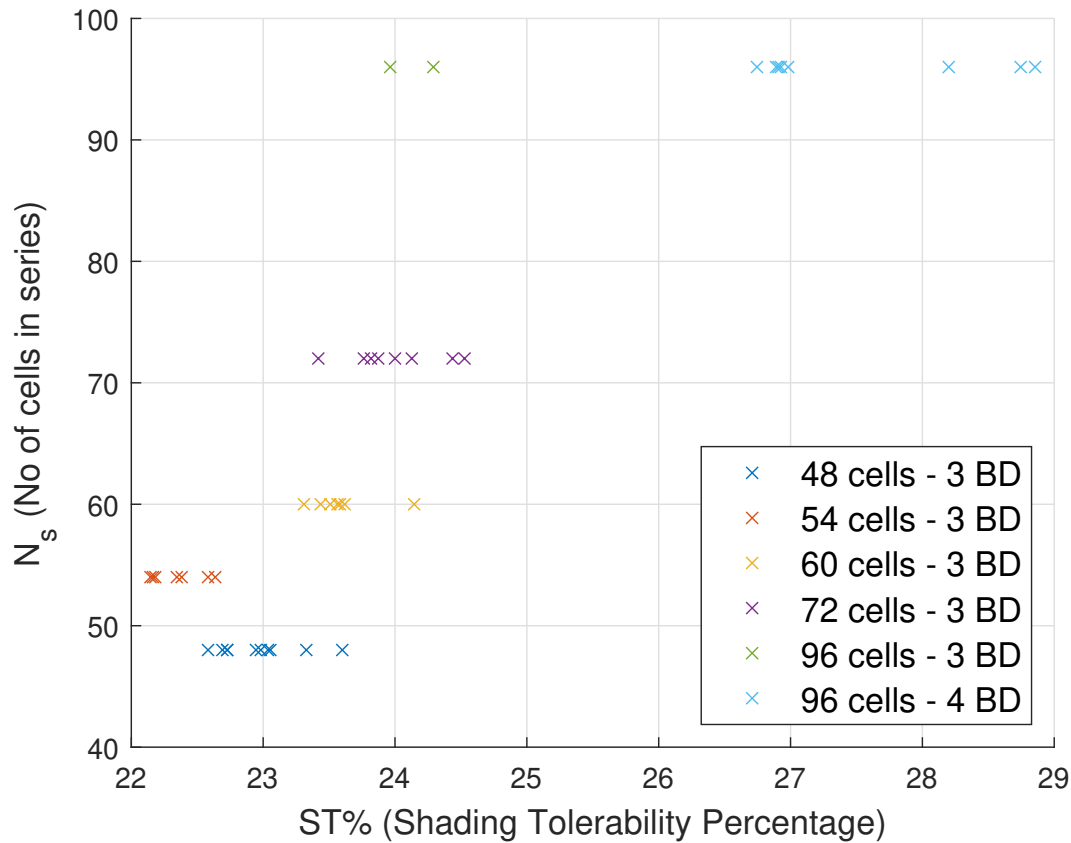


Figure 4.14: Shading Tolerability Percentage (ST%) as a function of N_s (number of cells in series in the PV module) for different PV module and bypass configurations (BD represents number of bypass diodes).

ber of bypass diodes could be one of the factors contributing to coefficient λ as defined in section 4.4.2.

Configuration of module/bypass diodes

It is also interesting to note the significant difference between the ST of the 96 cells modules with 4 bypass diodes (12 rows x 8 columns modules with bypass diodes in a [2 2 2] configuration), with all the rest of the other modules. The range of ST of these specific modules is considerably higher than the rest of the modules seen in this work. This could be because of the double impact of having a different configuration, as well as having more bypass diodes in connection.

Another aspect that can be noted is that there does not seem to be any substantial difference between the 96 cell module with 3 bypass diodes in a [2 4 2] configuration, and for example the 72 cell module with 3 bypass diodes in a [2 2 2] configuration. It could be considered from the results that the 96 cell module with 3 bypass diodes has a slightly higher shading tolerability than for example the 60 cell and 48 cell modules. However, there are not enough data points for this module to make a definitive analysis here (as it a slightly unconventional configuration).

Number of cells in module

One interesting trend is that, while there seems to be some scattering/outliers, figure 4.14 does seem to show that there seem to be clusters of ranges of ST% based on the number of cells/configuration of the PV module. For example, the 48 cell (dark blue), 60 cell (yellow), and 72 cell (purple) modules are similar in the fact that they are all configured with 6 columns of cells and 3 bypass diodes in a [2 2 2] configuration. The only difference between them is the number of rows of cells in the module (8 for

48 cell, 10 for 60 cell, and 12 for 72 cell). Therefore these three types of modules should be able to be compared quite objectively. It can be seen that, based on the clusters and ranges of the values for each type of module, as N_s increases for these modules, so to an extent does ST%. This may show a dependency of shading tolerability of a module of similar configurations on the total number of cells.

This is interesting as in Ziar et al., it was mathematically shown that ST should be inversely proportional to $n + 1$, where n represents the number of series-connected cells [28]. One potential reason for the trend seen here is that the impact of the bypass diode forward voltage drop could have more of an impact on a smaller number of cells (for the same configuration of the module). This is due to the fact that the relative voltage drop would be larger when compared with the voltages of 4 cells in series as opposed to the voltages of 6 cells in series for example. In order to truly see the actual trend with number of cells in series, it could be interesting to check this experimentally and/or on a cell level (with respect to shading).

Cell Technology

One more interesting point to note here is with respect to some of the outliers in certain ranges. For the 60 cell modules for example, almost all of the calculated ST points are clustered around 23.5%, apart from one which is above 24%. Similarly, for the 96 cell module with 4 bypass diodes, once again, most of the ST values are around 26.8%, apart from the three that are greater than 28%. What is interesting to note here is that all 4 of these outliers have 'special' cell technologies described on their datasheets. For example, the two highest ST values for the 96 cell module with 4 bypass diodes belong to Panasonic modules using Panasonic 'HIT heterojunction cells'. These are special heterojunction cells developed by Panasonic which combine crystalline and thin-film technology [90]. It is interesting to note also that one of the two higher STs in the 72 cell module range (the values around 24.5%) also belongs to a Panasonic module using HIT heterojunction technology. The third outlier in the 96 cell, 4 bypass diode modules values belongs to a Triex Silevo module, where the cell technology on the datasheet is listed as 'Triex' cells. These are defined as 'Silevo's proprietary hybrid tunneling junction cell technology' [91]. Finally, the outlier in the 60 cell module ST values, lying above 24% belongs to a QCells PV cell module, which uses Q.ANTUM cells, which apparently has an impact on the cell interconnection, removing the gaps in individual cell rows [92]. Taking these examples into account, it could be theorized that specific cell technologies such as these can have a positive impact on shading tolerability of modules. Once again, cell technology could potentially be a contributor to the coefficient λ as defined in section 4.4.2.

54 cell module results

Another interesting outcome that can be seen from figure 4.14 is that the STs of the 54 cell, 9 rows x 6 columns modules with 3 bypass diodes in a [2 2 2] configuration seem to be the lowest out of all. This could just be due to the configuration of the module. However, there is one other possibility. In the modeling of the sections, this configuration of module is the only one which has sections that span across two bypass diode strings. All the other configurations sections do not have this aspect. This means that the 54 cell module experiences shading scenarios in this model where the shading of one section can impact two bypass diode strings, which does not happen in the other modules. It is not clear whether this is actually the reason why overall ST% calculated is lower than the others, however it could be one of the possibilities.

Temperature coefficients

One further point that was checked was whether there was a correlation between the temperature coefficients for voltage K_V and current K_I for each module, with the ST of that module. The temperature coefficients indicate how the voltages and currents of a PV module are impacted with respect to temperature. PV module voltages generally decrease with increasing temperature (and therefore K_V is negative), while currents generally increase (K_I is positive). The (negative) change in voltage is generally much larger than the respective (positive) change in current. Thereby, the impact on overall power generally has more contribution from K_V than from K_I .

With respect to K_I , no clear correlation was seen with ST. This makes sense since, as explained, the change in current with respect to temperature is not very high (comparatively with voltage), and

thereby should not have too much of an effect on the output power.

However, some interesting results were seen for the correlation of K_V with the ST of the module, when looking at specific configurations. The correlation was checked with the use of the Pearson correlation coefficient. The Pearson correlation coefficient ranges from -1 to 1, representing strong negative correlation to strong positive correlation respectively. A value of 0 indicates that no correlation exists. The results of the calculation of the Pearson correlation coefficient between the two variables can be seen in table 4.3.

Table 4.3: Pearson correlation coefficients when comparing K_V with ST% for each module configuration.

Module Type	Pearson Correlation Coefficient (K_V vs ST%)
48 cell, 8 rows x 6 columns, 3 bypass diodes	0.50
54 cell, 9 rows x 6 columns, 3 bypass diodes	0.55
60 cell, 10 rows x 6 columns, 3 bypass diodes	0.97
72 cell, 12 rows x 6 columns, 3 bypass diodes	0.93
96 cell, 12 rows x 6 columns, 3 bypass diodes	0.97

As is shown in table 4.3, while the smaller modules show a slight positive correlation (while the coefficient is small, there still exists a slight positive correlation), it can be seen that there is an extremely strong positive correlation for the bigger modules. This shows that as K_V becomes more positive (or alternatively, less negative), the ST of the respective module becomes larger. This can be justified, as a less negative value for K_V indicates that there is less loss of voltage at higher temperatures, which in turn indicates there is less loss of power, which should positively impact ST.

One more interesting insight from checking the correlation of K_V with ST is with respect to the high ST outliers discussed in the previous section. As was explained, these outliers for the 60 cell and 96 cell modules seemed to have higher STs than the general range of values that was seen for these configurations. This could be potentially due to the fact that all these outliers were using a 'special' cell technology when compared to the others, which could be contributing to a higher ST based on cell technology. However, here it was also seen that for the Panasonic HIT cells and Qcells Q.ANTUM cells specifically, these modules also had the least negative values of K_V when compared to the remaining modules of the respective configuration. Therefore, the impact of K_V could also be contributing to the higher ST values in these cases. It is however interesting to note that the Triex cells module (another high ST outlier in the 96 cell module group) did not have a less negative K_V , but in fact the most negative K_V when compared to the other 96 cell modules. Therefore, it is not necessary that K_V was the only influence in these outlier cases, and more likely it is some combination of both the cell technology and the K_V . Regardless, from this analysis, it can be concluded that K_V could also be a potential contributor to the coefficient λ .

T_{NOCT}

Another level of correlation that was investigated was whether the T_{NOCT} of a module had any impact on the ST. It was desired to investigate this while making sure no other aspects of the module were contributing to the change in ST. Therefore, one of the modules that ST was already calculated for was considered again with only the T_{NOCT} changed.

The range of T_{NOCT} values that were seen for all the modules considered in this work was from $42^\circ C$ to $48^\circ C$. In order to be able to effectively see whether there was an impact, a module with a T_{NOCT} on one extreme of the range, specifically $48^\circ C$ was chosen. Then, the T_{NOCT} was changed to the other extreme, $42^\circ C$, and the ST was calculated again for comparison. The results can be seen in table 4.4.

Table 4.4: ST calculation for same PV module - modelling impact of T_{NOCT} .

Module	N_s	Config	$P_{mpp}(W)$	BD	BD Config	$T_{NOCT}(^{\circ}C)$	ST	ST%
Schott Poly 185 DG	48	8x6	185	3	[2 2 2]	48	0.1264	22.98%
Schott Poly 185 DG	48	8x6	185	3	[2 2 2]	42	0.1295	23.55%

It can be seen that the ST increased slightly with the decrease of the T_{NOCT} value. This could be explained by the fact that the performance of a PV module generally becomes worse with higher temperatures (when compared to STC temperature). A higher T_{NOCT} value implies that under the same conditions, the operating cell temperature of the module is higher in relation to if the same module had a lower T_{NOCT} . Therefore the performance should also be slightly lower - assuming all other parameters remain the same.

This of course is a theoretical approach to investigating the impact of T_{NOCT} on shading tolerability. In reality, two modules would have many differing parameters apart from T_{NOCT} which could have an impact. Additionally, this impact is based on the utilization of the NOCT model to calculate cell temperature. The effect on ST could differ if a different model/method was used to determine cell temperature.

It can also be seen that the impact of T_{NOCT} in this case is not too high - although this can be attributed to the fact that the range of T_{NOCT} seen in commercial modules is not too large. Regardless, it has been shown that T_{NOCT} does seem to have some impact on ST. In this way, it can be considered that it could also contribute in some way to the λ coefficient.

Other correlations checked

There were also a number of other additional aspects checked to see if there was a correlation with ST. It was explored if the nominal power of the PV module (at STC) had an impact on the shading tolerability of the module. This started with the process of choosing the modules for which to calculate ST for. One of the things kept in mind when choosing modules was to choose a wide range of nominal powers. Then the value of nominal power was checked against the calculated ST. This check was done also specifically for each of the 6 configurations chosen in order to remove the effect of (N_s) which could also be impacting ST. In this way the impact of nominal power could be more objectively observed. However, no apparent correlation was found between the nominal power of the PV module and its calculated ST. This result does also seem to make sense. This is because within the ST calculation there is a normalization with respect to the nominal module power, and therefore it should not be impacting the ST value between modules with different nominal powers.

Another property that was checked for correlation with ST was whether the cell technology being mono c-Si or poly c-Si had any impact. Once again, this was checked overall and for each of the specific configurations considered. However, no clear correlation for either of the two types with the ST value was found in this case either.

4.5.2. ST visualization

Figure 4.15 illustrates the ST of the modules in a visual format, by showing the P_{mpp} as a fraction of the module $P_{mod_{mpp}}$ with respect to the shaded area of the module (based on the number of sections shaded).

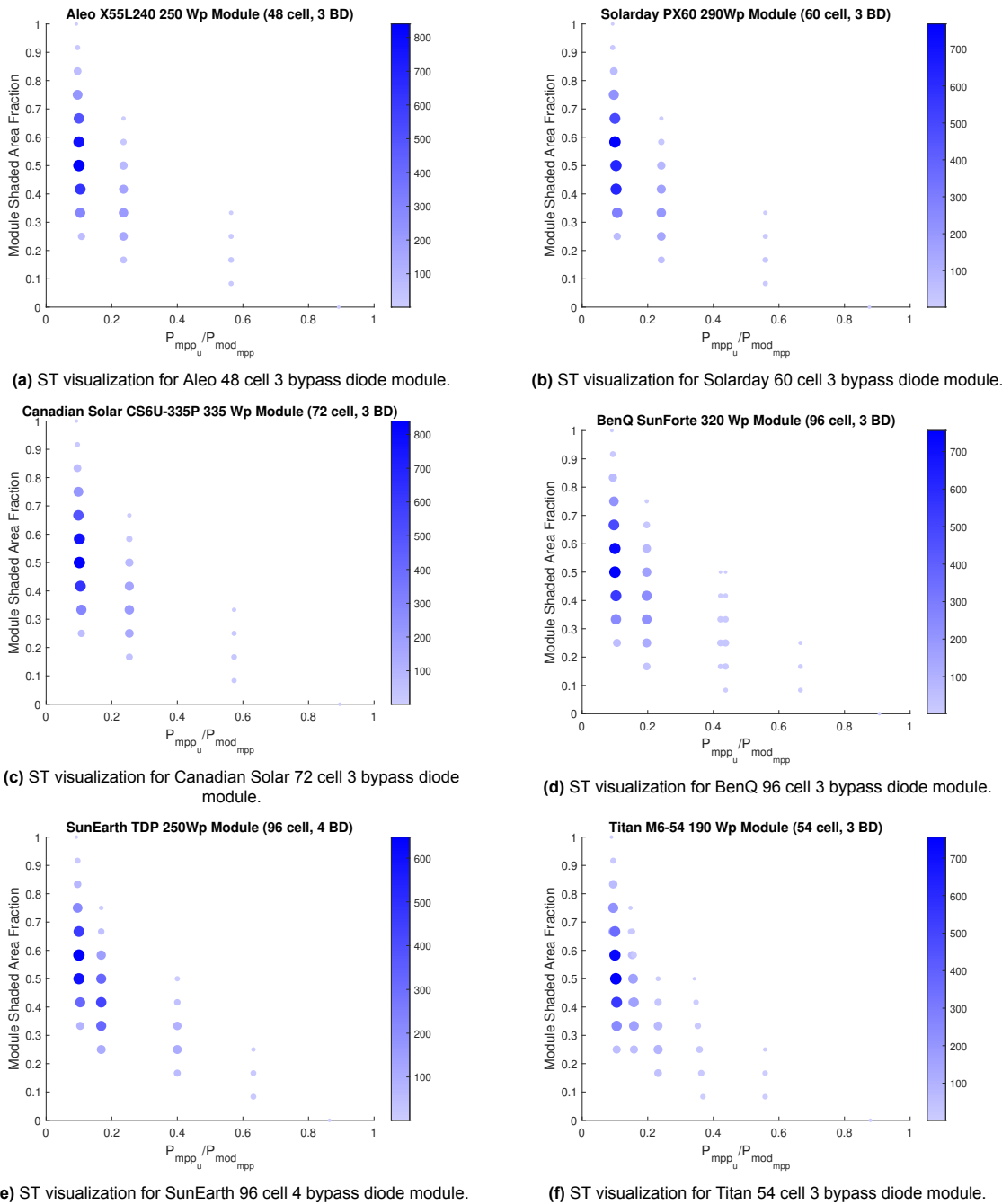


Figure 4.15: Visualization of ST for each module configuration (Module shaded area vs. operating power as a function of module nominal power).

The size and colour of the data points is related to the number of times that value occurs within the 4096 scenarios that exist for 12 sections and 2 irradiance levels. The colorbar on the right side of the figures gives an indication of how the colours of the data points correspond to the number of times (scenarios in which) that data point occurs.

One representative figure is shown for each type of module configuration explored. It can be seen that the 48 cell, 60 cell, and 72 cell modules with 3 bypass diodes have plots which are quite similar, with respect to the data points seen and how many times they occur. This can be expected as these 3 modules have very similar configurations, as well as splitting configurations, with the only difference between them being the number of rows of cells. It can also be seen that these modules seem to have 3

distinct 'lines' of data points, where the same/similar operating powers are attributed to various shaded area fractions. Alternatively, it can also be seen that for the same shading fraction, there exist different operating powers. This is explained by the different ways in the sections (out of the 12 sections) can be shaded. For example, take 3 shaded sections. If all 3 sections lie within the same bypass diode string, the operating power will be much higher than if each of the 3 sections lies within a different bypass diode string (as in the first case only one bypass diode string of cells is affected by shading, whereas in the second the entire module is). It can also be seen that in the latter case, the operating power should be similar to any number of sections shaded, where there exists at least one shaded section in each bypass diode string.

By contrast, the 96 cell module with 4 bypass diodes, the 96 cell module with 3 bypass diodes, and the 54 cell module with 3 bypass diodes have slightly different looking plots with respect to the distribution of data points. Once again, this can be attributed to the different configurations of these modules, as well as to the different ways in which they are split. Some interesting points to note are that the plot of the 54 cell 3 bypass diode seems to be shifted to the left a little bit when compared to the others. This corresponds with how this module seems to have the lowest range of ST% when compared with the other configurations. Similarly the 96 cell modules can also be seen to have more data points towards higher operating power values. However, specifically the 96 cell 4 bypass diode module is the only one which has dark blue data points in the second 'column' (out of four columns) in its plot, corresponding to higher operating powers. This also corresponding to the results seen for ST% where this module had significantly higher ST% values than the others.

It is therefore interesting also to have this view of the visualization of the ST in order to see the points at which the different modules are operating at the most, when subjected to the different shading scenarios.

4.6. Interesting insights on model from results

4.6.1. Example of same module with 3 bypass diodes and 6 bypass diodes

One of the types of modules for considered was a 60 cell module in a 10 rows x 6 columns configuration with 6 bypass diodes (so in a [1 1 1 1 1 1] configuration, with one bypass diode for each column of cells). The results are shown in table 4.5, along with the results for the same modules in a configuration with 3 bypass diodes in a [2 2 2] layout. For these two modules, the datasheets stated that the number of bypass diodes was 3/6. Therefore these modules could have either 3 or 6 bypass diodes depending on which specific model was chosen.

Table 4.5: ST calculation for two 60 cell modules with 6 bypass diodes vs with 3 bypass diodes.

Module	Cell Tech	N_s	Config	P_{mpp} (W)	BD	BD Config	V_{br}	T_{NOCT}	ST	ST%
Talesun TP660P	Poly c-Si	60	10x6	230	6	[1 1 1 1 1 1]	-18	45	0.1203	21.87%
Talesun TP660P	Poly c-Si	60	10x6	230	3	[2 2 2]	-18	45	0.1293	23.51%
UPT Solar UPT-C245P60	Poly c-Si	60	10x6	245	6	[1 1 1 1 1 1]	-18	46	0.1207	21.95%
UPT Solar UPT-C245P60	Poly c-Si	60	10x6	245	3	[2 2 2]	-18	46	0.1296	23.56%

What is interesting about these results is that, contrary to what would be predicted, the same modules with a larger number of bypass diodes are having lower values of ST. This does not theoretically make sense, since for the same modules having more bypass diodes should actually increase shading tolerability, as found with the 96 cell module.

When checking these results, it was found that the first main reason for this difference in ST was

because of the increased impact of the forward voltages of all the bypass diodes. Since these modules had double the number of bypass diodes, under shading conditions, depending on how many of the bypass diodes were activated, this led to lower values of P_{mpp} being calculated by the model for the 6 diode modules, due to additional forward voltage losses being taken into account, for certain shading scenarios. However, this should not necessarily lead to lower overall ST, as the impact of the forward voltages of the additional bypass diodes should be much more than canceled out by the better performance (and equivalently higher P_{MPP}) of the 6 bypass diode under a number of shading scenarios.

This leads to the second main reason for this difference in ST, and also to one of the limitations of this model. When considering both types of modules, the splitting configuration (into 12 sections) is the same, as depicted in figure 4.16.

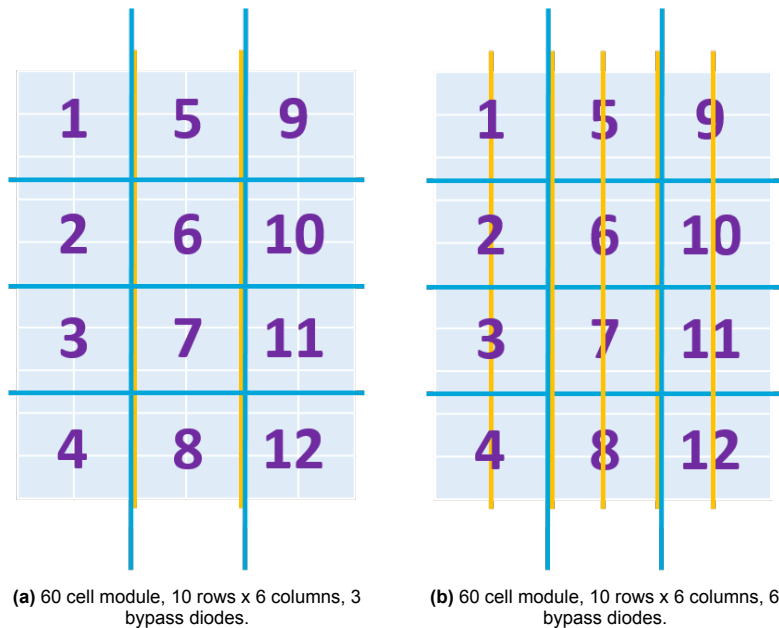


Figure 4.16: 60 cell module shown with 3 and 6 bypass diodes, with splitting configuration illustrated.

In figure 4.16, the orange lines represent the separation of separate bypass diode strings, while the blue lines represent the separation of sections. As can be seen, both types of modules have the same layout for the 12 sections they are split into.

Let us consider a scenario where only section 1 is shaded. The shading of the specific cells is exactly the same in the two modules. In the first case, 4 full cells and half of 2 cells are shaded, all of which are contained within one bypass string containing 20 cells. In the second case, 2 cells and half of one cell are shaded in each of two bypass strings containing 10 cells each. This essentially adds up to 4 full cells and half of 2 cells being shaded within 20 cells connected in series, and protected by one bypass diode in the 3 BD module and by 2 bypass diodes in the 6 BD module. The impact on the output power due to shading is essentially the same between the two modules. However, in the 6 BD module, there is double the amount of forward voltage drop due to bypass diodes since two bypass diodes are activated, as opposed to the first case where only one bypass diode is activated. In this way, the overall voltage of the string is lowered in the 6 BD module, thereby lowering the final output power as well. Since the section layout is the same between the modules, and all the sections cover two bypass diode strings, in all shading scenarios the module with 6 bypass diodes will have double the forward voltage drop, negatively impacting output power.

The positive effect of the bypass diodes is seen when considering the case that the first column of cells (not sections) is shaded. In the case of the module with 3 bypass diodes, the output of 20 cells would be impacted by the shading of these 10 cells, as all of these 20 cells are connected together in series in one bypass diode string. However, in the case of the module with 6 bypass diodes, only 10

cells are impacted by this shading (which are the 10 shaded cells), as only these 10 cells are connected to each other in series within one bypass string. The next 10 cells in series are connected to a different bypass diode, and therefore are not impacted by this shading. Therefore in the 3 BD module, one third of the module is impacted by this shading scenario, whereas only one sixth of the module is impacted in the second case. Therefore, for all shading scenarios that take place within any one column of cells, the module with 6 bypass diodes will perform significantly better, thereby demonstrating better shading tolerability. However, since this module is only split into 12 sections for the purposes of shading tolerability calculation, the smallest shading area never has less than two columns impacted. Therefore, the advantages of the module with 6 bypass diodes in a shading scenarios which lie within one column are never considered in the calculation of ST in this model. Herein lies one of the limitations of this model. In order to have more accurate ST values for comparison between modules in cases such as this, the introduction of a larger number of sections (which are smaller in area) would be something to consider for future work in this model.

4.6.2. Effects of lower breakdown voltages

As discussed in section 3.2, one insight gained in the process of lab validation was the significant positive impact of lower breakdown voltages on the operating power of a PV module when only one or two cells are shaded. In these specific cases, low breakdown voltages, such as those seen in the case of IBC cells, mean that the bypass diode for the string is not necessarily immediately activated. This is because the overall voltage of the string, taking the reverse bias negative voltages into account, does not necessarily drop below the forward voltage of the bypass diode. Therefore, in the case of one or two cells shaded (for low breakdown voltage cases), the entire string of cells connected to the diode is not necessarily bypassed, and therefore the output power of the PV module remains relatively high. This is in comparison to modules which have cells with average/high breakdown voltages, where even one cell being shaded would cause the bypass diode to be activated, and the entire string of cells to be bypassed. This is due to the high negative voltages of that cell in reverse bias, leading to a string voltage that would fall below the forward voltage of the bypass diode, thereby activating it.

Once again, due to the decision to section the model into 12 equal sections, this is one of outcomes that is not necessarily reflected in the calculated ST of a module. This is because each section generally has at least 4 cells or more (considering the smallest module size of a 48 cell module). Since the effects of lower breakdown voltages are usually seen if only one or two cells are shaded, this is one of the positive impacts of lower breakdown voltage technologies that is not necessarily taken into account during the calculation of ST values when considering the smallest area for shading to be one of 12 sections. In future work with this model, it would be interesting to look at cell level sections for shading, if it is possible to optimize the simulation times as well (as the long simulation times are one of the roadblocks for doing this for a large number of modules). Considering cell level shading of a module could allow the positive impacts of low breakdown voltages on the operating power of a PV module to be better taken into account in the ST calculation. This would potentially result in a slightly higher ST value for technologies with low breakdown voltages when comparing similar modules. In this way, breakdown voltage values could also contribute to the coefficient λ potentially.

4.6.3. Type of bypass diode

As explained in section 2.5.2, a representative p-n diode was used for modelling the bypass diodes in this model (as it is one of the common bypass diodes used in commercial applications). However, there are also modules that implement Schottky diodes. The main difference is that the forward voltage drop of Schottky diodes is smaller, around 0.4 V on average (compared to an average of around 0.7 V for a p-n diode), which is supposed to lead to better power efficiency [93]. In order to test if the type of diode has an impact on the shading tolerability of a PV module, one of the PV modules for which ST was already calculated, was computed again using a Schottky diode model. The IV characteristic of a representative Schottky diode was used in the modeling of the forward voltage drop of the bypass diode, as shown in figure 4.17 [94]. The curve was modeled using a straight line correlation based on the trend from $I = 0.1$ A to $I = 10$ A (as this is the general operating range), and the 25°C curve was considered for this modeling.

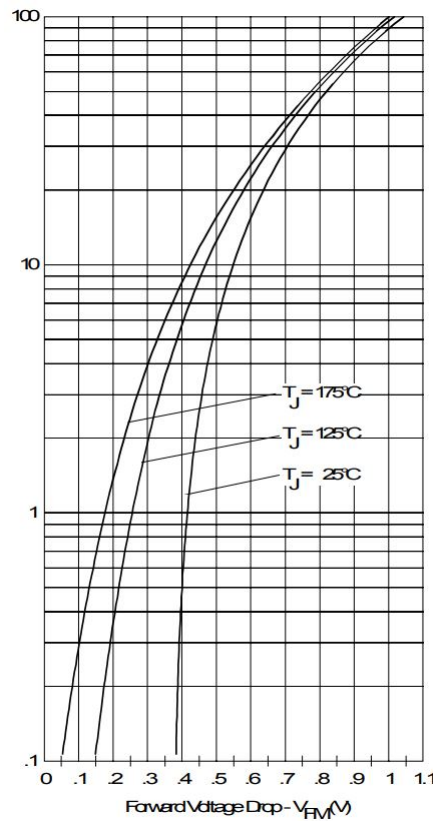


Figure 4.17: Forward voltage-current characteristic of JAMECO 80SQ Series Schottky diode [94]

The results of this test on the ST of a specific module are shown in table 4.6.

Table 4.6: ST calculation for same PV module - modelling impact of type of bypass diode (p-n vs Schottky).

Module	N_s	Config	P_{mpp} (W)	BD	BD Config	Diode Type	ST	ST%
Pixon PIX MP3 48	48	6x8	265	3	[2 2 2]	p-n	0.1268	23.05%
Pixon PIX MP3 48	48	6x8	265	3	[2 2 2]	Schottky	0.1305	23.73%

The impact of type of diode on ST is shown by the ST values calculated. It can be seen that the same panel, when modelled with a Schottky diode instead of a p-n one, shows a higher calculated ST value. This illustrates the benefits of a Schottky diode with respect to its lower forward voltage drop, which leads to less voltage loss in shading conditions. This contributes to better shading tolerability.

In this way the impact of the type of bypass diode on the ST value of a model is illustrated. It follows then that the type of bypass diode can also be one of the factors contributing to λ .

4.6.4. Effect of splitting configuration

One aspect noted in the analysis of the results was that the 54 cell module (with 3 bypass diodes) seemed to have an overall lower range of ST values than the other module configurations. One reason put forward for this was that it could simply be the configuration of this module that was affecting the ST results negatively. Another possible reason noted however, was that the splitting configuration of the 54 cell module was different when compared to the other 6 column modules in that it was split in a 3x4 configuration instead of a 4x3 configuration. Because of this splitting configuration, some of the resulting sections included cells from two different bypass diode strings. In contrast, for the other

configurations, each section was within only one bypass diode string. Therefore, for the 54 cell module, there were relatively more shading scenarios where two bypass diode strings of cells were affected, which would have an impact on the overall output power of the module.

In order to test this theory, it was decided to run the shading tolerability calculation for a 72 cell module (12 rows x 6 columns, 3 bypass diodes) with a 3x4 splitting configuration instead of the 4x3 splitting configuration tried earlier. The resulting split is illustrated in figure 4.18.

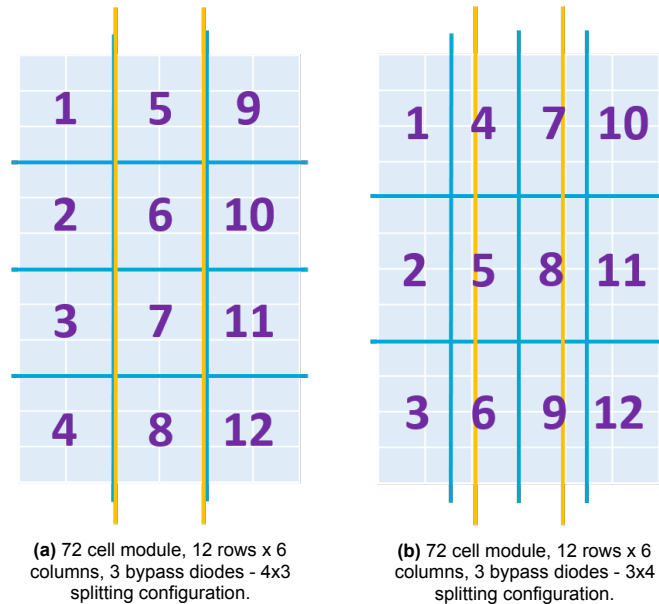


Figure 4.18: 72 cell module with 4x3 and 3x4 splitting configurations illustrated.

As can be seen, with this split, sections 4 to 9 now have cells from two bypass diode strings. Therefore if these sections are shaded, two bypass diode strings could be affected.

The result of the ST calculation can be seen in table 4.7, along with the ST value for the same module under the original splitting configuration. It can be seen that with this 3x4 splitting configuration, the ST value is lower than that calculated earlier. In fact, the resulting ST value is lower than the full range of ST values seen earlier for the 72 cell modules tested. This confirms the theory that one of the reasons for the 54 cell modules ST values being lower than the others could be due to the way the module was split. It could also indicate that if the 54 cell modules were split in the same way as the other 6 column modules, a clear trend would be seen for $ST\%$ vs N_s for all the configurations considered.

Table 4.7: ST calculation for same 72 cell modules with different splitting configurations.

Module	N_s	Config	P_{mpp} (W)	BD	BD Con- fig	Splitting Config	ST	ST%
PVSupers SuperHCSeries 72M	72	12x6	390	3	[2 2 2]	4x3	0.1307	23.76%
PVSupers SuperHCSeries 72M	72	12x6	390	3	[2 2 2]	3x4	0.12687	23.05%

With this finding, it can be seen that the splitting configuration of the module also has an impact on the calculated ST for the module. However, the comparison within each module configuration's ST results, and also between the 48 cell, 60 cell, and 72 modules are still valid, as they are all split with the same splitting configuration. It can even be argued that the comparison to the 96 cell modules are also

still valid, as they are split in the same way with respect to all sections only containing cells from one bypass diode string (although the 96 cell modules are split 3x4). Therefore, actually, trying to find the most symmetrical splitting configuration generally works well, as it sets out a standard for all modules (in that most symmetrical takes into account also if sections are within a bypass diode string or not). In this way, it makes it easier to compare modules of different configurations objectively.

However, as has been seen, it is not always the case – as here the most symmetric split of the 54 cell module resulted in different layouts of the sections. Additionally, it is seen that the splitting configuration of the module also has an impact on the ST value of the module. It could then be interesting to try all splitting configurations in the calculation of ST of a module, and take an average value of the results to obtain a more accurate value for ST at that value of c (where in this case $c = 12$).

However, since computational time could become an issue here, another possible way to get a more objective ST could be as follows. As discussed earlier, potentially the most accurate way to calculate ST would be at a cell level, to really see the full shading tolerability potential of the respective module. Therefore if ST is calculated for one module for each specific configuration at a cell level, this can be compared with the ST value obtained from all the different splitting configurations. The splitting configuration which provides the ST value that tends closest to the cell level ST value can be used as the splitting configuration when calculating ST at that value of c . This can be done for every configuration. In this way, the necessity of calculating for all possible splitting configurations can be eliminated, and a more objective way of comparing STs of different module configurations can be obtained.

4.7. Further Recommendations

To conclude, in this chapter, the development of the shading tolerability calculator in MATLAB was explained, and the results of the calculation of the shading tolerability parameter (ST) of a number of modules were presented and analysed. In this section, a few recommendations for the further development of this model/calculator are given.

One aspect which could be interesting to look into and integrate in this model in the future is the time dependence of ST. At the moment, shading tolerability of a module has been considered without taking time impacts into account. However, when looking at shading tolerability of a module in the short term vs long term, the parameter could change.

For example, as has been explained, depending on the model and its characteristics, partial shading can lead to hotspots, which can cause degradation and damage to a PV module over time, diminishing its overall performance. Since based on the features of the module, the impact on degradation can be different from module to module, it would likely contribute to the overall long term shading tolerability of a PV module. It could be beneficial, then, to model the impact of hotspots/degradation of a module over time due to partial shading with respect to the shading tolerability of a module.

This also leads into the impact of temperature. At the moment, temperature is modeled through the NOCT model, where it is taken into account that the incident irradiance has impact on the temperature of a cell. As mentioned earlier, the NOCT model is quite a simplistic model. While it meets the requirements of the model at this time, it could be interesting to look into other models, specifically those that once again take the impact of time into account with respect to temperature.

The temperature of a module also depends on the operation of a module. As explained, partial shading leads to higher temperatures due to power dissipation/hotspots. Higher temperatures tend to result in worse performance of PV modules (when compared to STC conditions). Therefore, to be able to get a more accurate view of the shading tolerability of a PV module, it could be good to model the cell temperature impact due to heating because of power dissipation in partial shading conditions, of a PV module.

5

Half-Cell Butterfly Module Case Study

This chapter will detail the final part of this work, which was to perform a case study regarding half-cell butterfly modules. In section 5.1, some background will be given on the half-cell butterfly module. Next, in section 5.2, the modelling of the half-cell butterfly module in this work will be explained, with respect to the IV simulation part of the model. Finally, in section 5.3, the calculation of the ST for two specific half-cell butterfly modules will be discussed and reviewed.

5.1. Half-Cell Modules

A half-cell module, as the name suggests, is a PV module containing half-cells instead of full solar cells. A half-cell is essentially a normal (full) solar cell that is cut in half. Some traditional full cell PV module configurations, as has been seen in the previous chapter, are 60 cells (10 rows x 6 columns) and 72 cells (12 rows x 6 columns) modules. The corresponding half-cell modules for these would be 120 half-cells (20 rows x 6 columns) and 144 half-cells (24 rows x 6 columns) [95]. The area of a solar cell is proportional to the amount of current it can generate (which is part of the principle that was used to calculate the overall irradiance of a partially shaded cell in Chapter 2). Therefore, a half-cell generates half as much current as its full cell counterpart [95, 96]. Since resistive power losses are directly proportional to the square of the current ($P = I^2R$), one of the advantages of a half-cell is that resistive losses are reduced to one quarter (specifically the losses that result from the series resistance that is part of the connection of different cells in a module) [96, 97, 98]. This also means that hotspot impact (due to partial shading) should be less in the case of half-cell modules, which is another benefit [99]. Additionally, half-cells can be placed closer to one another in a module (since the power output of an individual half-cell is lower, so is the required distance between cells), and therefore have a more effective module area utilization. [95]

With the change from full cell to half-cell also comes a change in the configuration of the module, with half-cell modules generally being in a series-parallel-series configuration, which is also sometimes called a 'butterfly configuration' [95, 100]. The best way to explain this is to first consider a conventional 60 (full) cell PV module in the layout 10 rows x 6 columns (with 3 bypass diodes in a [2 2 2] configuration). The corresponding half-cell module, as mentioned, would be a 120 half-cell, 20 rows x 6 columns PV module. The layout of this module would have a 'top' and a 'bottom' section, essentially two strings that are connected in parallel, with each having 60 half-cells in a 10 rows x 6 columns layout connected in series. This is illustrated in figure 5.1 which shows a schematic of 120 half-cell PV module.

The effect of this series-parallel-series configuration is also that the halving the current of each individual cell does not impact the output power of the module negatively (as currents are added in parallel connections). Therefore, the output current and voltage of half-cell modules are comparable to conventional modules [99, 95, 100]. Another aspect that can be noted here is the configuration of the bypass diodes in the half-cell butterfly module. As can be seen, there are three bypass diodes which are each connected to 20 half-cells each in the top and bottom section (where the 20 cells in the top section are connected in parallel with those in the bottom section). In this way, due to the parallel connection

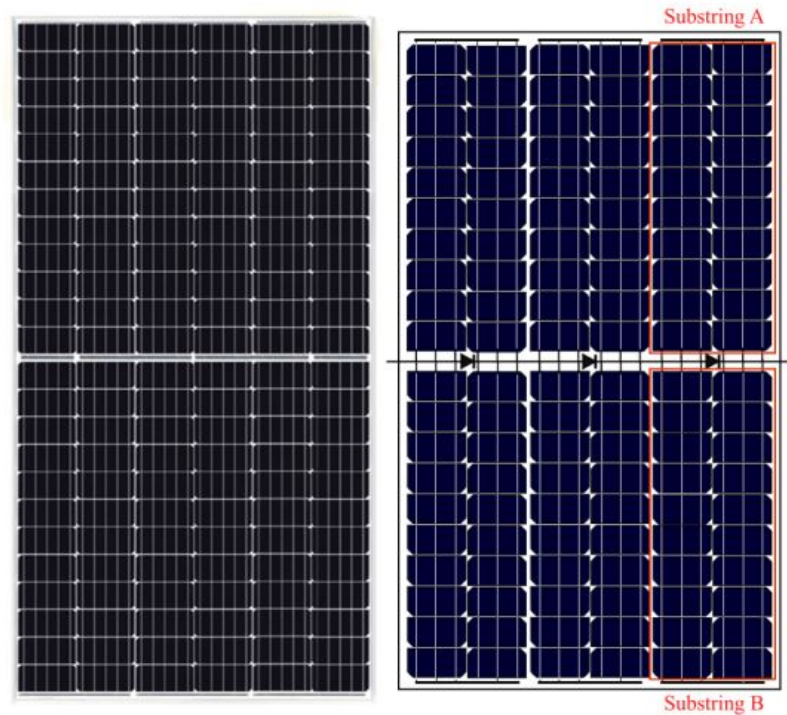


Figure 5.1: 120 half-cell butterfly module, with series-parallel-series schematic shown. Figure taken from [95].

of the top and bottom sections, and the bypass diode configurations, the half-cell butterfly module effectively has 6 distinct substrings. This is in comparison with the 3 substrings that the corresponding conventional 60 full cell module has (where every 20 cells in series is connected to one of the three bypass diodes). In this way, the half-cell butterfly is supposed to have a better shading response due to its series-parallel-series connection and bypass diode configuration [95, 101, 96].

This can be illustrated through an example: assume the bottom right corner of both types of modules is shaded (so 4 full cells at the bottom of the last two columns, and correspondingly, 8 half-cells at the bottom of the last two columns). In the conventional module, the impact of these shaded cells would affect the entire substring of 20 cells, which is one third of the module's output. In contrast, in the half-cell module, only one out of the 6 substrings would be affected, which is only one sixth of the module's output. Thereby, in this way, the half-cell butterfly module's performance under the same shading conditions should generally be better.

Half-cells are already quite prevalent in the market, with some studies predicting they will take over more than 60% of the market share by 2030 [102]. Also, given all of their proposed benefits, especially their supposed ability to be able to withstand shading with better performance due to the configuration of the modules, there are strong reasons as to why this type of module is interesting to explore from a shading tolerability parameter perspective, which is why this case study was undertaken.

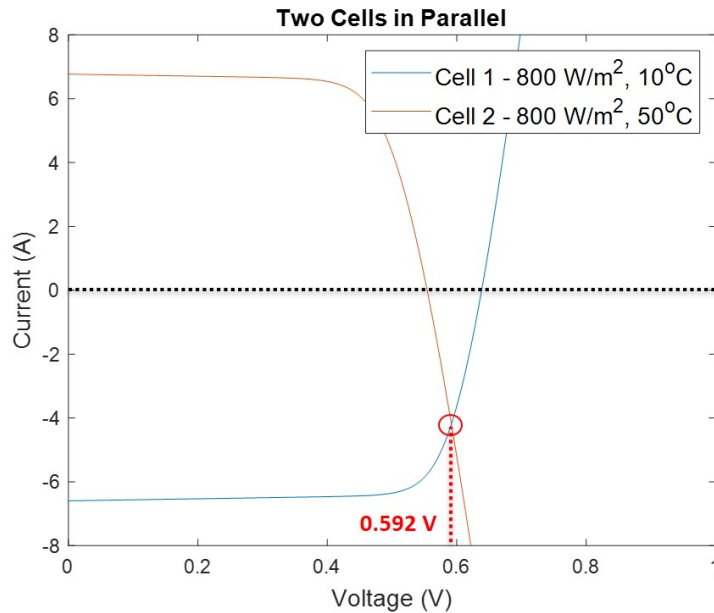
5.2. Half-cell Butterfly IV Characteristics Modelling

The first step of this study was to model the connection of the half-cell butterfly module in MATLAB in order to generate the IV characteristics of the module under different conditions.

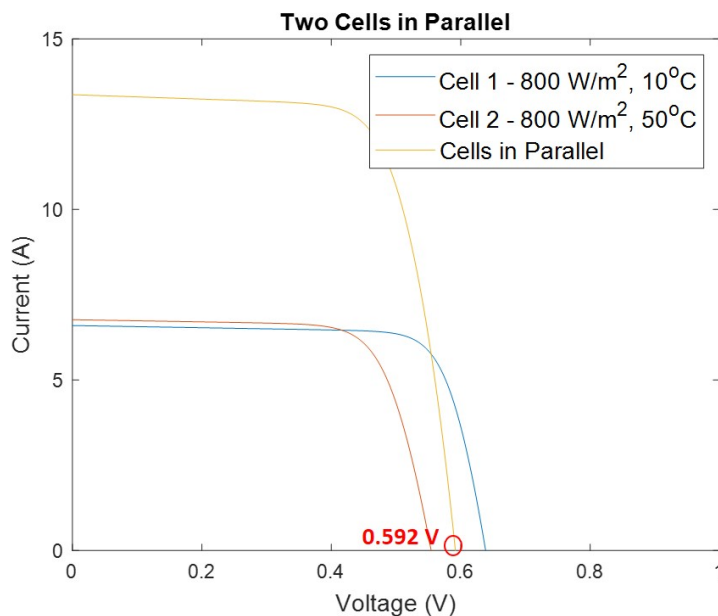
Parallel Connection Modelling

A main point here is the parallel connection that is seen in this type of module, which means the parallel connection of strings needs to be able to be modelled. Consider two cells connected in parallel. In contrast to a series connection, when cells are connected in parallel, the voltage across them is equal while the currents at each voltage point are added up [68]. In the case of mismatch situations between

cells (facing different conditions) that are connected in parallel, a similar method is used to determine the resulting voltage of the connected cells as was used to determine the current of series connected mismatched cells, explained in section 2.5.2. That is, for two cells under different conditions connected in parallel, the resulting V_{oc} can be determined by flipping the IV characteristic of one around the x-axis and finding the intersection with the IV characteristic of the other. In theory, then, similar to the series connection, adding up all the current points at a given voltage point, including the negative current points, should give the same result. Once again, both methods were checked to make sure the same value of V_{oc} was being obtained for each. The results can be seen in figure 5.2.



(a) Method 1: Plot showing intersection of plots of two solar cells in parallel facing different conditions, with one plot flipped across the x-axis.



(b) Method 2: Plot showing resulting IV curve of two solar cells in parallel facing different conditions, obtained by the addition of the current points.

Figure 5.2: Plots showing two cells in parallel and methods of calculating V_{oc} .

As is shown, the resulting V_{oc} in both cases is the same, and so the method of adding up all the

current values at the specific voltage points is used for modelling parallel connections.

Half-cell Module Connection

There are three steps in modelling the connection of the cells in the half-cell module. As mentioned, the half-cell butterfly layout has 6 distinct substrings laid out in a series-parallel-series configuration with three bypass diodes distributed evenly between them. The connection is modeled as follows:

1. The IV characteristics of each distinct substring are obtained, using the method described in section 2.5.2 for series connection of cells within each substring
2. Then each substring in the top section is added to its corresponding parallel substring in the bottom section, with the IV characteristics being calculated for each resulting combined substring using the method described for parallel connection in the previous section.
3. Finally, the three resulting substrings are added together once again in a series connection, but this time taking the impact of the bypass diode connected to each into account (the modeling of bypass diode implementation is also explained in section 2.5.2).

To illustrate the modelling of the half-cell butterfly module, examples of two IV curves simulated by this model for different shading conditions are shown in figures 5.3a and 5.4a. The respective shading scenario is shown with an illustration in figures 5.3b and 5.3b respectively. The dashed green line represents the parallel connection between the top and bottom parts of the module.

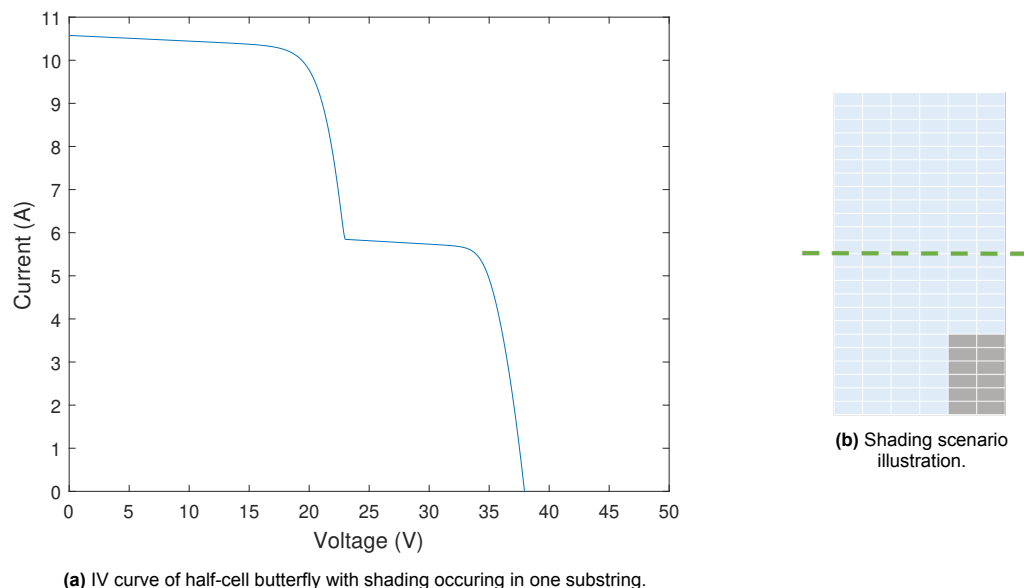


Figure 5.3: IV characteristic of a representative half-cell butterfly module (JA Solar JAM60S10 Half-Cell Module) with one substring partially shaded. Shaded cells (grey) receive irradiance of 100 W/m^2 , while unshaded cells (blue) receive irradiance of 1000 W/m^2 .

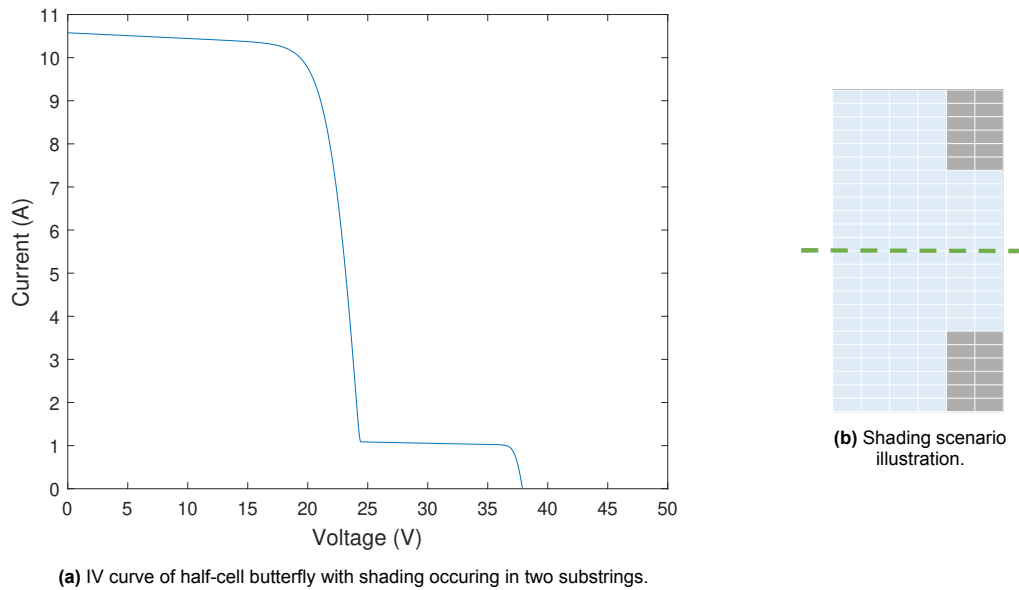


Figure 5.4: IV characteristic of a representative half-cell butterfly module (JA Solar JAM60S10 Half-Cell Module) with two substrings (connected in parallel) partially shaded. Shaded cells (grey) receive irradiance of 100 W/m^2 , while unshaded cells (blue) receive irradiance of 1000 W/m^2 .

The parallel connection modelled between the respective substrings can be seen in the difference between figures 5.3 and 5.4. The figures show the difference in the resulting IV characteristics (and specifically the difference in the height of the knee of the right part of the IV curve) between the two scenarios where in one only the bottom part is partially shaded, in comparison to the other where both the top and bottom parts are shaded.

5.3. Shading Tolerability

Now that the calculation of the IV characteristics of a half cell butterfly module under different conditions has been modelled, the next step is the modelling of the shading scenarios, similar to what was done in the previous chapter for conventional modules.

For the half cell butterfly module shading scenarios, the same conditions are considered. That is, the module is split into 12 (geometrically) equal sections, where it is considered that shaded sections receive an irradiance of 100 W/m^2 and unshaded 1000 W/m^2 . However, the configuration of a half cell butterfly module is quite different from conventional modules (due to the splitting of the module into two parts that are connected through parallel connection, with bypass diodes being connected 'in the middle'). Because of this, the modelling of the shading scenarios for the butterfly module will have to be rethought in some ways. Consider figure 5.5 showing a schematic for the splitting of a 144 half-cell module (24 rows x 6 columns). For reference, the conventional module counterpart of this (which is the 72 cell, 12 rows x 6 columns module from earlier) is also shown next to it.

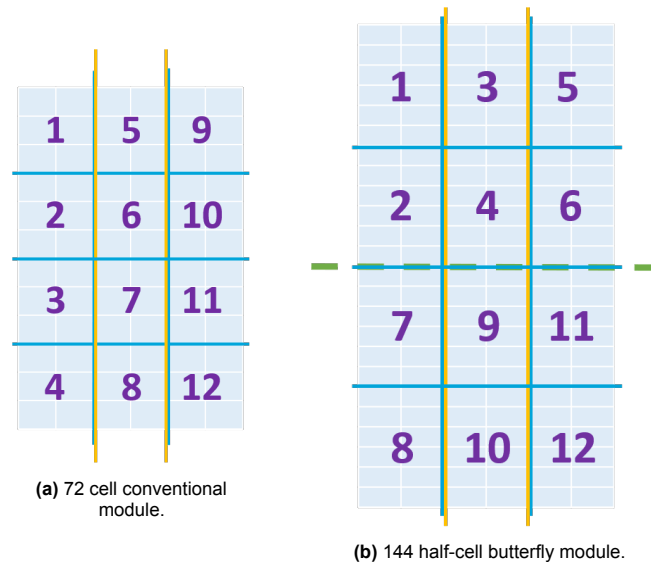


Figure 5.5: 72 cell conventional module layout vs 144 half-cell butterfly module layout.

As can be seen from figure 5.5, as before, the 12 sections are split in almost exactly the same way as for the 72 cell module from earlier. The main difference is that instead of 6 cells per section, there are now 12 half cells per section. In figure 5.5b, the green dashed line represents the division of the top and bottom sections of the module, which are connected to each other in a parallel connection. The yellow lines represent the division of the bypass diodes, and the blue lines the division of the sections, similar to earlier.

The first change with respect to shading scenarios is how the module itself is modeled. For the purposes of studying this module, the top and bottom sections can be almost be considered as two separate modules connected to each other in parallel (and both with connections to the same three bypass diodes). Due to this, the numbering of the sections is also changed accordingly, as can be seen in figure 5.5.

The difference in connection and configuration has impact on how to calculate the equivalent scenarios in this case, as the symmetry of this module is different from that of the conventional 72 cell module from earlier.

5.3.1. Equivalent Scenarios

Vertical Symmetry

First, let the case of vertical symmetry be considered. Here it will become apparent why the two sections are modeled separately. In the previous chapter, it was explained how the 72 cell module has vertical symmetry in that all the sections within a column of sections are essentially equal, with each section in the column having 6 cells within the same bypass diode string. However, with this module, this is no longer the case, due to the top and bottom halves of the module being different sections connected in parallel.

Here, the implication of equal and equivalent section comes into play once again. To rephrase in a simple way from the definitions given in the previous chapter, equal sections are sections with the same number (and ratios) of cells within the same substring, while equivalent sections are sections with the same number (and ratios) of cells within equivalent substrings. An example of equivalent substrings are two substrings, each connected to a different bypass diode, but with the same number of cells in each. The illustration of the substrings in both the 72 cell conventional module as well as the 144 cell module can be seen in figure 5.6.

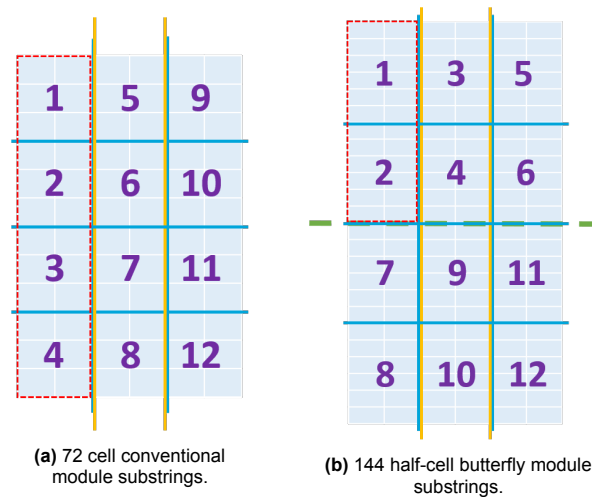


Figure 5.6: 72 cell conventional module substrings vs 144 half-cell butterfly module substrings.

In figure 5.6, the red dotted borders represent one substring. In the 72 cell module, the highlighted substring has sections 1, 2, 3 and 4; and the total number of substrings is three (as the three bypass diodes naturally section the module into three segments). However, in the 144 half cell module, as was explained in section 5.1 (and illustrated in figure 5.1), the number of substrings is doubled (to six substrings), due to addition of the parallel connection between the top and bottom sections. The illustration of one of the substrings can be seen in figure 5.6b, with the highlighted substring consisting of sections 1 and 2.

With this illustration, it can be seen how the vertical symmetry has been impacted. Sections 1 and 2 belong to a different substring than sections 7 and 8 due to the parallel connection, and therefore all four sections cannot be thought of as equal anymore. Therefore, the modelling of vertical symmetry needs to change accordingly. This is now why the top and bottom parallel sections of this module are modeled separately. Vertical symmetry can then be applied for each of the sections separately.

It should be noted that for the half cell butterfly module, as earlier, the total possible number of shading scenarios is still 4096, as there are still 2 irradiance levels (shaded or unshaded) and 12 total sections ($2^{12} = 4096$). However, since the top and bottom sections have been separated, there are 6 sections in each, and thereby $2^6 = 64$ scenarios for each separately. The scenarios for each section are illustrated in figure 5.7.

	1	2	3	4	5	6
1	0	0	0	0	0	0
2	1	0	0	0	0	0
3	0	1	0	0	0	0
...
25	1	1	0	0	1	0
26	1	1	0	0	0	1
...
64	1	1	1	1	1	1

(a) All possible shading scenarios (top section).

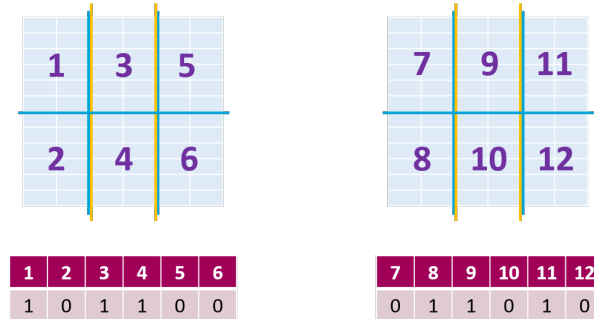
	7	8	9	10	11	12
1	0	0	0	0	0	0
2	1	0	0	0	0	0
3	0	1	0	0	0	0
...
25	1	1	0	0	1	0
26	1	1	0	0	0	1
...
64	1	1	1	1	1	1

(b) All possible shading scenarios (bottom section).

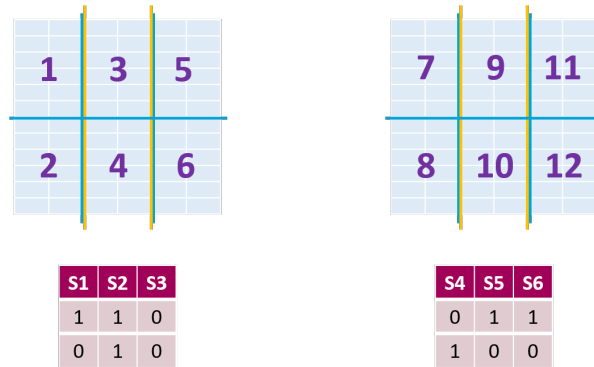
Figure 5.7: All possible shading scenarios shown separately for top and bottom sections of the half cell butterfly module.

It should be noted that when putting them together this is still $64 \cdot 64 = 4096$ scenarios. This is as each scenario from the top section can occur with all scenarios from the bottom section.

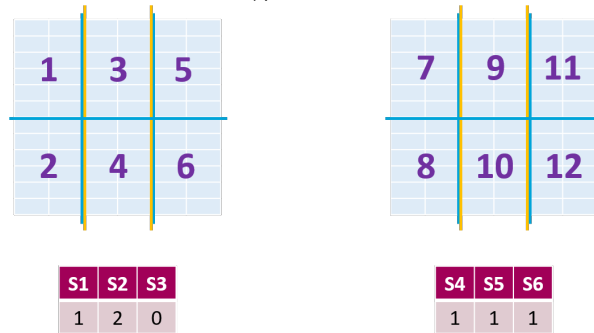
The same method to take vertical symmetry into account from the previous chapter is then applied for both sections. Each scenario is reshaped to match the configuration of the sections in of the top and bottom sections, and then each column is added up (due to the sections within each column being equal as explained). This process is shown in figure 5.8 for one specific scenario. Here 'S1' represents substring 1, and so on.



(a) Example scenario.



(b) Reshaping of example scenario based on layouts of each (top and bottom) part of the module.



(c) Addition of sections in each column for each (top and bottom) part of the module.

Figure 5.8: Example showing vertical symmetry of each of the top and bottom sections of the half-cell module for one scenario.

Then once again, as before, duplicates are counted and removed – except this time this is done separately for each of the top and bottom sections. This results in a reduction of scenarios from 64 each for the top and bottom parts of the module to 27 unique scenarios each for each part. This implies that at this stage the total number of scenarios has been decreased from 4096 scenarios to $27 \cdot 27 = 729$ scenarios, a significant reduction. Now that the duplicate scenarios due to the vertical symmetry within each section have been determined (and removed), the unique scenarios for each section can be put back together again.

Further Symmetry

When putting the unique scenarios for the top and bottom sections together, a few things need to be kept in mind. One is that, as mentioned before, to get all possible shading scenarios for the half cell module as a whole, it should be taken into account that each scenario for the top scenario should be put together with all the scenarios for the bottom section. Another point to be kept in mind is that the number of times each scenario occurs needs to be kept track of (and calculated when putting the scenarios back together). An illustration can be seen through figure 5.9.

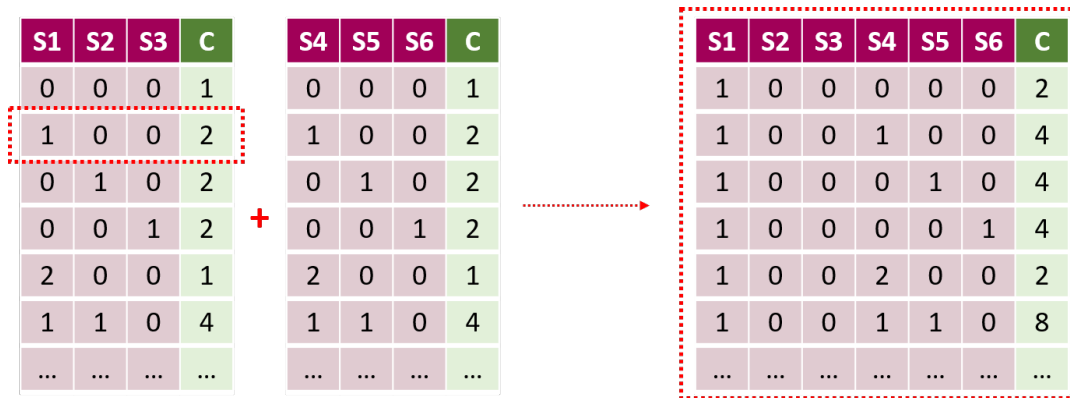


Figure 5.9: Putting the scenarios of the top and bottom parts of the module back together.

Figure 5.9 shows an example considering the second scenario for the top section. The green ‘C’ column keeps track of the counts of each scenario (the number of different ways (times) that scenario can occur). The second scenario for the top section is put together with each scenario from the bottom section, and the counts are multiplied to get the total number of possible counts for the resulting scenario. This is done for all the scenarios with the top and bottom sections.

Now, the remaining symmetry for this module can be taken into account. Here it is important to note the configuration of the module. The top and bottom sections are connected in parallel – therefore, each substring is connected in parallel to its corresponding substring. For example, S1 is connected to S4, S2 to S5, and S3 to S6. Therefore here, the symmetry will have to consider these connected parallel substrings as pairs, and not individually anymore. The next symmetry then, is the fact that each pair of connected substrings can be thought of as equivalent (so the order between them doesn’t matter). What this means is that if for example one section in S1 and 2 sections in S4 are shaded (with all the rest of the sections in the module unshaded), this is the same as if one section in S3 and 2 sections in S6 are shaded (with the rest unshaded). Therefore, columns of the connected parallel substrings are sorted to find the duplicates in this scenario and count and remove them. An example can be seen in 5.10.

Figure 5.10 shows 3 example scenarios. As can be seen, the columns of each pair of parallel connected substrings are sorted to take into account the equivalency of the resulting parallel connected substrings, and then the duplicates are removed. In this way, the last 2 unique scenarios shown are reached. At each point, the counts for each scenario are kept track of, by adding the counts of each duplicate scenario (to assign to the final unique scenario).

The final symmetry that is present in this case of the butterfly half-cell module is the symmetry between the top and bottom sections. Take an example where one section in substring S1 in the top part of the module is shaded (and all other sections are unshaded). This is essentially the same scenario if only one section in substring S4 in the bottom part is shaded. In both cases, 12 half-cells within one bypass diode string of 24 half cells are shaded within one of the two parallel sections in the module. Taking this symmetry into account essentially means that the top and bottom parts of the module can be thought of as equivalent (and interchangeable). Therefore, in the same way, the top and bottom sections are sorted with respect to each other to find the duplicate scenarios. An example can be seen with 3 scenarios shown in figure 5.11.

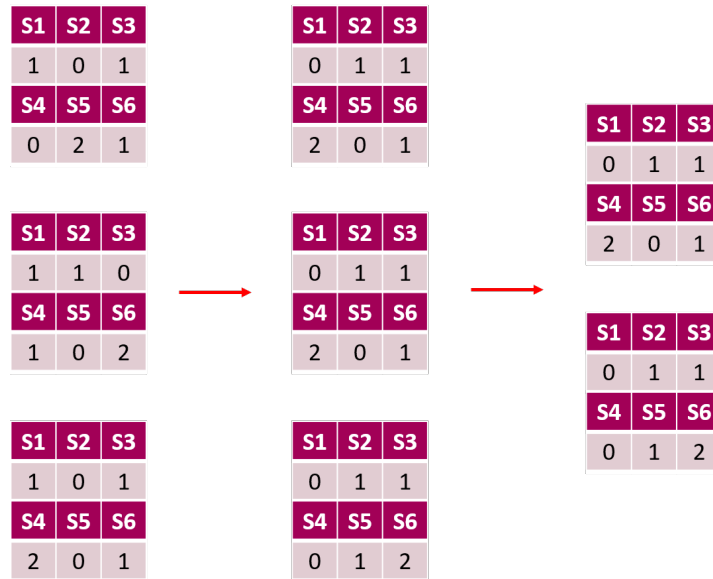


Figure 5.10: Example scenarios showing consideration of symmetry of parallel substring pairs in half-cell butterfly module.

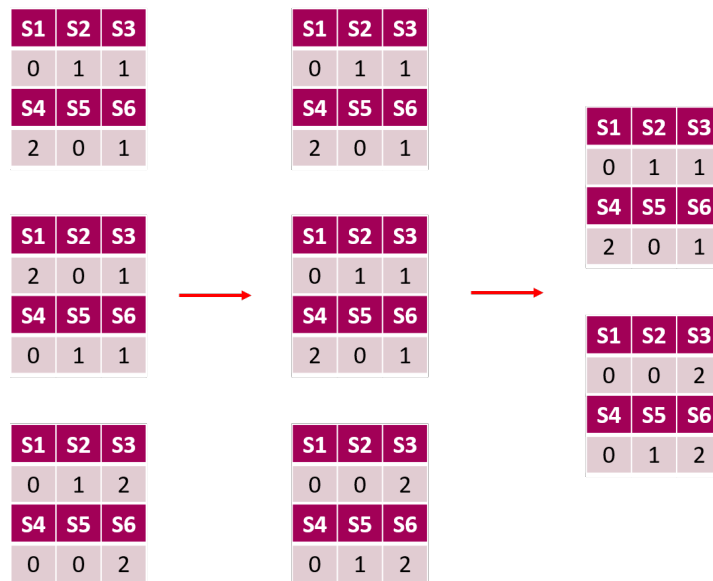


Figure 5.11: Example scenarios showing consideration of symmetry of top and bottom parts in half-cell butterfly module.

As can be seen in figure 5.11, the top and bottom parts of the module are sorted with respect to each other to find the duplicate scenarios with respect to their symmetry. In this example, the duplicate scenarios are the first and second scenario shown. It can be seen that the top and bottom parts can be flipped and are interchangeable. The duplicates are found and removed (with the counts of each scenario being kept track of as before), and the final two unique scenarios are arrived at as shown.

In this way, the symmetries of the half-cell butterfly module have been taken into account to remove the duplicate scenarios and arrive at the final unique scenarios. For both of the types of half-cell butterfly modules mainly seen in the market (120 half-cell modules (20 rows x 6 columns) and 144 half-cell modules (24 rows x 6 columns)), the total number of scenarios that need to be considered for the simulations is decreased from 4096 to 120 scenarios taking all symmetries of the module into account. It can be seen that the increase in complexity with regards to the configuration of half-cell

butterfly modules compared with conventional modules results in more unique shading scenarios that need to be considered overall.

5.4. Results and Discussion

The ST of two half-cell butterfly modules were calculated as part of this case study. This was done utilizing the developed model for the simulation of the IV characteristics of a half-cell module, as well as the results of the symmetry with respect to the respective shading scenarios. The two configurations considered were the 120 half-cell module and 144 half-cell module as these are the primary commercial half-cell butterfly module configurations. The results of ST calculation for these modules can be seen in table 5.1.

Table 5.1: ST calculation for two half-cell butterfly PV modules.

Module	Cell Tech	Half-Cells	Config (CxR)	P_{mpp} (W)	T_{NOCT}	ST	ST%
JASolar JAM60S10	Mono c-Si	120	6x20	340	45	0.2310	42.00%
JASolar JAM72S10	Mono c-Si	144	6x24	420	45	0.2340	42.55%

It can be seen that there is a significant (positive) difference between the shading tolerability of the butterfly half-cell module when compared to the conventional modules explored in the previous chapter. With calculated values of ST% being around 42%, the shading tolerability parameter of the half-cell butterfly modules is almost twice as much as most of the conventional modules seen. Compared to the highest ST value seen for the conventional modules, which was 28.85% for the Panasonic HIT KURO 96 cell module with 4 bypass diodes, the ST% is around 1.5 times higher. These values are also in a similar range to the value calculated for a representative half-cell butterfly module (which was around 46%) by Klasen et al. in their work [36].

This increase in ST is likely because of the additional parallel connection that the half-cell butterfly module has, which contributes to making it more resistant to shading conditions (with respect to output operating power of the module). As was briefly explained in section 5.1, due to the series-parallel-series configuration of the half-cell butterfly module (with the inclusion of 3 bypass diodes), the module is essentially split into 6 substrings. This is in comparison to the 3 substrings that its conventional module counterpart is split into. In this way, one shaded section affects less cells. For example, assume one section in one substring is shaded. This mostly affects the current the cell can produce (voltage decreases as well but not as much as current). As explained earlier, in a series connection of cells (as you have in a substring), the current running through them is limited by the cell with the lowest current. In the conventional module, the shaded section would then directly impact one third of the cells in the module, whereas in the half-cell butterfly, it would only be one sixth of the module. Of course, the parallel connection means that the cells in the corresponding substring connected in parallel will also be somewhat affected. However, since in a parallel connection, the limited variable is the voltage, not the current, the overall output power does not get impacted as much as when all the cells are connected in series.

The visualization of the ST for the two modules can be seen in figure 5.12.

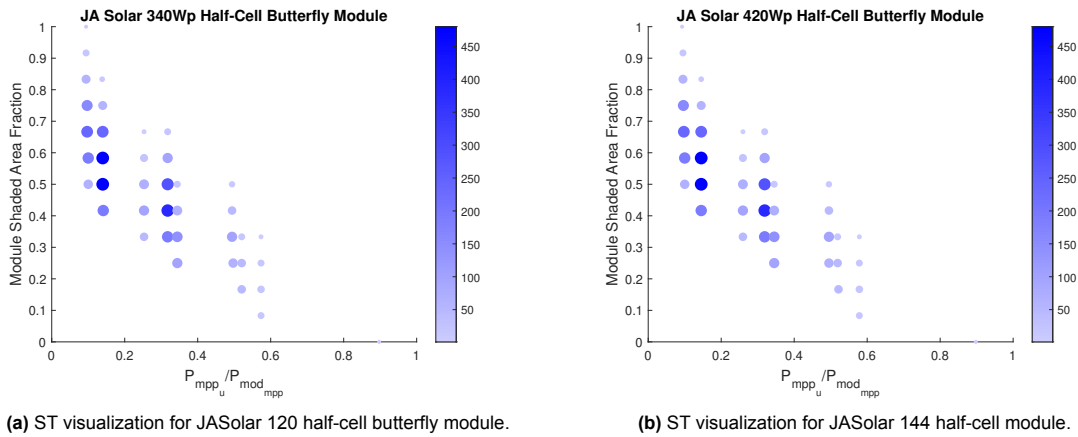


Figure 5.12: Visualization of ST for two configurations of half-cell butterfly modules (Module shaded area vs. operating power as a function of module nominal power).

Once again, the plots give an indication of which power points the module is operating at the most, under various shading conditions (the darker and larger the circle, the more occurrences at that operating power point). One main difference that is visible in these plots is the increase in the levels of operating power that are seen, which is illustrated by the increase in the 'vertical lines' of the data points. This can presumably be attributed to the difference in configuration, and specifically once again to the additional parallel connection in half-cell butterfly modules leading to a greater number of power levels the module operates at. Additionally, it can now be seen that the largest number of scenarios does not occur at the lowest level of operating power, as was the case in the conventional modules. Now, the largest number of scenarios are seen in the second and fourth levels of operating power (higher levels). This follows the fact that the shading tolerability of the half-cell butterfly modules is higher than that of the conventional modules.

Therefore, in this chapter, the development of the modelling of a half-cell butterfly module with respect to IV characteristics determination and ST calculation was presented as a case-study. It was seen that the half-cell butterfly modules have significantly higher STs than their conventional module counterparts, and conventional modules in general. This can be credited to the difference in configuration that makes this type of module more resistant to shading overall.

The other aspect shown by this case study is the adaptability of the developed model and code for different configurations of PV modules. The model has been developed at a cell level, and both series and parallel connections have been modeled, as well as the operation and impact of bypass diodes within a PV module. In this way, this model can be adapted to essentially simulate almost any type of configuration of module, with the building blocks developed in this code.

For future work, it would be interesting to model not only a larger number of half-cell butterfly modules (to see if any of the same/different trends are observed as the conventional modules), but also to model the operation of various configurations of PV modules. It would also be useful to do some practical measurements of half-cell butterfly modules in order to compare the calculated values with real life results to measure and optimize the accuracy of the model (which unfortunately was not able to be done with this work due to the constraints of time, etc.). It should also be noted that at the moment, the model still has potential to be optimized further with respect to speed when considering the simulations for the half-cell butterfly module configuration. This should be a prime point to keep in mind when moving forward with any new configuration.

6

Conclusion/Recommendations

The main aim of this work was the development of a model in MATLAB that can easily calculate the shading tolerability of a PV module as a numerical parameter, to be used for characterization and comparison purposes. Below, the objectives of this work introduced in chapter 1 will be revisited in order to detail if/how they were achieved, and the main findings will be discussed. Finally, further recommendations for the continuation of this research will be provided.

6.1. Conclusions

A summary of how the main objectives of this work (which were laid out in chapter 1) were achieved is given in the points below.

1. **Develop a MATLAB based code for IV/PV curve creation of PV modules:** The development of a MATLAB based model for the calculation of current and voltage characteristics of PV modules under different conditions was explained in Chapter 2. The only inputs to the model were required to be either values that could be found on a PV module datasheet and/or could be estimated knowing other details about the PV module.

The model was based on the two diode model for parameter extraction and initially developed at a cell level under standard test conditions. Irradiance and temperature dependencies were added to the parameters, to account for various non STC conditions that a PV module can face. The NOCT model was used to calculate cell temperature.

The series connection of cells within a PV module was modeled in order to be able to determine the current and voltage characteristics at a module level. This was initially done for homogeneous conditions over the entire module, and later for non-homogeneous non STC conditions, or more specifically partial shading conditions on a PV module. This was done by considering current limitation by the cell producing the lowest current in a series connection. In the modeling of partial shading conditions, a number of aspects were added. The first was the ability to deal with less than cell level shading. The next was the modeling of the reverse bias region of a shaded cell. Finally, the operation of bypass diodes in a PV module (and under partial shading conditions) was implemented. In this way, the development of a MATLAB based model for IV/PV curve creation of PV modules was completed.

The final model was validated with laboratory measurements done by Eurac Research that were kindly provided to us as part of this work. The measurements were done for a 60 cell Canadian Solar PV module with 3 bypass diodes. The results of the validation against these measurements were positive, with the error in P_{MPP} calculation always remaining below 4.5%. This validation completed the process of the development of the MATLAB based model for IV/PV curve creation of PV modules, thereby successfully completing the first objective of this thesis.

2. **Simulate and study different solar modules' performance at various shading conditions:** The next objective was the simulation and study of different solar modules' performance under various shading conditions. This was explained in Chapter 4. The model was chosen to be studied under two irradiance levels (shaded = $100 W/m^2$ and unshaded = $1000 W/m^2$). It was also

decided to split the considered module into 12 (geometrically) equal sections, with one section being the smallest area that could be shaded. It was determined that there were 4096 possible shading scenarios for these specific conditions.

One of the goals of the model was to relatively quickly be able to calculate shading tolerability of a module. Therefore, to optimize the speed of the model, a study was carried out regarding the identification of duplicate scenarios based on the configuration of the PV module, its components, and the splitting of the module. The most common configurations of series connected PV modules found commercially were considered. It was found that in most cases, there were a much smaller number of unique scenarios than the total 4096. The largest number of unique scenarios resulting for one of the configurations was 100, while the smallest number was as low as 35. This consideration of duplicate scenarios resulted in reducing the required simulation time from around 120 hours to less than 2 hours on average. This led to a significant increase in the speed in which shading tolerability was calculated, a real advantage of this work.

Finally, based on the remaining unique scenarios, various shading conditions on the PV module were simulated to check the performance of the PV module (or alternatively to check the impact on operating power at any condition (P_{MPP})). This successfully concluded the second objective of this thesis.

3. **Design a MATLAB based calculator for shading tolerability (ST):** The primary aim of this thesis was to design a MATLAB based calculator for shading tolerability (ST). The main variable required for the ST calculation was the operating power P_{MPP} of the module under various shading conditions. This was achieved as explained in Chapter 4, based on the results of the first two objectives. The equation for ST developed by Ziar et al. [28] was slightly amended to take into account the specifics of this work with respect to shading scenarios considered. In this way, the primary objective of this thesis was successfully completed.
4. **Calculate ST for a number of PV modules and analyse results:** With the development of the shading tolerability calculator, the ST values of more than 40 different PV modules were calculated, creating a small database of ST values. The values of ST% for the modules considered ranged from 22% to 29%. Trends were analysed to check if any correlations were visible. It was found that the increase in number of bypass diodes (while taking into account the configuration of the module) resulted in a considerably higher ST. Specifically, out of the configurations considered, the 96 cell PV modules with 4 bypass diodes performed the best with respect to shading tolerability. The temperature coefficient of open circuit voltage, K_V also showed some correlation with the ST of a module. Within the same type of configuration of PV module, it was observed that generally as K_V became less negative across a range of modules, the value of ST tended to increase. It was also found that there seemed to be some dependence shown on the number of cells in the module for similarly configured modules, with the increase in number of cells generally resulting in a slightly higher range of ST values. A number of other factors were also checked in various ways to see their impact on ST. Finally a case study was carried out where the ST of a relatively newer type of PV module configuration, the half-cell butterfly module, was calculated (for two configurations). In order to perform this calculation, it was first required to model the connection of a half-cell PV module to be able to determine the IV characteristics when building up from a cell level. Part of this was the implementation of the modeling of parallel connections, as well as taking into account the different configuration of a half-cell butterfly PV module when compared to conventional modules. The results of the case study showed that the calculated ST of a half-cell butterfly module was almost double that of the conventional modules (with results giving an ST% of around 42% for both modules tested), highlighting its superior response to shading conditions, mainly due to its distinctive configuration. It also demonstrated the adaptability of the code developed in this work, with the building blocks to be able to model many different types of configurations of PV modules.

6.2. Further Recommendations

To conclude this thesis, a number of further recommendations are proposed as potential future areas of research and/or improvement for this work.

- **Recommendations with respect to model:**

- **Further speed optimization**

In this work, the speed of the model was optimized greatly through various methods as detailed. However, the further optimization of speed in some other aspects with respect to this model would open up the avenue for many of the other further recommendations.

- **Shading scenarios and sections**

In this work, the number of sections to split the module into to investigate the shading scenarios was doubled based on previous work done by Ziar et al., and Mishra et al. However, it was found that there were a few characteristics of PV modules that were not really taken into account due to the size of the sections. An example was the case of doubling the bypass diodes in a module, where the scenarios where this would positively impact P_{mpp} were not taken able to be taken into account due to the size of the sections.

Therefore, it is recommended that shading tolerability of PV modules is explored with more/smaller sections, and ideally at a cell level (with respect to the smallest area that can be shaded). Currently one of the main reasons this was unable to be done was due to the major increase in scenarios that this would result in, which, with the speed of the model as it is, would make the ST calculation extremely long.

However, if the speed of the model was further optimized - this, combined with the method of checking for equivalent scenarios to reduce the number of scenarios that need to be simulated that was described in this work, would reduce the overall simulation time required. This could make it potentially possible to calculate ST with a larger number of (smaller) sections. It would be interesting to explore if this value was very different from using 12 sections.

- **Irradiance levels**

At the moment, two irradiance levels were considered in the ST calculation. In Ziar et al., it was proven through both mathematical and experimental means that the trends seen with two irradiance levels should be the same as those seen with irradiance levels tending to infinity. Regardless, it could be interesting to explore 3, 4, etc., irradiance levels in the ST calculation to see if there was any impact on the ST of difference modules.

- **Impact of lower breakdown voltages**

If it is possible to reduce the simulation time enough to calculate at a cell level, it would be interesting to explore the impact of lower cell breakdown voltages on ST. The positive effect of lower breakdown voltages on output operating power would generally only be seen in the case of one or two cells shaded with a bypass diode string. Therefore, the impact on ST could only be seen if shading scenarios were explored at a cell level.

- **Modeling of temperature**

At the moment, temperature of the cell/module is modeled using the NOCT model. While this model has many advantages with respect to its integration into this model, it does also have a number of simplifications. Therefore, using a more comprehensive model for the calculation of cell temperature could lead to better accuracy of ST of a model.

- **Hotspots**

Going further on the previous point, partial shading conditions can lead to the increase of temperature of and around the shaded cells due to power dissipation, which can lead to hotspots. To be able to integrate the change in temperature based on partial shading could also make the temperature of the module and therefore its calculated ST more accurate.

- **Degradation/Time Impact**

Additionally, the increase in temperature and presence of hotspots can lead to the degradation of the module over time. This would lead to decreased output with respect to the operating power of the module over time. Therefore, it could be insightful to include the change in operating power of a PV module over time due to effects such as this in the calculation of the ST of the module. The better ability of a module to withstand such temperature increase and the resulting hotspots would mean the performance over time of that module would be less negatively impacted. In this way, the overall shading tolerability of a PV module over a longer period of time could be different than the instantaneous ST that has been calculated now. The inclusion of the impact of time on the ST of a PV module could allow for an updated time dependent ST characteristic that could provide more insight on the overall shading tolerability of a PV module.

- **Other recommendations for future work:**

- **Database of ST values**

- With the developed model, the development of a bigger database of ST values can be created. Many more PV modules can be considered in the calculation of the ST values, spanning across larger ranges of configurations and types.

- **Development of mathematical expression for λ**

- One of the specific advantages of this work has been that the model developed gives the ability to isolate certain parameters of a PV module and check their specific impact on the shading tolerability parameter, ST. In this way, one parameter of a certain PV module can be changed at a time to see how it affects the ST value. This was illustrated in the cases of T_{NOCT} , type of bypass diode, etc. Utilizing this additional capacity of the module can contribute to the development of a mathematical expression for λ , for which not many specific details have been found until this time. This work can be used to study the specific impacts that certain parameters have on the ST of a module when looked at in isolation. The way in which certain parameters (that affect ST) can offset or cancel out each other can also be analyzed. In this way, a more complete picture of which parameters contribute to ST and what their relationships are with respect to each other can be examined, with respect to λ .

References

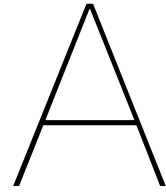
- [1] IRENA. *Solar Energy*. 2022. URL: <https://www.irena.org/solar> (visited on 07/25/2022).
- [2] S. Vemuru, P. Singh, and M. Niamat. "Modeling Impact of Bypass Diodes on Photovoltaic Cell Performance Under Partial Shading". In: *2012 IEEE International Conference on Electro/Information Technology* (2012), pp. 1–5.
- [3] N. D. Kaushika and A. K. Rai. "An investigation of mismatch losses in solar photovoltaic cell networks". In: *Energy* 32.5 (2007), pp. 755–759.
- [4] H. Patel and V. Agarwal. "MATLAB-Based Modeling to Study the Effects of Partial Shading on PV Array Characteristics". In: *IEEE Transactions on Energy Conversion* 23.1 (2008), pp. 302–310.
- [5] P. Manganiello, M. Balato, and M. Vitelli. "A survey on mismatching and aging of PV modules: The closed loop." In: *IEEE Transactions on Industrial Electronics* 62.11 (2015), pp. 7276–7286.
- [6] S. K. Das et al. "Shading mitigation techniques: State-of-the-art in photovoltaic applications". In: *Sustainable Energy Reviews* 78 (2017), pp. 369–390.
- [7] S. Fadhel et al. "PV shading fault detection and classification based on I-V curve using principle component analysis: Application to isolated PV system". In: *Solar Energy* 179 (2019), pp. 1–10.
- [8] S. Moballegh, J. Jlang, and M. Vitelli. "Modeling, prediction, and experimental validations of power peaks of PV arrays under partial shading conditions". In: *IEEE Transactions on Sustainable Energy* 5.1 (2013), pp. 293–300.
- [9] F. Belhachat and C. Larbes. "Modeling, analysis and comparison of solar photovoltaic array configurations under partial shading conditions". In: *Solar Energy* 120 (2015), pp. 399–418.
- [10] R. G. Vieira et al. "A comprehensive review on bypass diode application on photovoltaic modules". In: *Energies* 13.10 (2020), p. 2472.
- [11] M. R. Maghami et al. "Power loss due to soiling on solar panel: A review". In: *Renewable and Sustainable Energy Reviews* 59 (2016), pp. 1307–1316.
- [12] O. Bingöl and B. Özkava. "Analysis and comparison of different PV array configurations under partial shading conditions". In: *Solar Energy* 160 (2018), pp. 336–343.
- [13] L. L. Jiang, D. L. Maskell, and J. C. Patra. "A novel ant colony optimization-based maximum power point tracking for photovoltaic systems under partially shaded conditions". In: *Energy and Buildings* 58 (2013), pp. 227–236.
- [14] Y. J. Wang and P. C. Hsu. "An investigation on partial shading of PV modules with different connection configurations of PV cells". In: *Energy* 36.5 (2011), pp. 3069–3078.
- [15] C. E. Chamberlin et al. "Effects of mismatch losses in photovoltaic arrays". In: *Solar Energy* 54.3 (1995), pp. 165–171.
- [16] D. Picault et al. "Forecasting photovoltaic array power production subject to mismatch losses". In: *Solar Energy* 84.7 (2010), pp. 1301–1309.
- [17] P. Bauwens and J. Doutreloigne. "Reducing partial shading power loss with an integrated Smart Bypass". In: *Solar Energy* 103 (2014), pp. 134–142.
- [18] J. Bai et al. "Characteristic output of PV systems under partial shading or mismatch conditions". In: *Solar Energy* 112 (2015), pp. 41–54.
- [19] R. Ramaprabha and B. L. Mathur. "A Comprehensive Review and Analysis of Solar Photovoltaic Array Configurations under Partial Shaded Conditions". In: *International Journal of Photoenergy* (2012), pp. 1–16.
- [20] P. R. Satpathy and R. Sharma. "Reliability and losses investigation of photovoltaic power generators during partial shading". In: *Energy Conversion and Management* 223 (2020), p. 113480.

- [21] Y. El Basri et al. "A proposed graphical electrical signatures supervision method to study PV module failures". In: *Solar Energy* 116 (2015), pp. 247–256.
- [22] J. A. Tsanakas, L. Ha, and C. Buerhop. "Faults and infrared thermographic diagnosis in operating c-Si photovoltaic modules: A review of research and future challenges". In: *Renewable and sustainable energy reviews* 62 (2016), pp. 695–709.
- [23] H. Kawamura et al. "Simulation of I–V characteristics of a PV module with shaded PV cells". In: *Solar Energy Materials and Solar Cells* 75.3-4 (2003), pp. 613–621.
- [24] E. V. Paraskevadaki and S. A. Papathanassiou. "Evaluation of MPP Voltage and Power of mc-Si PV Module Partial Shading Conditions". In: *IEEE Transactions on Energy Conversion* 26.3 (2011), pp. 923–932.
- [25] H. Mohammed, M. Kumar, and R. Gupta. "Bypass diode effect on temperature distribution in crystalline silicon photovoltaic module under partial shading". In: *Solar Energy* 208 (2020), pp. 182–194.
- [26] A. Dolara et al. "Experimental investigation of partial shading scenarios on PV (photovoltaic) modules". In: *Energy* 55 (2013), pp. 466–475.
- [27] E. I. Batzelis, P. S. Georgilakis, and S. A. Papathanassiou. "Energy models for photovoltaic systems under partial shading conditions: a comprehensive review". In: *IET Renewable Power Generation* 9.4 (2015), pp. 340–349.
- [28] H. Ziar et al. "Quantification of Shading Tolerability for Photovoltaic Modules". In: *IEEE Journal of Photovoltaics* 7.5 (2017), pp. 1390–1399.
- [29] First Solar. *First solar technology advantage brochure*. Tempe, AZ, USA, 2015, pp. 1–7.
- [30] WürthSolar. *GeneCIS solar module 80 W datasheet*. Germany, 2008.
- [31] Hanergy. *PowerFlex BIPV datasheet*. Beijing, China, 2013, pp. 1–2.
- [32] A. Leon-Garcia. *Probability, Statistics, and Random Processes for Electrical Engineering*. 3rd ed. Englewood Cliffs, NJ, USA: Pearson/Prentice-Hall, 2008.
- [33] L. Inoue. *Decision Theory: Principles and Approaches*. Hoboken, NJ, USA: Wiley, 2009.
- [34] S. Mishra et al. "Selection Map for PV Module Installation Based on Shading Tolerability and Temperature Coefficient". In: *IEEE Journal of Photovoltaics* 9.3 (2019), pp. 872–880.
- [35] S. Mishra. "Selection Map for PV Module Installation Based on Shading Tolerability and Temperature Coefficient". MA thesis. Delft NL, 2018.
- [36] N. Klasen et al. "A Comprehensive Study of Module Layouts for Silicon Solar Cells Under Partial Shading". In: *IEEE Journal of Photovoltaics* 12.2 (2022), pp. 546–556.
- [37] N. Klasen et al. "Performance of shingled solar modules under partial shading". In: *Progress in Photovoltaics: Research and Applications* 30.4 (2022), pp. 325–338.
- [38] PVEducation. *IV Curve*. URL: <https://www.pveducation.org/pvcdrom/solar-cell-operation/iv-curve> (visited on 08/18/2022).
- [39] Titan. *PV Module TITAN M6-54*. India.
- [40] K. Ishaque, Z. Salam, and H. Taheri. "Simple, fast and accurate two-diode model for photovoltaic modules". In: *Solar Energy Materials and Solar Cells* 95.2 (2011), pp. 586–594.
- [41] A. Askarzadeh and A. Rezazadeh. "Extraction of maximum power point in solar cells using bird mating optimizer-based parameters identification approach". In: *Solar energy* 90 (2013), pp. 123–133.
- [42] D. S. H. Chan and J. C. H. Phang. "Analytical methods for the extraction of solar-cell single- and double-diode model parameters from IV characteristics". In: *IEEE Transactions on Electron devices* 34.2 (1987), pp. 286–293.
- [43] A. A. Elbaset, H. Ali, and M. Abd-El Sattar. "Novel seven-parameter model for photovoltaic modules". In: *Solar energy materials and Solar cells* 130 (2014), pp. 442–455.

- [44] V. J. Chin, Z. Salam, and K. Ishaque. "An accurate modelling of the two-diode model of PV module using a hybrid solution based on differential evolution". In: *Energy conversion and management* 124 (2016), pp. 42–50.
- [45] J. P. Charles et al. "A critical study of the effectiveness of the single and double exponential models for I–V characterization of solar cells". In: *Solid-State Electronics* 28.8 (1985), pp. 807–820.
- [46] F. J. Bryant and R. W. Glew. "Analysis of the current-voltage characteristics of cadmium sulphide solar cells under varying light intensities". In: *Energy Conversion* 14.3-4 (1975), pp. 129–133.
- [47] A. Askarzadeh and A. Rezaazadeh. "Parameter identification for solar cell models using harmony search-based algorithms". In: *Solar Energy* 86.11 (2012), pp. 3241–3249.
- [48] D. F. Alam, D. A. Yousri, and M. B. Eteiba. "Flower pollination algorithm based solar PV parameter estimation". In: *Energy Conversion and Management* 101 (2015), pp. 410–422.
- [49] H. Wei et al. "Extracting solar cell model parameters based on chaos particle swarm algorithm". In: *2011 International conference on electric information and control engineering*. IEEE. 2011, pp. 398–402.
- [50] M. Ye, X. Wang, and Y. Xu. "Parameter extraction of solar cells using particle swarm optimization". In: *Journal of Applied Physics* 105.9 (2009), p. 094502.
- [51] V. Khanna et al. "A three diode model for industrial solar cells and estimation of solar cell parameters using PSO algorithm". In: *Renewable Energy* 78 (2015), pp. 105–113.
- [52] M. Zagrouba et al. "Identification of PV solar cells and modules parameters using the genetic algorithms: Application to maximum power extraction". In: *Solar energy* 84.5 (2010), pp. 860–866.
- [53] J. A. Jervase, H. Bourdoucen, and A. Al-Lawati. "Solar cell parameter extraction using genetic algorithms". In: *Measurement science and technology* 12.11 (2001), p. 1922.
- [54] M. Hejri et al. "An analytical-numerical approach for parameter determination of a five-parameter single-diode model of photovoltaic cells and modules". In: *International Journal of Sustainable Energy* 35.4 (2016), pp. 396–410.
- [55] N. D. Kaushika and N. K. Gautam. "Energy yield simulations of interconnected solar PV arrays". In: *IEEE Transactions on Energy Conversion* 18.1 (2003), pp. 127–134.
- [56] G. Petrone and C. A. Ramos-Paja. "Modeling of photovoltaic fields in mismatched conditions for energy yield evaluations". In: *Electric power systems research* 81.4 (2011), pp. 1003–1013.
- [57] B. C. Babu and S. Gurjar. "A novel simplified two-diode model of photovoltaic (PV) module". In: *IEEE journal of photovoltaics* 4.4 (2014), pp. 1156–1161.
- [58] X. Gao et al. "Lambert W-function based exact representation for double diode model of solar cells: Comparison on fitness and parameter extraction". In: *Energy conversion and management* 127 (2016), pp. 443–460.
- [59] L. Fialho et al. "Effect of Shading on Series Solar Modules: Simulation and Experimental Results". In: *Procedia Technology* 17 (2014), pp. 295–302.
- [60] Y. Chen, Y. Sun, and Z. Meng. "An improved explicit double-diode model of solar cells: Fitness verification and parameter extraction". In: *Energy Conversion and Management* 169 (2018), pp. 345–358.
- [61] M. Hejri et al. "On the parameter extraction of a five-parameter double-diode model of photovoltaic cells and modules". In: *IEEE Journal of Photovoltaics* 4.3 (2014), pp. 915–923.
- [62] K. Ishaque, Z. Salam, and Syafaruddin. "A comprehensive MATLAB Simulink PV system simulator with partial shading capability based on two-diode mode". In: *Solar Energy* 85 (2011), pp. 2217–2227.
- [63] D. Sera, R. Teodorescu, and P. Rodriguez. "PV panel model based on datasheet values". In: *Proceedings of the IEEE International Symposium on Industrial Electronics (ISIE)* (2007), pp. 2392–2396.

- [64] M. G. Villalva, J. R. Gazoli, and E. R. Filho. "Comprehensive approach to modeling and simulation of photovoltaic arrays". In: *IEEE Transactions on power electronics* 24.5 (2009), pp. 1198–1208.
- [65] C. Sah. *Fundamentals of solid-state electronics*. Singapore: World Scientific Publishing Co. Pvt. Ltd., 1991.
- [66] S. Chih-Tang, R. N. Noyce, and W. Shockley. "Carrier generation and recombination in pn junctions and pn junction characteristics". In: *Proceedings of the IRE* 45.9 (1957), pp. 1228–1243.
- [67] MathWorks. *fzero*. 2022. URL: <https://www.mathworks.com/help/matlab/ref/fzero.html> (visited on 08/02/2022).
- [68] A. Smets et al. *Solar Energy: The Physics and Engineering of Photovoltaic Conversion Technologies and Systems*. UIT Cambridge, 2015.
- [69] J. W. Stultz. "Thermal and other tests of photovoltaic modules performed in natural sunlight". In: *Journal of Energy* 3.6 (1979), pp. 363–372.
- [70] W. Herrmann, W. Wiesner, and W. Vaassen. "Hot spot investigations on PV modules – New concepts for a test standard and consequences for module design with respect to bypass diodes". In: *Conference Record of the Twenty Sixth IEEE Photovoltaic Specialists Conference-1997*. IEEE. 1997, pp. 1129–1132.
- [71] T. H. Jung et al. "Output characteristics of PV module considering partially reverse biased conditions". In: *Solar Energy* 92.2 (2013), pp. 214–220.
- [72] K. A. Kim et al. "A dynamic photovoltaic model incorporating capacitive and reverse-bias characteristics". In: *IEEE Journal of Photovoltaics* 3.4 (2013), pp. 1334–1341.
- [73] H. Patel and V. Agarwal. "Maximum power point tracking scheme for PV systems operating under partially shaded conditions". In: *IEEE Transactions on Industrial Electronics* 55.4 (2001), pp. 1689–1698.
- [74] R. E. Hanitsch, D. Schulz, and U. Siegfried. "Shading effects on output power of grid connected photovoltaic generator systems". In: *Rev. Energ. Ren. : Power Engineering* (2001), pp. 93–99.
- [75] J. W. Bishop. "Computer simulation of the effects of the electrical mismatches in photovoltaic cell interconnection circuits". In: *Solar Cells* 25 (1988), pp. 73–89.
- [76] V. Quaschnig and R. Hanitsch. "Numerical simulation of current–voltage characteristics of photovoltaic systems with shaded solar cells". In: *Solar Energy* 56.6 (1996), pp. 513–520.
- [77] A. Calcabrini et al. "The Relevance of the Cell's Breakdown Voltage in the DC Yield of Partially Shaded PV Modules". In: *2021 IEEE 48th Photovoltaic Specialists Conference (PVSC)*. IEEE. 2021, pp. 0092–0094.
- [78] O. Breitenstein et al. "Understanding junction breakdown in multicrystalline solar cells". In: *Journal of applied physics* 109.7 (2011), p. 5.
- [79] H. Chu et al. "Shade performance of a back-contact module assembled with cells featuring soft breakdown characteristic". In: *Energy Procedia* 92 (2016), pp. 540–545.
- [80] J. Bauer et al. "Avalanche breakdown in multicrystalline solar cells due to preferred phosphorous diffusion at extended defects". In: *Progress in Photovoltaics: Research and Applications* 21.7 (2013), pp. 1444–1453.
- [81] X. Sun et al. "A physics-based compact model for CIGS and CdTe solar cells: From voltage-dependent carrier collection to light-enhanced reverse breakdown". In: *2015 IEEE 42nd Photovoltaic Specialist Conference (PVSC)*. IEEE. 2015, pp. 1–6.
- [82] P. Szaniawski et al. "Light-enhanced reverse breakdown in Cu (In, Ga) Se₂ solar cells". In: *Thin Solid Films* 535 (2013), pp. 326–330.
- [83] T. J. Silverman et al. "Thermal and electrical effects of partial shade in monolithic thin-film photovoltaic modules". In: *IEEE Journal of Photovoltaics* 5.6 (2015), pp. 1742–1747.
- [84] A. Woyte, J. Nijs, and R. Belmans. "Partial shadowing of photovoltaic arrays with different system configurations: literature review and field test results". In: *Solar energy* 74.3 (2003), pp. 217–233.

- [85] N. G. Dhere et al. "The reliability of bypass diodes in PV modules". In: *Reliability of photovoltaic cells, modules, components, and systems VI*. Vol. 8825. SPIE. 2013, pp. 110–117.
- [86] SEMIKRON. *F 1200A ... F 1200G - Datasheet*. 2011.
- [87] Canadian Solar. *CS6P 220/225/230/235/240/245/250P*. Canada.
- [88] M. Dallapiccola et al. "Simplified Method for Partial Shading Losses Calculation for Series Connected PV Modules with Experimental Validation". In: *35th European Photovoltaic Solar Energy Conference and Exhibition*. Vol. 1614. 2018, p. 6.
- [89] M. Dallapiccola et al. "Explicit Model Based on Approximated I-V Curves for Partial Shading Modelling of Photovoltaic Systems". In: *36th European Photovoltaic Solar Energy Conference and Exhibition*. 2019, pp. 1492–1496.
- [90] Panasonic Industry. *Product Notices - Heterojunction technology for increased solar yield*. 2019. URL: <https://industry.panasonic.eu/panasonic-industry-news/heterojunction-technology-increased-solar-yield> (visited on 08/12/2022).
- [91] Silevo. *Triex U-Series U305 Watt*. Silevo Inc., 2014, pp. 1–2.
- [92] QCells. *Q.ANTUM DUO Z TECHNOLOGY*. URL: <https://www.q-cells.eu/products/technology/qantum.html> (visited on 08/12/2022).
- [93] SINOVOLTAICS. *Bypass Diodes*. URL: <https://sinovoltaics.com/learning-center/basics/bypass-diodes/> (visited on 08/16/2022).
- [94] JAMECO Electronics. *Schottky Rectifier 80 SQ... Series (Jameco Part Number 1558946)*. California, USA.
- [95] D. D. B. Mesquita et al. "A review and analysis of technologies applied in PV modules". In: *2019 IEEE PES Innovative Smart Grid Technologies Conference-Latin America (ISGT Latin America)*. IEEE. 2019, pp. 1–6.
- [96] H. Hanifi, J. Schneider, and J. Bagdahn. "Reduced shading effect on half-cell modules—Measurement and simulation". In: *31st European Photovoltaic Solar Energy Conference and Exhibition*. 2015, pp. 2529–2533.
- [97] T. Tang et al. "A quantitative comparison between double glass photovoltaic modules using half-size cells and quarter-size cells". In: *IEEE Journal of Photovoltaics* 7.5 (2017), pp. 1298–1303.
- [98] S. Guo et al. "A quantitative analysis of photovoltaic modules using halved cells". In: *International Journal of Photoenergy* 2013 (2013).
- [99] J. Qian et al. "Comparison of half-cell and full-cell module hotspot-induced temperature by simulation". In: *IEEE Journal of Photovoltaics* 8.3 (2018), pp. 834–839.
- [100] M. T. Sarniak. "Modeling the functioning of the half-cells photovoltaic module under partial shading in the matlab package". In: *Applied Sciences* 10.7 (2020), p. 2575.
- [101] M. Chiodetti et al. "Half-Cell Module Behaviour and Its Impact on the Yield of a PV Plant". In: *36th European Photovoltaic Solar Energy Conference and Exhibition*. 2019, pp. 1444–1448.
- [102] K. Brecl, M. Bokalič, and M. Topič. "Annual energy losses due to partial shading in PV modules with cut wafer-based Si solar cells". In: *Renewable Energy* 168 (2021), pp. 195–203.



Canadian Solar Validation Results

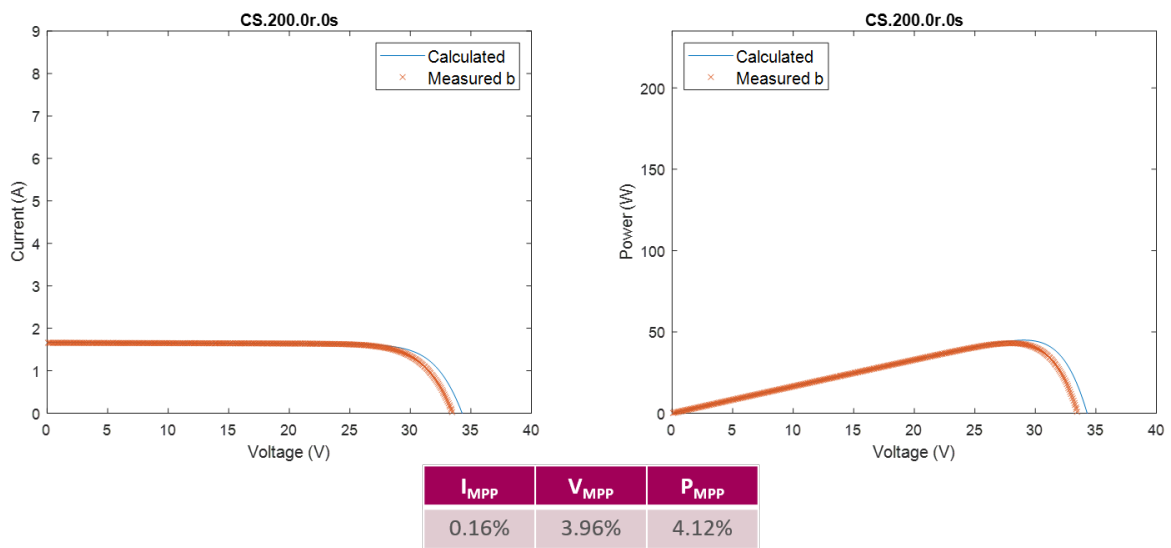


Figure A.1: IV and PV plots showing calculated values in comparison to measured values for the Canadian Solar CS6 230P module under partial shading conditions, with errors at MPP. Shading case G200_0ratio_0strings.

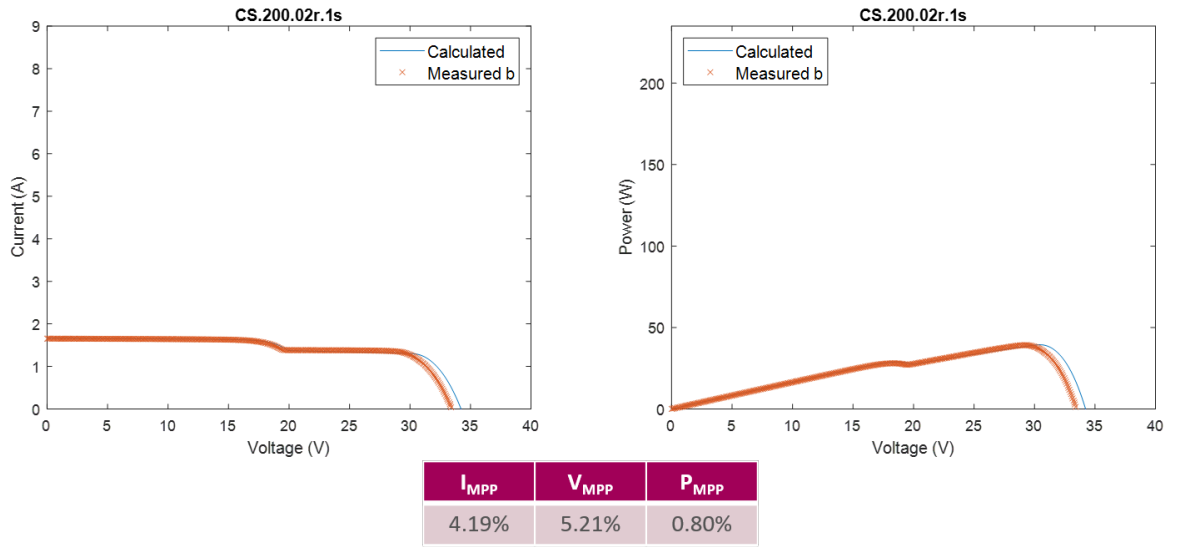


Figure A.2: IV and PV plots showing calculated values in comparison to measured values for the Canadian Solar CS6 230P module under partial shading conditions, with errors at MPP. Shading case G200_02ratio_1strings.

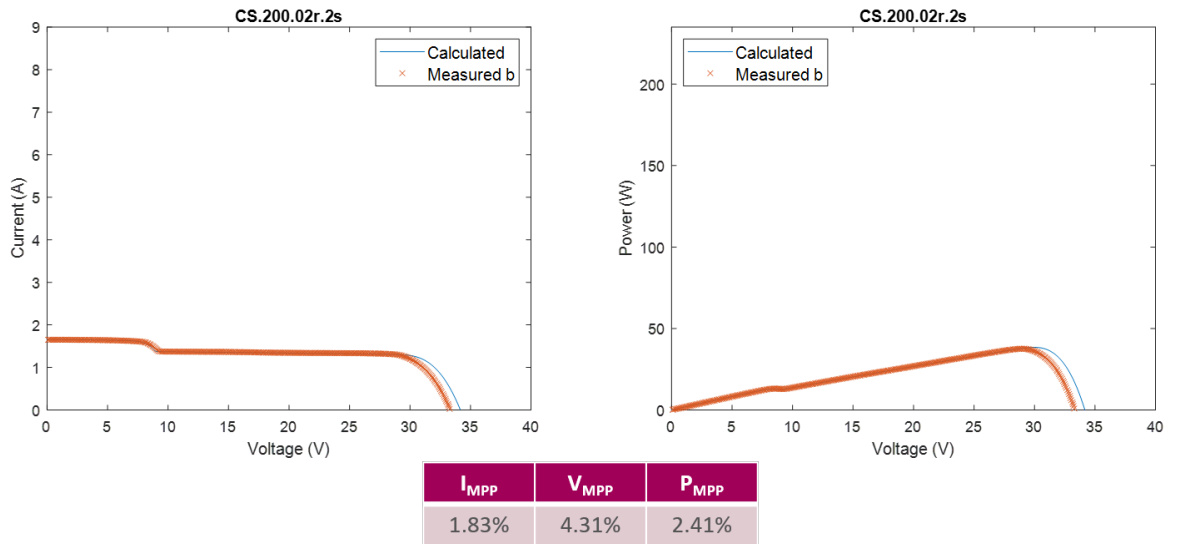


Figure A.3: IV and PV plots showing calculated values in comparison to measured values for the Canadian Solar CS6 230P module under partial shading conditions, with errors at MPP. Shading case G200_02ratio_2strings.

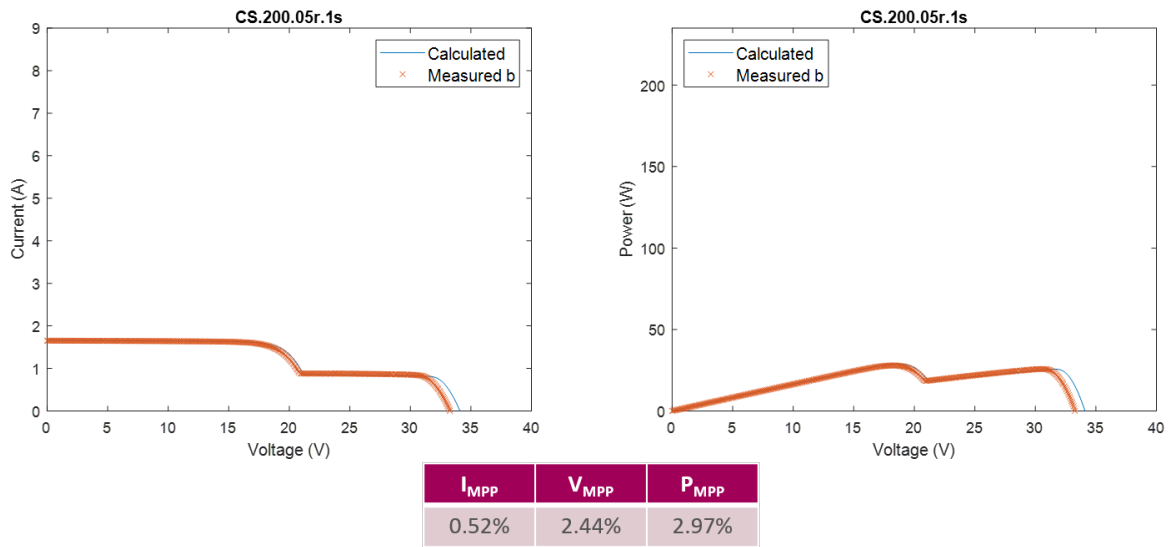


Figure A.4: IV and PV plots showing calculated values in comparison to measured values for the Canadian Solar CS6 230P module under partial shading conditions, with errors at MPP. Shading case G200_05ratio_1strings.

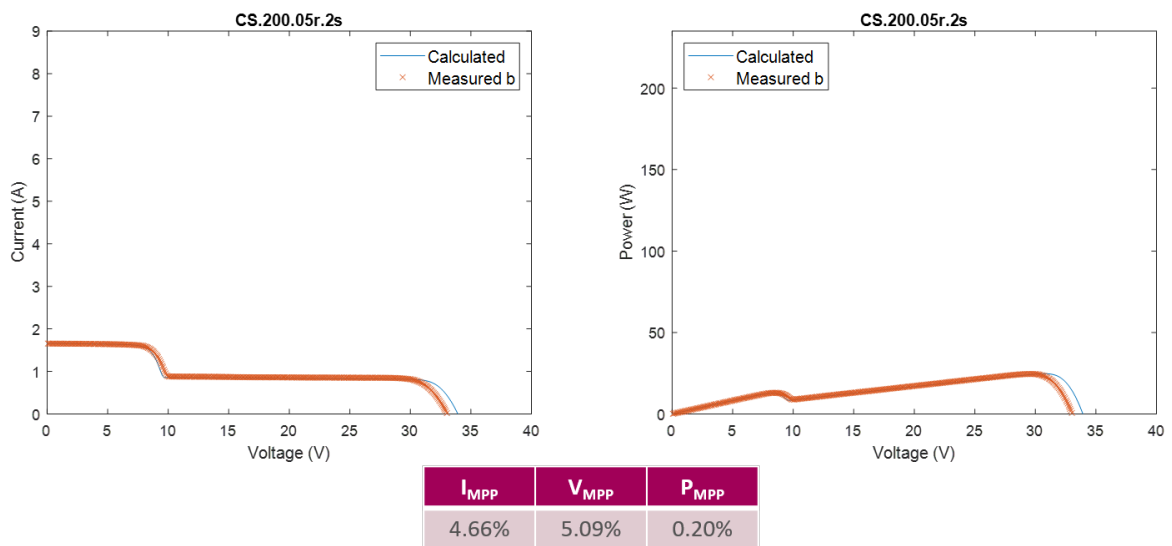


Figure A.5: IV and PV plots showing calculated values in comparison to measured values for the Canadian Solar CS6 230P module under partial shading conditions, with errors at MPP. Shading case G200_05ratio_1strings.

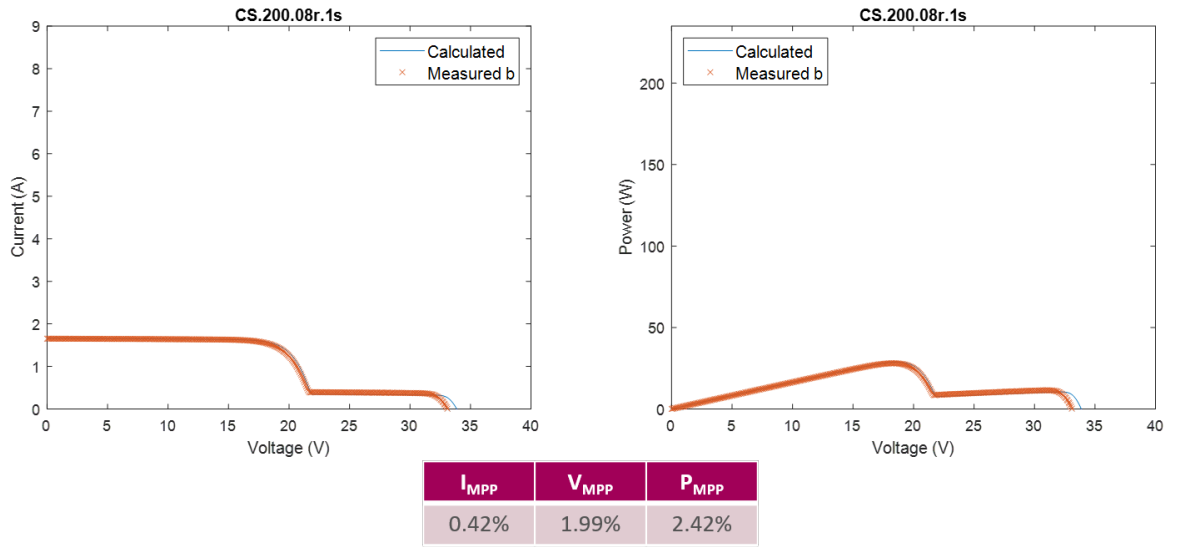


Figure A.6: IV and PV plots showing calculated values in comparison to measured values for the Canadian Solar CS6 230P module under partial shading conditions, with errors at MPP. Shading case G200_08ratio_1strings.

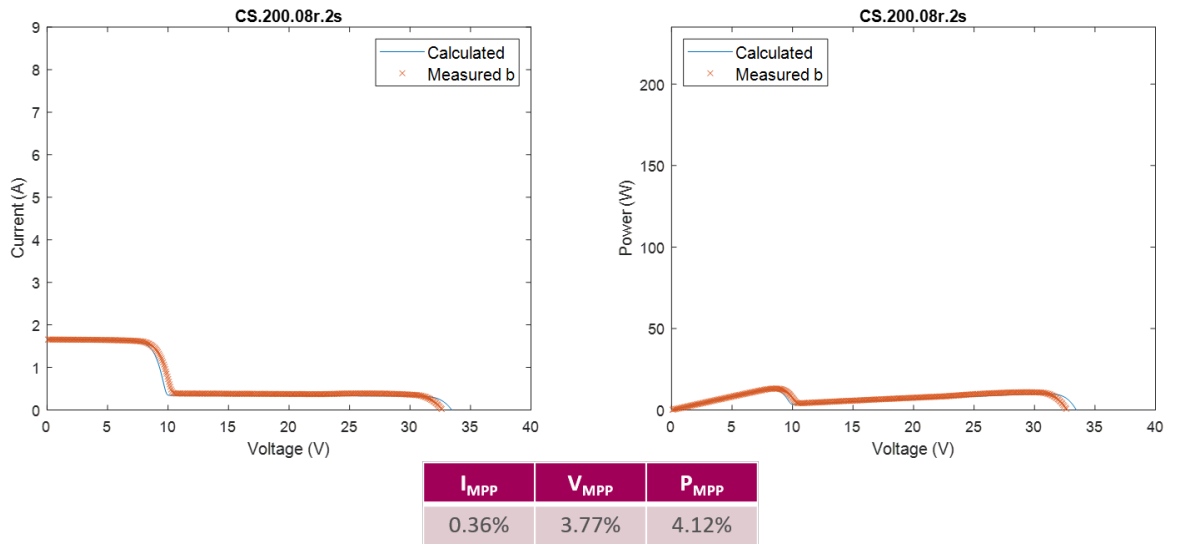


Figure A.7: IV and PV plots showing calculated values in comparison to measured values for the Canadian Solar CS6 230P module under partial shading conditions, with errors at MPP. Shading case G200_08ratio_2strings.

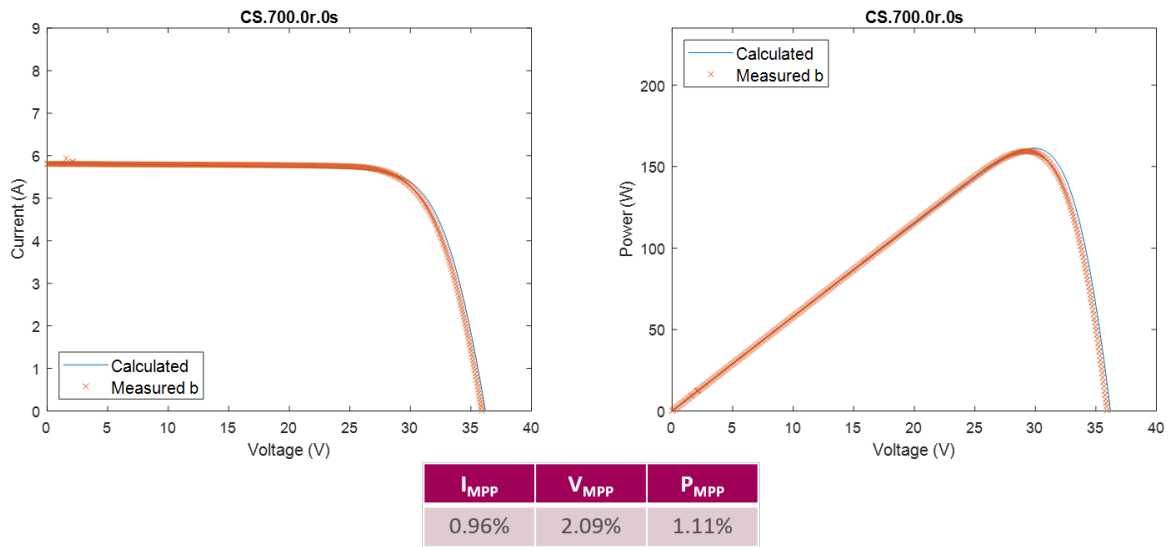


Figure A.8: IV and PV plots showing calculated values in comparison to measured values for the Canadian Solar CS6 230P module under partial shading conditions, with errors at MPP. Shading case G700_0ratio_0strings.

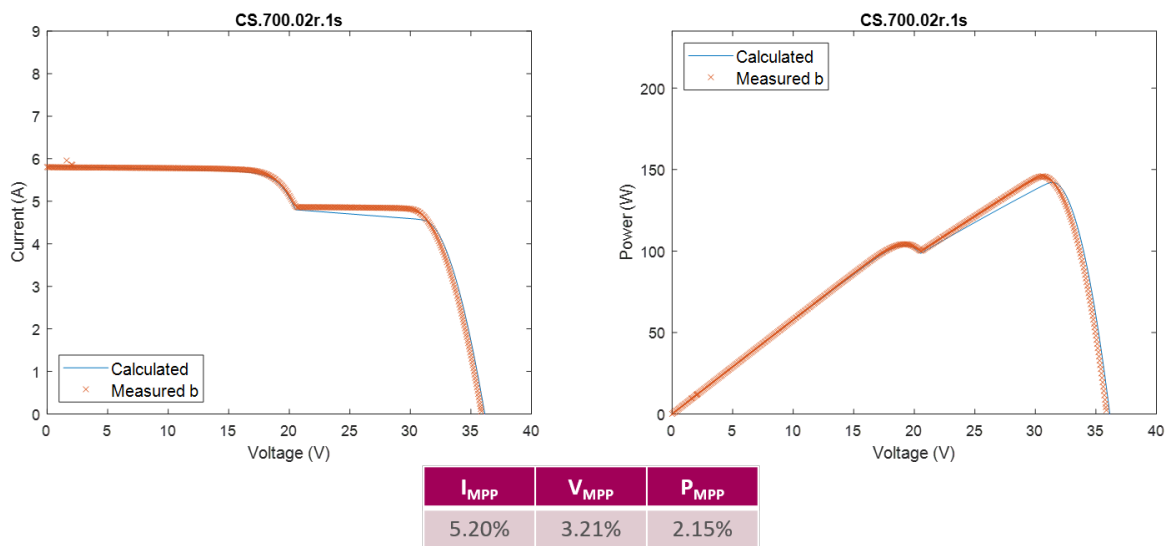


Figure A.9: IV and PV plots showing calculated values in comparison to measured values for the Canadian Solar CS6 230P module under partial shading conditions, with errors at MPP. Shading case G700_02ratio_1strings.

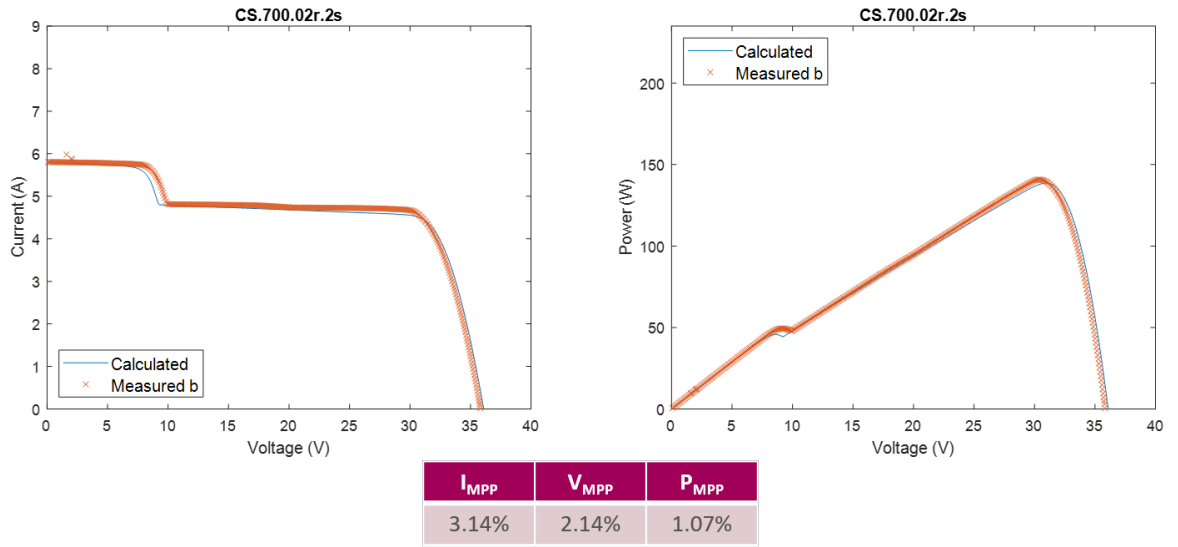


Figure A.10: IV and PV plots showing calculated values in comparison to measured values for the Canadian Solar CS6 230P module under partial shading conditions, with errors at MPP. Shading case G700_02ratio_2strings.

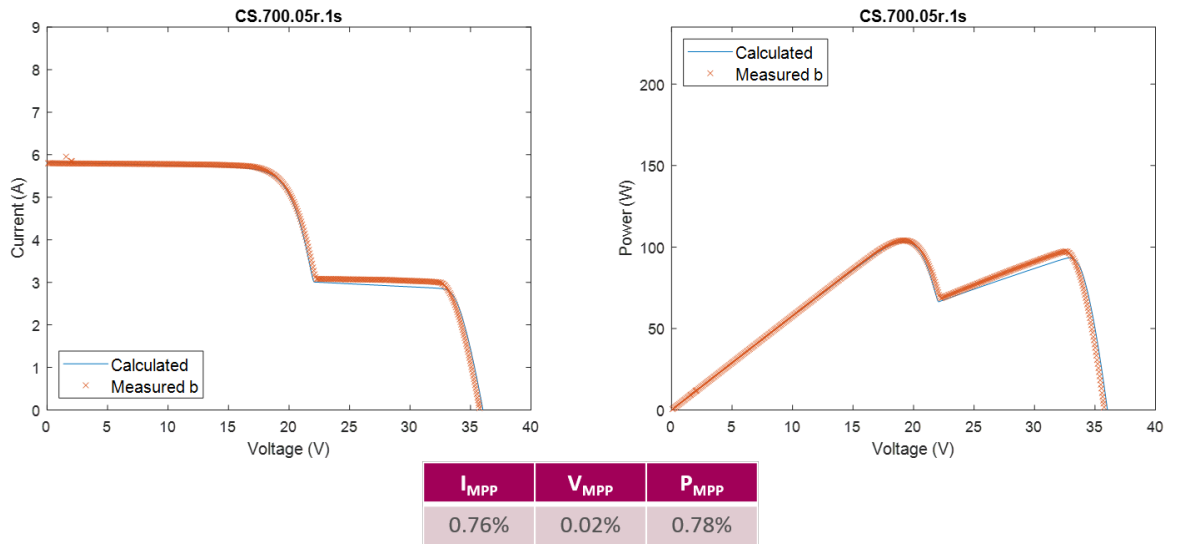


Figure A.11: IV and PV plots showing calculated values in comparison to measured values for the Canadian Solar CS6 230P module under partial shading conditions, with errors at MPP. Shading case G700_05ratio_1strings.

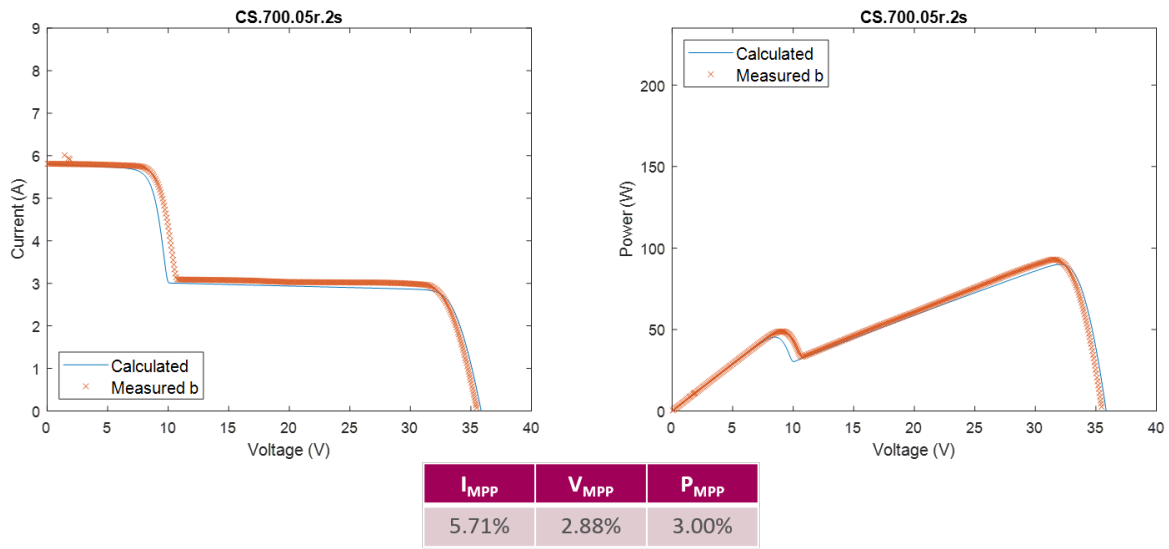


Figure A.12: IV and PV plots showing calculated values in comparison to measured values for the Canadian Solar CS6 230P module under partial shading conditions, with errors at MPP. Shading case G700_05ratio_1strings.

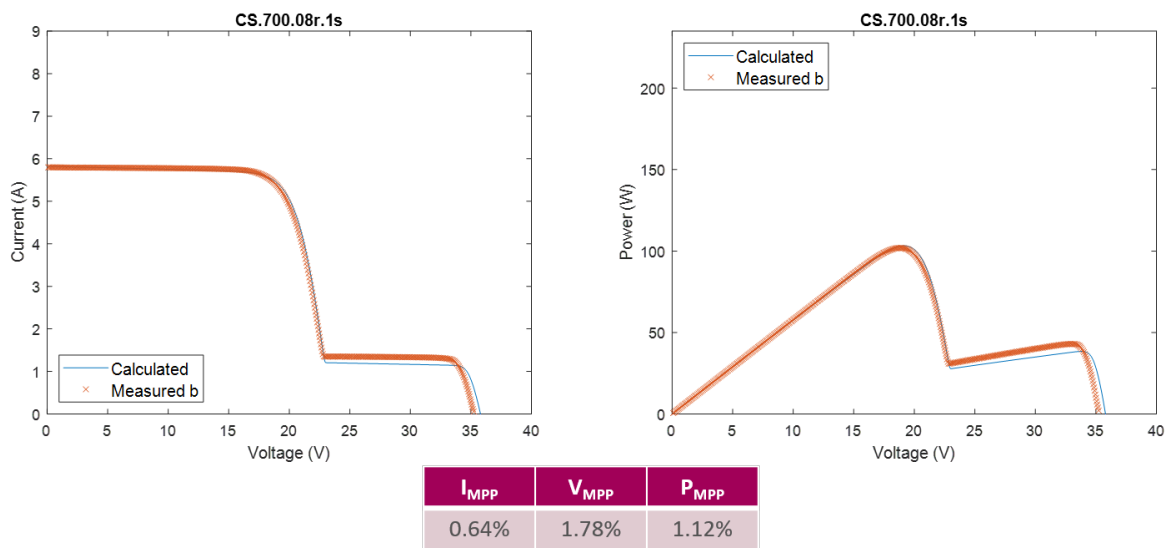


Figure A.13: IV and PV plots showing calculated values in comparison to measured values for the Canadian Solar CS6 230P module under partial shading conditions, with errors at MPP. Shading case G700_08ratio_1strings.

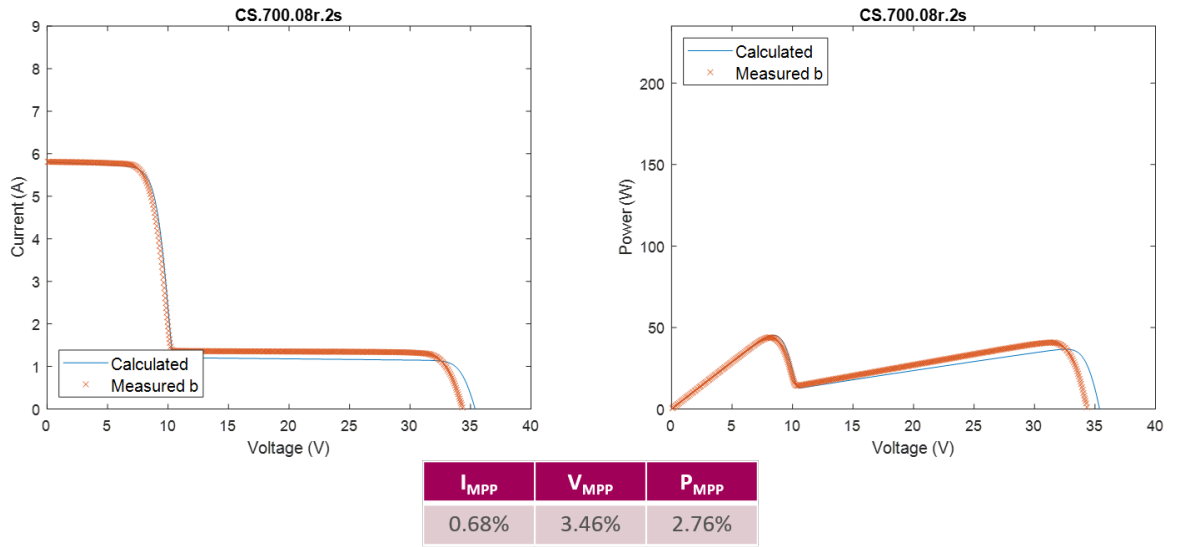


Figure A.14: IV and PV plots showing calculated values in comparison to measured values for the Canadian Solar CS6 230P module under partial shading conditions, with errors at MPP. Shading case G700_08ratio_2strings.

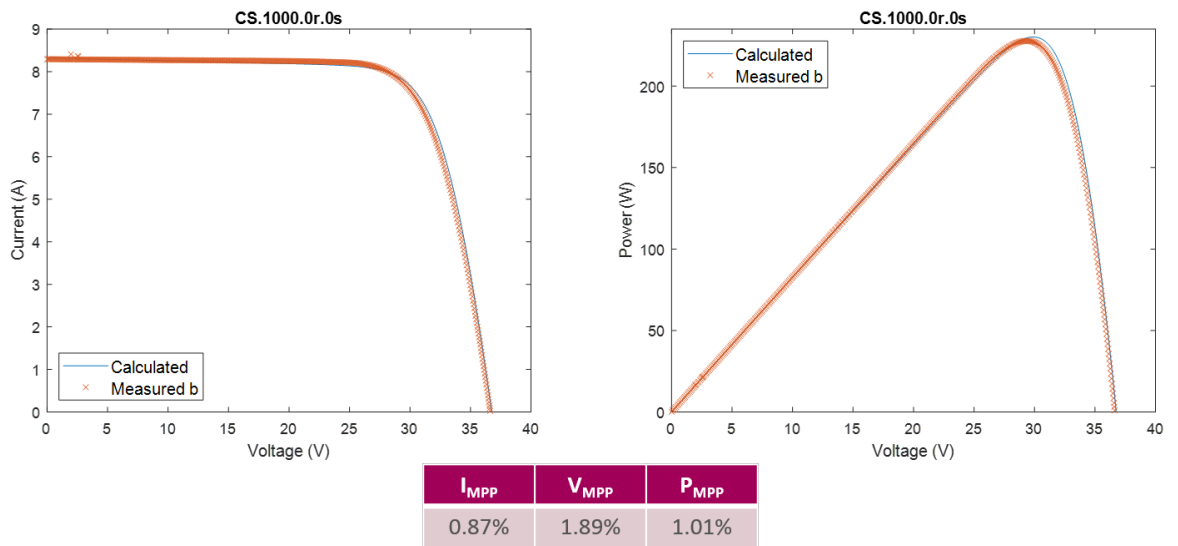


Figure A.15: IV and PV plots showing calculated values in comparison to measured values for the Canadian Solar CS6 230P module under partial shading conditions, with errors at MPP. Shading case G1000_0ratio_0strings.

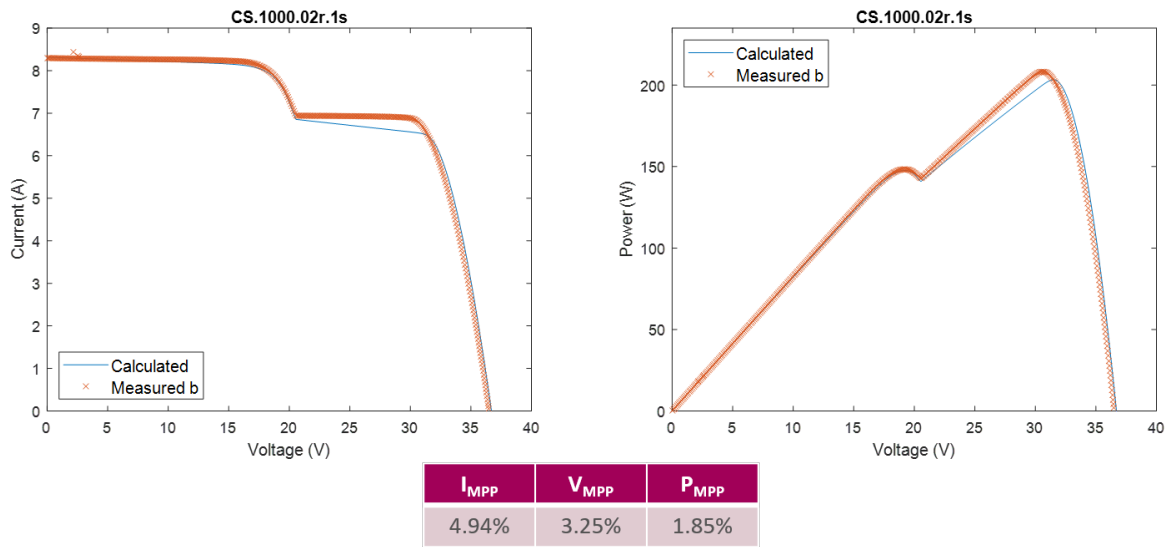


Figure A.16: IV and PV plots showing calculated values in comparison to measured values for the Canadian Solar CS6 230P module under partial shading conditions, with errors at MPP. Shading case G1000_02ratio_1strings.

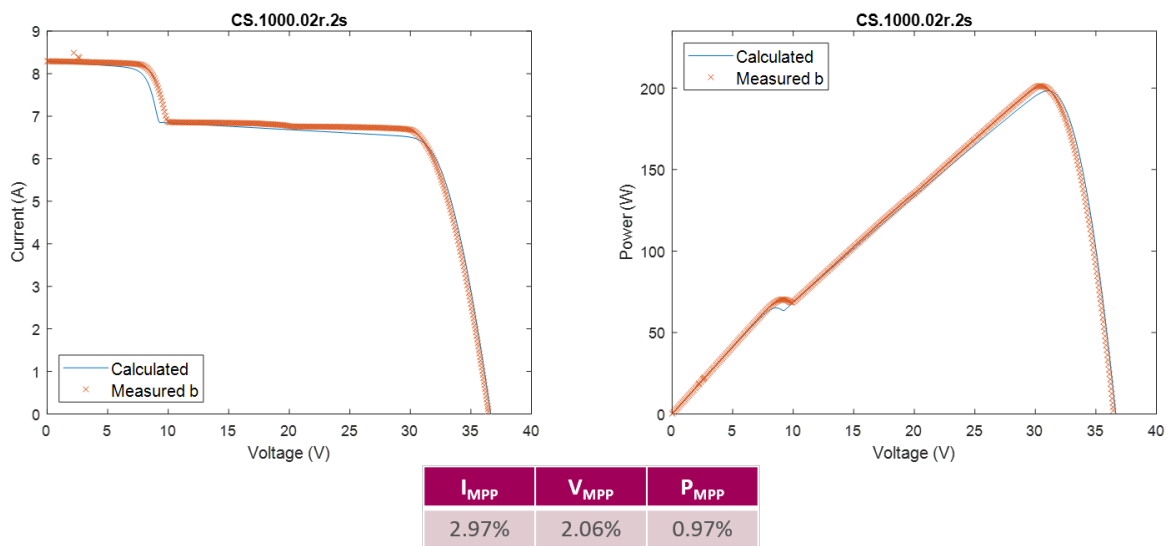


Figure A.17: IV and PV plots showing calculated values in comparison to measured values for the Canadian Solar CS6 230P module under partial shading conditions, with errors at MPP. Shading case G1000_02ratio_2strings.

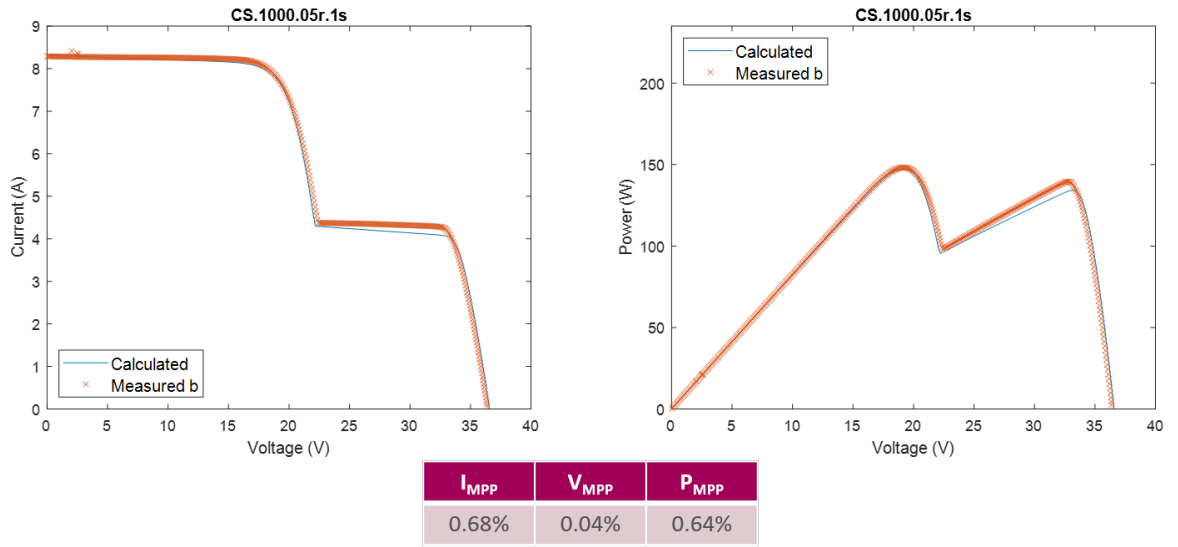


Figure A.18: IV and PV plots showing calculated values in comparison to measured values for the Canadian Solar CS6 230P module under partial shading conditions, with errors at MPP. Shading case G1000_05ratio_1strings.

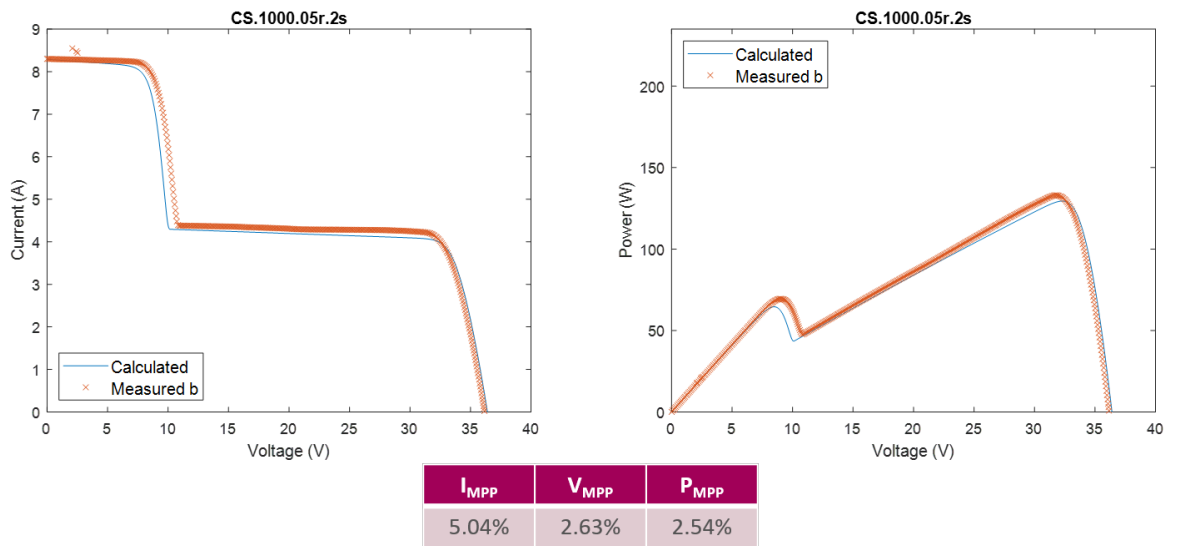


Figure A.19: IV and PV plots showing calculated values in comparison to measured values for the Canadian Solar CS6 230P module under partial shading conditions, with errors at MPP. Shading case G1000_05ratio_1strings.

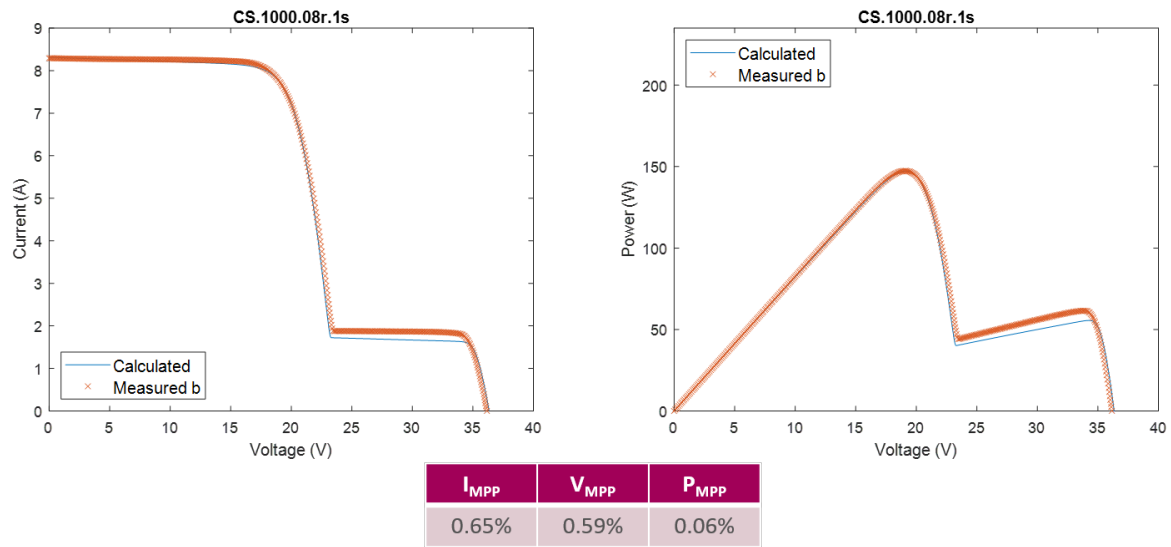


Figure A.20: IV and PV plots showing calculated values in comparison to measured values for the Canadian Solar CS6 230P module under partial shading conditions, with errors at MPP. Shading case G1000_08ratio_1strings.

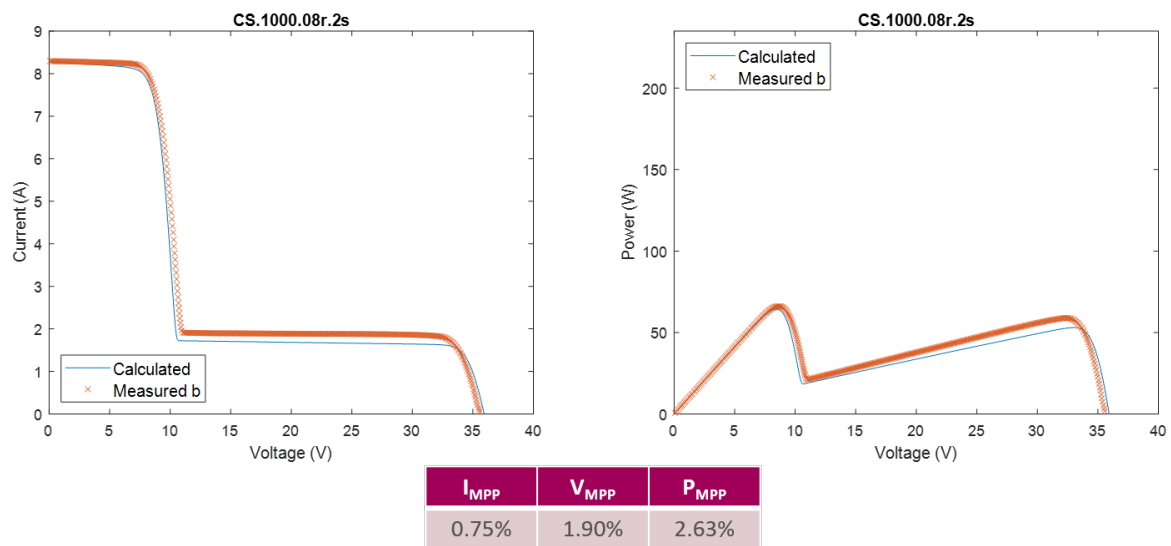


Figure A.21: IV and PV plots showing calculated values in comparison to measured values for the Canadian Solar CS6 230P module under partial shading conditions, with errors at MPP. Shading case G1000_08ratio_2strings.